Development of the SAQM-AERO Model and its Application in the San Joaquin Valley of California

Donald Dabdub*

Laurel L. DeHaan*

Naresh Kumar†

Fred Lurmann†

John H. Seinfeld (P.I.)‡

Prepared for California Air Resources Board and the

California Environmental Protection Agency

ARB Contract #93-304

February 9, 1998

* Department of Mechanical Engineering and Aerospace Engineering, University of California, Irvine, CA 92697-3975.

† Sonoma Technological, Inc., 5510 Skyland Blvd., Suite 101, Santa Rosa, CA 95403-1083.

‡ Division of Engineering and Applied Science, California Institute of Technology, Pasadena, CA 91125.

The statements and conclusions in this Report are those of the contractor and not necessarily those of the California Air Resources Board. The mention of commercial products, their source, or their use in connection with material reported herein is not to be construed as actual or implied endorsement of such products.

This Report was submitted in fulfillment of ARB Contract #92-304 and project title "Development of the SAQM-AERO Model and its Application in the San Joaquin Valley of California" by the California Institute of Technology under the sponsorship of the California Air Resources Board. Work was completed as of April 22, 1997.

Table of Contents

List of Figures and List of Tables	i
Abstract	1
Executive Summary	2
1. Introduction	5
2. Diagnosis of Ozone in the San Joaquin Valley of California	2-1
3. Implementation of a New Gas-Phase Chemistry Solver	3-1
4. Incorporation of Aerosol Species in SAQM	4-1
5. A New Time Step Algorithm	5-1
6. References	6-1

LIST OF FIGURES

Figure		Page
2-1.	SAQM model domain.	2-19
2-2.	Low level MM5 wind field from noon August 4, 1990.	2-20
2-3.	Execution time as a function of number of nodes when parallelizing the chemistry loop of the SAQM. Theoretical time presented is calculated from Amdahl's law. Time reported corresponds to a 24 hour standard simulation of the San Joaquin Valley of California	2-21
2-4.	Execution time as a function of number of nodes when parallelizing various operators of the SAQM. Theoretical time presented is calculated from Amdahl's law. Time reported corresponds to a 24 hour standard simulation of the San Joaquin Valley of California.	2-22
2-5.	Ozone mixing ratio from observations (dotted) and model base case (solid).	2-23
2-6.	Ozone mixing ratio from observations (dotted), model base case (solid), and the model with zero wind (dashed).	2-24
2-7.	Ozone mixing ratio from observations (dotted), model base case (solid), and the model with zero boundary conditions (dashed).	2-25
2-8.	Vertically integrated, area average ozone mixing ratio from the model base case (solid), and the model with zero boundary conditions (dashed).	2-26
2-9.	Ozone mixing ratio from observations (dotted), model base case (solid), and the model with zero ozone boundary conditions (dashed).	2-27
2-10.	Ozone mixing ratio from observations (dotted), model base case (solid), and the model with zero emissions (dashed).	2-28
2-11.	Ozone mixing ratio from observations (dotted), model base case (solid), and the model with zero deposition (dashed).	2-29

LIST OF TABLES

Table		Page
2-1.	Discretization of the grid using σ-coordinates.	2-17
2-2.	Differential species defined in the chemical mechanism.	2-17
2-3.	Boundary mixing ratios for the lowest level of the SAQM used in the August 3-5, 1990 episode.	2-18
2-4.	Measures of model error in ozone predictions.	2-18
2-5.	Summary of the SAQM computational profile for a base case episode.	2-18

LIST OF FIGURES

Figure		Page
3-1.	Predicted concentrations of NO, NO_2, O_3, HNO_3, OLE, FORM, and ALD2 for the three different solvers	3-7
3-2.	Predicted concentrations of C2O3, NO_3, HO_2, XO2, and CRO for the three different solvers	3-8
3-3.	Predicted concentrations of CRES, XO2N, OH, and ROR for the three different solvers	3-9
3-4.	An example of the CHEMPARAM file used in the SAQM	3-13
3-5.	The CHPARM.COM include file used in SAQM-IEH	3-19
3-6.	BLK_DAT2 FORTRAN block data file used in SAQM-IEH	3-19
3-7.	Time-series plots of O_3 comparing results from SAQM-IEH and SAQM-STD	3-21
3-8.	Time-series plots of NO_2 comparing results from SAQM-IEH and SAQM-STD	3-24
3-9.	Time-series plots of O_3 comparing results from SAQM-IEH and LSODE	3-28
3-10.	Time-series plots of O_3 comparing results from SAQM-300 and SAQM-1200	3-33

LIST OF TABLES

Table		Page
3-1.	Initial concentrations of species for the box model test problem	3-3
3-2.	The slow reacting, fasting reacting, and steady-state species assignments for CB-IV in the SAQM-IEH solver	3-6
3-3.	CPU times taken by different solvers for the test problem	3-10
3-4.	Structure of data on the CHEMPARAM file	3-12
3-5.	Comparison of SAQM ozone predictions at high ozone station with the IEH and standard chemistry solvers	3-27
3-6.	Comparison of SAQM ozone predictions with different chemistry solvers	3-31
3-7.	Comparison of CPU time used by the SAQM-STD and SAQM-IEH	3-31

LIST OF FIGURES

Figure		Page
4-1.	Schematic of the individual steps and logic in the aerosol module	4-8
4-2.	Experimental data for size dependence of particle deposition velocities	4-14
4-3.	Examples of the "nsect.inc" and "param.inc" include files in the SAQM-AERO model	4-16
4-4.	Time-series plot of observed (•••) and predicted (—) PM_{10} SO_4 concentrations	4-24
4-5.	Time-series plot of observed (•••) and predicted (—) PM_{10} NO_3 concentrations	4-25
4-6.	Time-series plot of observed (•••) and predicted (—) HNO_3 concentrations	4-28
4-7.	Time-series plot of observed (•••) and predicted (—) TNO3 concentrations	4-29
4-8.	Time-series plot of observed (•••) and predicted (—) PM_{10} NH_4 concentrations	4-31
4-9.	Time-series plot of observed (•••) and predicted (—) NH_3 concentrations	4-32
4-10.	Time-series plot of observed (•••) and predicted (—) TNH4 concentrations	4-34
4-11.	Time-series plot of observed (•••) and predicted (—) PM_{10} OM concentrations	4-35
4-12.	Time-series plot of observed (•••) and predicted (—) PM_{10} EC concentrations	4-37
4-13.	Time-series plot of observed (•••) and predicted (—) PM_{10} mass concentrations	4-38
4-14.	Spatial distribution of predicted PM_{10} SO_4 concentrations on August 6, 1990	4-42
4-15.	Spatial distribution of predicted PM_{10} NO_3 concentrations on August 6, 1990	4-43
4-16.	Spatial distribution of predicted HNO_3 concentrations on August 6, 1990	4-44
4-17.	Spatial distribution of predicted PM_{10} NH_4 concentrations on August 6, 1990	4-45
4-18.	Spatial distribution of predicted NH_3 concentrations on August 6, 1990	4-46
4-19.	Spatial distribution of predicted PM_{10} OM concentrations on August 6, 1990	4-47
4-20.	Spatial distribution of predicted PM_{10} EC concentrations on August 6, 1990	4-48
4-21.	Spatial distribution of predicted PM_{10} mass concentrations on August 6, 1990	4-49

LIST OF TABLES

Table | Page

4-1. Equilibrium relations in the SEQUILIB aerosol module 4-3

4-2. Secondary organic aerosol yields for the CB-IV chemical mechanism organic classes 4-10

4-3. Assignment of C10 biogenic species emissions to CB-IV compound classes 4-10

4-4. Aerosol production reactions for the CB-IV mechanism 4-11

4-5. Description of important parameters used in the aerosol module 4-17

4-6. Surface layer concentrations of new species in the initial concentration and boundary condition files 4-19

4-7. Total emissions for the modeling domain used in the simulation for Friday, August 3, 1990 4-21

4-8. Comparison of mean observed and predicted concentrations ($\mu g/m^3$) of aerosol species for August 3-6, 1990 4-22

4-9. Surface temperature and relative humidity in the SJV modeling domain on August 3-6, 1990 4-26

4-10. Observed and predicted PM_{10} mass concentrations ($\mu g/m^3$) at routine monitoring stations on August 3, 1990 4-39

LIST OF TABLES

Table Page

5-1. 24-hr average predicted concentrations of PM species (in $\mu g/m^3$) for the base case and alternate time step case on August 6, 1990 5-3

5-2. 24-hr average predicted concentrations of gas-phase species (in ppb) for the base case and alternate time step case on August 6, 1990 5-4

Abstract

Mathematical models of acid deposition are complex, requiring significant expenditure of computation time for their implementation. The overall goal of this project was threefold: (1) to prepare and test the SAQM model for use in simulating ozone and acid deposition in California; (2) to improve the computational efficiency of SAQM through improvement of computational algorithms within it and through implementation of parallel computing; and (3) to develop, implement, and apply an efficient aerosol module in SAQM. This report contains a description of each of these three tasks. In preparation and testing of SAQM, simulations of ozone air quality in the San Joaquin Valley during the August 3-6, 1990 episode were carried out and are reported. These simulations augment and support those carried out previously by the Air Resources Board and summarized in San Joaquin Valley Air Quality Study: Policy-Relevant Findings, California Air Resources Board, November 1996.

Executive Summary

The SAQM model was developed for simulation of ozone and acid deposition on the regional scale. This model is particularly relevant for large areas of California, especially the San Joaquin Valley. The present report is directed at a comprehensive analysis of SAQM, its numerical routines, its performance in ozone simulation, its overall computational efficiency, and the addition of an aerosol module to it. In preparation and testing of SAQM, simulation of ozone in the San Joaquin Valley during the August 3-6, 1990 episode were carried out. Diagnosis of the relative contributions of inflow material and local Valley emissions to ozone levels at Valley sites is in general accord with conclusions presented in San Joaquin Valley Air Quality Study, Policy-Relevant Findings, California Air Resources Board, November 1996.

The photochemical mechanisms used in gridded air quality models include fairly detailed treatment of the inorganic reactions and fairly condensed representations of the organic reactions of importance in the atmospheric chemistry of the NO_x,/VOC/O_3,/SO_2/HNO_3 chemical system. Periodically, the photochemical mechanisms need to be updated to incorporate more recent chemical kinetic and mechanistic data. Likewise, there is a need to implement alternate chemical mechanisms to assess the sensitivity of model results, to the choice of chemical mechanism. The original SAQM model was set up with the chemical mechanisms implemented in a "hardwired" fashion. Implementation of alternate chemical mechanisms in this format is time-consuming and prone to error because all of the reactions are hand-coded. Numerous modern air quality models (RPM, CAMx, UAM/FCM, etc.) have chemical compilers and flexible chemical mechanism interfaces to facilitate incorporation of the new reactions and/or alternate mechanisms. Hence, one of the objectives was to change the chemical mechanism interface so that the chemistry could more easily be updated.

Another objective was to evaluate the numerical methods used to integrate the gas-phase chemical kinetic rate equations. Integrating the system of 30 to 50 ordinary differential equations (ODEs) that describe the gas-phase chemistry takes a large amount of computer time.

The chemical kinetic equations are complex, nonlinear, and numerically stiff. The most accurate method for solving stiff systems of ODEs is the Gear method (Gear, 1971; Hindmarsh, 1980). For gridded air quality models, where the equations need to be solved at thousands of grid points, the Gear method is inefficient and time consuming. Various fast chemical kinetic solvers have been developed for use in air quality models that are significantly faster than the Gear solver. The numerical method used in the SARMAP air quality model (SAQM) is based on the algorithm used in the Regional and Acid Deposition Model (RADM) (Chang et al., 1987). In the last decade significant advancements have been made towards developing faster and more accurate numerical methods. Hence, it was desirable to replace the original SAQM solver with a new generation solver. Furthermore, the implementation of a more flexible chemical mechanism interface could be more readily accomplished if the model's numerical solver was more robust and required less mechanism-specific hardwired coding.

This report includes a review of the SAQM's original chemical solver and a comparison with a modern implicit-explicit hybrid (IEH) chemistry solver (Sun et al., 1994; Kumar et al., 1995). Based on the review, the IEH solver has been implemented in the SAQM and tested against the original model.

Incorporation of aerosol species in acid deposition models is essential because the wet and dry deposition of particles containing sulfate, nitrate, and ammonium can affect the acidity of deposited materials. In this study, the SAQM model was extended to treat aerosol species of importance in California. The extension involved adding an aerosol module to simulate the gas-aerosol partitioning of relevant species, the evolution of the aerosol size distribution (optionally), the production of secondary organic aerosol species, and the dry deposition of particles. The version of the model with aerosol species is referred to as SAQM-AERO.

Major features of this aerosol module are:

- Simulation of the aerosol concentrations of all the major primary and secondary components of atmospheric PM, including sulfate, nitrate, ammonium, chloride, sodium, elemental carbon, organic carbon, water, and other crustal material.

- A sectional approach for characterization of the continuous aerosol size distribution, typically extending from 0.01 to 10 μm for aerosols and from 0.01 to 30 μm when fog droplets are present, with user-specified size bins. The model can also be applied with a single aerosol size bin.
- An algorithm to simulate the mass transfer occurring between the gaseous and aerosol species during condensation and evaporation. The effects of nucleation and coagulation are ignored in the algorithm.
- An algorithm to simulate the distribution of aerosol species concentrations based on the thermodynamics of the sulfate/nitrate/chloride/ammonium/sodium/water chemical system.
- Production of condensable organic species from oxidation of gaseous organic compounds based on the organic aerosol yields reported by Pandis et al. (1992).
- An algorithm to approximate effects of fogwater condensation and evaporation on the growth and shrinkage of the aerosol/fog droplet-size distribution.
- An algorithm to simulate particle deposition and gravitational settling for particles of various sizes.
- Incorporation of ammonia (NH_3) and hydrochloric acid (HCl) as gas-phase species in the model.

In reviewing the logic incorporated into the SAQM model for ways to improve its computational efficiency, we discovered that the model did not check that the time step used for horizontal advection would ensure numerical stability.

A more robust design is to assign an upper limit on the integration time step and then choose the actual time step based on the Courant stability criteria (both for the horizontal and vertical advection) at the beginning of each hour of simulation. This may lead to a variable number of time steps for each hour, but ensures numerical stability under all conditions. A new subroutine TMSTPS was written to calculate the transport time step based on the Courant limit in the horizontal and vertical directions. A new variable DTMAX was added to the user input file to specify the maximum time step to be used by the model for transport operator.

1. Introduction

Acidic deposition represents one of the most complex atmospheric phenomena to model, as it involves an intricate coupling of gas-phase chemistry, aerosol and droplet chemistry, and deposition. Nonetheless, in order to assess the effectiveness of emission control measures on acid deposition detailed mathematical models are required. The regional-scale acid deposition model RADM was developed by Chang and co-workers for the NAPAP program, and that model was updated for application to California and given the acronym SAQM. Of particular interest has been the application of SAQM to understand air quality in the San Joaquin Valley. Prior to the present study, SAQM did not include a treatment of aerosol processes, so it had limited utility as an acid deposition model. also, its implementation required significant amounts of computing time, making the model of limited usefulness as a tool to evaluate a wide range of potential control strategies.

The principal directions of the present study were to add an aerosol component to SAQM and to improve its computational efficiency. Chapter 2 describes SAQM and its application to simulation of gas-phase atmospheric chemistry in the San Joaquin Valley. Computational improvements in the model are presented in Chapter 3. Implementation of a size- and composition-resolved aerosol module is described in Chapter 4. Finally, Chapter 5 presents a minor time-step improvement made to SAQM.

2. Diagnosis of Ozone in the San Joaquin Valley of California

2.1 Introduction

Ozone levels in the San Joaquin Valley of central California exceeded the national ambient air quality standard for ozone an average of 64 days a year between 1987 and 1989 (Lagarias and Sylte, 1991). Nationwide, this number of violations is second only to the South Coast Air Basin of California. In addition, three of the counties within the San Joaquin Valley are consistently among the ten areas with highest ozone levels in the U.S. (Ranzieri and Thuillier, 1994). High ozone levels in many well studied metropolitan areas, such as the South Coast Air Basin of California, are primarily due to local emissions. However, in the primarily rural San Joaquin Valley a major question is to what extent episodes of poor air quality are due to local versus transported emissions.

The goal of this paper is to analyze the nature of the ozone problem in the San Joaquin Valley. To do so we employ the SARMAP Air Quality Model (SAQM), which was based on the Regional Acid Deposition Model (RADM) developed by Chang *et al.* (1987), and has undergone a number of improvements including an updated advection scheme and an updated chemical mechanism (DaMassa *et al.*, 1996). While our principal goal is to diagnose the sources and sinks of ozone in the San Joaquin Valley, we begin the paper with a brief description of the SAQM, including some new features that have been added to the original model.

In the next section the original model together with a new surface layer submodel will be presented and the model numerics will be discussed; in the third section the parallelization of the model to achieve computational efficiency will be addressed; and the fourth section will present an analysis of San Joaquin Valley air quality. For this study we consider the three day period, August 3 to 5, 1990, plus a spin-up period, starting on August 2 at noon GMT.

2.2 Model Description

The SARMAP Air Quality Model is designed to compute the concentrations of atmospheric trace species based on the numerical solution of the atmospheric diffusion equation in an Eulerian modeling framework. Mathematically, the dynamics of each species i are described by the following system of conservation equations (McRae *et al.*, 1982):

$$\frac{\partial c_i}{\partial t} + \nabla \cdot \mathbf{u} c_i = \nabla \cdot (\mathbf{K} \cdot \nabla c_i) + R_i(\mathbf{c}, T) + S_i(\mathbf{x}, t) + \frac{\partial c_i}{\partial t}|_{clouds}, \qquad (1)$$

where $c_i(\mathbf{x}, t)$ are the elements of the gas-phase species concentration vector $\mathbf{c}$, t is time, $\mathbf{x} = (x, y, z)$, $\mathbf{u} = (u, v, w)$ is the advective flow field, $\mathbf{K}$ is the eddy diffusivity tensor, R_i is the rate of chemical production and loss of species i, T is the temperature, and S_i is the volumetric source of i from emissions and deposition. The last term in Equation (1) accounts for cloud processes, which are not used in the simulations presented in this paper.

Many components of the model, including vertical diffusion and photolysis rates, are computed according to Chang *et al.* (1987). The dry deposition parameterization is based on Chang *et al.* (1987), but has been modified to account for land types that are present in the San Joaquin Valley (Hubbe and Pederson, 1994).

2.2.1 Spatial Resolution

The model domain is the San Joaquin Valley of California and the surrounding area. (**Figure 1**). The latitude and longitude of the west and east corners of the modeling domain are (34.54472,-122.89846) and (39.08257,-118.21475), respectively. The Valley runs from the northwest to the southeast, and is surrounded by the Coast Range on the west and the Sierra Nevada Range on the east. The domain is divided into a regular grid of approximately 12 × 12 km in the horizontal direction. Vertically, the SAQM originally used a 15-layer terrain following $\sigma-$coordinate system. The $\sigma-$coordinate system used is defined as follows:

$$\sigma = (p - p_{top})/(p_s - p_{top}) \qquad (2)$$

where p is the pressure at the level where σ is evaluated, p_s is the surface pressure, and p_{top} is the pressure at the top of the modeling region (10 kPa or

approximately 16 km for this application). A Surface Layer Submodel (SLS) (Chang *et al.*, 1996) has been added to the original SAQM. The SLS replaces the bottom layer of the original model with three layers, or two extra levels. **Table 1** shows the discretization of the original 16 level vertical grid together with the two additional SLS levels marked "a" and "b". Also in **Table 1** are the pressure and height corresponding to the sigma levels assuming a 1000 hPa surface and a standard atmosphere. The SLS has improved the emission resolution of the model by reducing the dilution of ground level emissions injected into the model. In addition, diagnostic tests have shown that the nighttime dry deposition has increased with the SLS, bringing model results closer to observations. All simulations described subsequently include the SLS.

2.2.2 Emissions

Hourly species emissions data are required for each grid cell. A list of chemical species tracked by the model is given in **Table 2**. The species accounted for in the emissions inventory are SO2, SULF, NO2, NO, ALD, HCHO, PAR, ETH, OLE, ISO, TOL, XYL, CO, and HONO. The emissions inventory used to simulate the August 1990 episode was created using the SARMAP Emission Inventory Model (SEIM), also known as GEMAP (Geocoded Emissions Modeling and Projection) (Magliano, 1994). The baseline input data for GEMAP were obtained from the California Air Resources Board emission inventory section.

2.2.3 Meteorological Variables

Three-dimensional advective and temperature fields are provided as hourly input to Equation(1) from the SARMAP Meteorological Model (SMM), which is based on the mesoscale meteorological model, MM5 (Grell *et al.*, 1993), with only minor adjustments, primarily the domain of the model. The MM5 (or SMM) is capable of predicting the general northwesterly flow in the Valley, as well as the morning downslope and the afternoon upslope flows that are characteristic of the Valley in summertime (Seaman *et al.*, 1995). A typical daytime, low level wind flow pattern for the simulation period is shown in **Figure 2**. Here, relatively strong winds can be seen coming from the Pacific, through the San Francisco Bay area, and predominantly continuing to the

southeast in the Valley. Mountains that surround the Valley generally exhibit weaker, less uniform flow. Observations show that the nighttime conditions produce stronger downwind flow in the Valley. In addition, at sunrise a cyclonic circulation, known as the Fresno eddy, usually appears just south of Fresno (Roberts *et al.*, 1995).

2.2.4 Boundary and Initial Conditions

The horizontal boundary conditions used when solving Equation (1) are

$$u_i c_i - K_{ii} \frac{\partial c_i}{\partial x_i} = F_{b,i}. \tag{3}$$

The horizontal flux, $F_{b,i}$ of species i, at the boundary is computed as

$$F_{b,i} = V_p c_{b,i}, \tag{4}$$

where V_p is the normal wind component at the boundary, $c_{b,i}$ is the boundary concentration during inflow conditions, or the concentration next to the boundary during outflow conditions.

The vertical boundary conditions used when solving Equation (1) are

$$K_{zz} \frac{\partial c_i}{\partial \sigma} = v_{d,i} c_i \qquad \text{at} \qquad \sigma = 0.999 \tag{5}$$

$$K_{zz} \frac{\partial c_i}{\partial \sigma} = 0 \qquad \text{at} \qquad \sigma = 0.05 \tag{6}$$

where $v_{d,i}$ is the deposition velocity of species i. Because of the no-flux condition at the top of the modeling region, predictions are insensitive to upper boundary conditions for species concentration.

Boundary conditions are used to calculate the horizontal flux as described in Equation (4). The boundary concentrations used are time and space independent. Raw data to compute the boundary conditions were obtained from SARMAP field measurements (Blumenthal, 1993). **Table 3** shows the low level boundary concentrations that were used for simulations presented here. The use of an alternate set of boundary conditions, with reduced concentrations of volatile organic compounds, did not produce significantly different predictions from the use of the listed boundary concentrations.

Initial conditions used when solving Equation (1) are obtained from available measurements of vertical profiles of the stable species. Short-lived (free radical) species are initialized to zero since the photochemistry will generate a concentration for each of those species consistent with all other species in a short time. Initialization of the simulation is performed by running the model for 48 hours, repeating the same day twice. The resulting concentration field is then used as the initial conditions for the simulation.

2.2.5 Chemistry

Solution of the chemistry operator when solving Equation (1) accounts for chemical transformations within a given cell. The generic differential equation of chemical kinetics for each species i as included in the SAQM is expressed in the form

$$R_i(\mathrm{c}, T) = \frac{\partial c_i}{\partial t} = P_i - L_i = P_i - c_i/\tau_i \tag{7}$$

where P_i and L_i are the production and loss rates of species i. τ_i is the characteristic time scale for the first-order chemical loss.

The version of SAQM employed here uses the Carbon Bond Mechanism, version 4 (CBM4), which consists of 29 differential species (as shown in **Table 2**) in 83 reactions (Gery *et al.*, 1989). Other versions of SAQM use the Statewide Air Pollution Research Center (SAPRC) mechanism (Lurmann *et al.*, 1991).

2.2.6 Numerical Implementation

The temporal approximation of Equation (1) is obtained from the solution of the operator splitting sequence:

$$\mathrm{c}^{t+2\Delta t} = \mathcal{L}_x^{\Delta t}\mathcal{L}_y^{\Delta t}\mathcal{L}_z^{\Delta t}\mathcal{L}_c^{2\Delta t}\mathcal{L}_{cl}^{2\Delta t}\mathcal{L}_z^{\Delta t}\mathcal{L}_y^{\Delta t}\mathcal{L}_x^{\Delta t}\mathrm{c}^t. \tag{8}$$

The time discretization used in this version of SAQM is comprised of a basic time step of 5 minutes for each operator, however each operator has control of its internal time discretization. The time step used by the advection, diffusion, and dry deposition calculations is typically half of the basic operator time step. Furthermore, the time step used in the chemistry operator is significantly smaller and highly dependent on the degree of stiffness of the

ordinary differential equations that describe the chemistry. Periods of sunset and sunrise present the highest degree of stiffness, when rapid changes occur in the concentrations of photochemically driven species.

2.2.7 Horizontal Advection

The solution of the advection operator when solving Equation (1) accounts for the transport of species under a given wind field. The two-dimensional advection equation is

$$\frac{\partial C}{\partial t} + \frac{\partial (uC)}{\partial x} + \frac{\partial (vC)}{\partial y} = 0. \tag{9}$$

Problems of numerical diffusion, peak concentration resolution, and spurious oscillations arise in the numerical solution of Equation (9) as both the amplitude and phase of different Fourier components of the solution tend to be altered by numerical schemes. Consequently, the main difficulty encountered in the solution of the advection operator is that of accuracy.

The horizontal advection operator of the SAQM is solved using ADI techniques (Yanenko, 1971), that is, decomposing the two dimensional problem described by Equation (9) by the successive solution of the x and y components

The BOTT method (Bott, 1989ab) develops further the polynomial fitting techniques proposed initially by Crowley (1968). The idea behind the solver is to approximate the concentration field by a fourth-order polynomial, guided by the curvature and magnitude of the concentration field. Fluxes are evaluated followed by their weighting and limitation to achieve positive definiteness and phase and amplitude error reduction.

2.2.8 Evaluation of the Model

We have assessed the ability of this version of SAQM to reproduce the observed ozone concentrations. A summary of the statistical evaluation of model performance for baseline conditions is presented in **Table 4**. Paired peak prediction accuracy, A_{ts}, is a stringent measure of the model's ability to reproduce a peak concentration at the same time and location as the observed

peak. It is computed as

$$A_{ts} = \frac{c_p(\widehat{x}, \widehat{t}) - c_o(\widehat{x}, \widehat{t})}{c_o(\widehat{x}, \widehat{t})} \cdot 100\% \tag{10}$$

where c_p is the predicted one-hour concentration, c_o is the observed hourly averaged concentration, $\widehat{x}$ is the monitoring station location of the peak concentration, and $\widehat{t}$ is the time of occurrence of the peak observation (Tesche *et al.*, 1990). The value given in **Table 4** is an average over all sites and over the three-day simulation.

The mean gross error is a measure of the differences between observed and predicted values over all times. It is computed as

$$E_d = \frac{1}{N} \sum_{i=1}^{N} \left| c_p(x_i, t) - c_o(x_i, t) \right| \tag{11}$$

where N is the number of observations from all sites for a particular day. In **Table 4**, this value is displayed first based on only ozone mixing ratios exceeding 40 ppb in the calculation, and then using a cutoff mixing ratio value of 1 ppb.

The version of SAQM with the SLS performs well within the statistical bounds of other urban/regional ozone simulations in reproducing peak values, and clearly reduces the paired peak error over the SAQM without the SLS. This improvement in predicting peak values is due to the reduced dilution of emissions with the SLS. Furthermore, an improvement in nighttime values with the SLS is seen in the mean gross error. When low nighttime values of less than 40 ppb are excluded from the statistic, the improvement due to the SLS is approximately 1 ppb. However, when values are considered as low as 1 ppb, the improvement is 5 times greater. The improved dry deposition with the SLS is the source of this reduction in error.

2.3 Aspects of the Parallelization of the Model

Parallelization is a tool that can reduce the computational time needed for implementation, thereby allowing further advancements in model physics that would have otherwise been too computationally intensive to perform (Dabdub and Seinfeld, 1996).

A profile of the code is shown in **Table 5**, indicating that the single most computationally intensive task in the SAQM is the solution of the chemistry operator. Numerically, this is equivalent to the the integration of a system of stiff ordinary differential equations (Equation 7). Simple stiff solvers would require extremely small steps to advance the solution of Equation (7) to maintain stability. Some general purpose solvers that implement variable order schemes require the computation of the Jacobian of the system. This would require a set of algebraic equations to be solved at each time step, which is a relatively time-consuming operation. Consequently, one of the main problems encountered in the solution of the chemistry operator is that of speed. Furthermore, the chemistry operation is dependent only on local data. That is, the predicted concentration after a chemistry step is dependent on the concentration of other species that are located in the same grid cell. Both observations suggest that an initial attempt to parallelize the code should focus on distributing the chemistry integration of all the grid cells equally among all the processors.

The computing paradigm used to implement the parallelization strategy described below is host/slave. The role of the host is to perform the I/O, to solve the horizontal and vertical transport operators, and to manage the data distribution used by the slaves. The role of the slaves is to receive the input data from the host, and to perform the computationally intensive work of solving the system of nonlinear ODEs from the chemistry operator. The communication channels required for this approach are only between the host and each slave. There is no inter-node communication needed to parallelize the chemistry operator. A parallel version of the code was developed to run on a network of IBM RISC 6000/390 workstations, networked using CDDI to form a distributed memory MIMD (multiple instruction/multiple data) computing platform. Message passing was performed using the P4 libraries and FORTRAN. **Figure 3** shows the time to perform a 24-hour simulation for the San Joaquin Valley using the SAQM. The theoretical curve plotted in **Figure 3** represents Amdahl's law, which shows the best possible time that can be obtained implementing the chemistry only in parallel,

$$S = \frac{1}{(1-P) + P/N} \tag{12}$$

where S is the ideal speed-up, N the number of processors, and P the fraction of the code that is implemented in parallel. The theoretical time is the best possible time as it assumes that all communications between the host and nodes are instantaneous. In practice, however, communication costs are sig-

nificant. In **Figure 3**, the difference in time between the sequential code and the parallel version using 1 processor shows the time cost of all model communication. A significant portion in the data flow is a result of double-precision arithmetic, which is used in all SAQM computations.

Use of a faster network would substantially increase the performance of the parallel implementation. However, higher performance could also be achieved by implementing the solution of the vertical and horizontal transport operators in parallel. **Figure 4** shows a comparison of the theoretical times obtained by implementing the horizontal and vertical operators of the model in parallel, which is equivalent to increasing the value of P in Equation 12. Notice that the impact of perturbing P on the performance of code is proportional to the value of P before the perturbation.

In brief, parallelization of the chemistry operator of atmospheric dynamical models is a relatively simple task, not involving any communication among the slave nodes. Parallel implementation of the chemistry, as described above, is independent of the numerical scheme and photochemical mechanism used.

2.4 Diagnosis of Ozone in the San Joaquin Valley

Diagnostic runs were performed using SAQM to study the major sources and sinks of ozone in the San Joaquin Valley. We focus on three sites that are representative of those in the Valley: Arvin, Fresno, and Livermore (see **Figure 1**). Arvin is a small farming town in the southeast corner of the region; Fresno is a city with a population of approximately 350,000 in the middle of the Valley; Livermore is a suburban city immediately east of the San Francisco Bay area and also near the influx boundary of the model. These three sites represent different types of locations and population densities, providing a reasonable spectrum of both air quality and model performance. Edison (**Figure 1**) is another location of interest in the San Joaquin Valley due to the high ozone concentrations observed there. Generally ozone in Edison behaves similarly to that in Arvin. There is a, however, single exception which will be discussed in Section 4.2.

2.4.1 Base Case

There are several key aspects of the dynamics of air pollution in the San Joaquin Valley that are illustrated by the base case. Over the three-day simulation, highest ozone levels were consistently found in four distinct areas: near the outflow of San Francisco, in the southern portion of the Valley, downwind from Fresno, and in the vicinity of Sacramento. In these locations it was not uncommon for the simulated ozone mixing ratio to exceed 140 ppb during the modeling period. San Francisco itself exhibited relatively clean air even though it contains some of the highest emissions in the modeling domain. It is observed from the base case simulation that local emissions from San Francisco are transported downwind in the Valley. Throughout the Valley the maximum ozone concentration occurs around 4 pm, while the minimum values vary in their time of occurence, generally between 4 am and 8 am.

Figure 5 shows both the observed (dotted) and the base case model predictions (solid) of ozone mixing ratio for the three-day period of the simulation. From observations we see that the average ozone mixing ratio in Arvin is greater than that of Fresno or Livermore. This is especially noticeable at night, when the ozone concentration in Arvin rarely decreases below 50 ppb.

Here we also examine the discrepancies that exist between predictions and observations. They include the predicted ozone mixing ratio dropping too early in the evening in Fresno and ozone values in Livermore that are consistently too high during the first two days of the period. To do so, we will examine the nature of the ozone problem in the San Joaquin Valley using several diagnostic runs of the SAQM. In all the following cases, perturbations to the model were implemented from the beginning of the spin-up period (noon GMT on August 2, 1990). Results will be presented as ozone mixing ratio beginning August 3 at the lowest vertical level of the model.

2.4.2 Three-Dimensional Wind Effect

The topography of the San Joaquin Valley produces an advective flow that varies throughout the Valley. The wind in Livermore, which is near the primary inflow into the Valley, is generally from west to east, and rarely falls below 3 m/s. The strongest winds in Livermore occur around midnight, at an average speed of over 6 m/s. Arvin, which is located at the end of

the Valley, has a more varied wind field. The strongest winds tend to be in the late evening, and are from the southwest. At other times of the day the wind is from the northwest (early morning), or from the east (late morning). Fresno is slightly east of the main down-valley flow. In Fresno, a maximum average wind of over 6 m/s occurs around 4 am, blowing primarily eastward. The winds reach a minimum speed in the evening, followed by a few hours of north-eastward winds.

In order to understand the effects of the advective flow on the pollutant distribution in the Valley, we have altered the meteorological inputs to SAQM. We will discuss a simulation in which the three-dimensional advective wind field and horizontal diffusion have been set to constant zero values. If the ozone concentration increases at a site under such a condition, it can be assumed that there is a significant dependence on emissions from that site, and will therefore indicate if the sources of ozone are local or non-local.

Figure 6 shows ozone levels under completely calm conditions. In Arvin there is a small, but rapid, increase in ozone mixing ratio at approximately 8:00 every morning, and a small, but rapid, decrease around 8:00 every evening. After each of these changes, the ozone level remains relatively constant for 12 hours. This indicates that the NO_x level in Arvin remains at a somewhat uniform level over the three day run. At sunrise the available NO_2 creates ozone and after that point the ozone mixing ratio is essentially unchanged. Likewise, in the evening, after the available NO acts as an ozone sink, there is little variation in the ozone concentration. It can also be seen that in this simulation the nighttime ozone values are higher than the base case. This is due to the small amounts of NO_x present in this rural town. There is little NO_2 to create ozone in the morning, and little NO to remove ozone in the evening. Both of these features suggest that there is a significant amount of NO_x transported to Arvin under base case wind conditions. Under such conditions the primary source of NO_x to Arvin is from locations upwind in the Valley, however, little NO_x from the San Francisco Bay area reaches Arvin (San Joaquin Valley Air Quality Study Policy Committee, 1996).

In the simulation with no wind, both Fresno and Livermore show an increase in ozone mixing ratio from 8 am to 8 pm. The area with the highest increase in ozone mixing ratio in the modeling domain is the San Francisco Bay Area (not shown), where peak ozone values tripled in comparison with the base case. This indicates that these sites have sufficient local sources to accumulate local emissions throughout the day when there are no winds. In

addition, these sites are predicted to exhibit daytime peaks higher than the base case when no winds are present, implying that emissions from these sites are transported downwind into the Valley under base case wind conditions.

The response of Edison to the case with no wind is similar to that of Fresno, with daytime values increasing by 25% and nighttime values increasing by as much as 75%. This is the one case where the dynamics of ozone in Edison do not behave similarly to Arvin, which is due to Edison's close proximity to large emission sources.

2.4.3 Boundary Condition Effect

In order to study the effects of the boundary air on the San Joaquin Valley, simulations were performed in which the boundary conditions were altered. In the first case all boundary conditions were set to zero. Comparison between the base case and that of zero boundary conditions demonstrates the effect of boundary transport on ozone concentrations. One would expect the largest differences in sites near the boundary where the air is advected into the region. Further simulations were made in which a subset of the boundary conditions were set to zero in order to test the sensitivity to specific components.

A large difference between the base case, and that with zero boundary conditions can be seen in Livermore (**Figure** 7), where ozone nearly vanishes when the boundary conditions are set to zero. Most sites in the northwest corner of the modeling region show a similar response to zero boundary conditions. Note that this is not a result of low emissions in Livermore, as it was determined previously that Livermore's ozone concentration is reasonably dependent on local emissions. However, there is a substantial dependence on boundary conditions because of Livermore's proximity to the region boundary where there is a large influx of material. In particular, a constant influx of 40 ppb of ozone from the boundary can generally be seen in Livermore.

Fresno also exhibits a notable decrease in ozone concentrations with zero boundary conditions. However, as expected, this decrease is smaller than that in Livermore, as Fresno is farther from the model boundary than Livermore.

Arvin, being the farthest from the influx model boundary, shows almost no sensitivity to the change in boundary conditions on the first day of the simulation. It takes approximately 24 hours for boundary air to be advected

to Arvin.

An overall evaluation of the effects of zero boundary conditions on ozone predictions is shown in **Figure 8**, which is the integrated total mass of ozone for the base case and that with zero boundary conditions. The rapid decrease in ozone mass over time when the boundary conditions are set to zero points clearly to the significant effect exerted by the boundary conditions on predicted ozone in the San Joaquin Valley.

To further test the sensitivity of ozone predictions to boundary conditions, diagnostic runs were made in which a subset of the boundary species concentrations were altered. While changes in many of the boundary concentrations produced differences of less than 5% in the model output, a case where only ozone was set to zero resulted in larger changes (**Figure 9**). Both Arvin and Fresno experienced reductions of 5% to 10% in ozone concentrations from the removal of ozone at the boundary. Livermore, on the other hand, experienced an ozone loss of approximately 50%. Furthermore, it can be seen that the sole source of nighttime ozone in Livermore is from advection into the region from the boundary.

Much of the sensitivity to the boundary conditions can be explained by the inherent meteorology of the area. Because of relatively brisk winds that blow from the Pacific, any species advected from the boundary has an impact on the San Joaquin Valley. For example, the estimated mixing ratio of NO_x at the boundary is 3 ppb, and emissions from certain locations can lead to local levels exceeding 100 ppb. Even so, under baseline conditions for this episode the total mass of NO_x in the Valley that originates from the boundary is four times that emitted in the Valley itself. This is significantly different from many other areas, such as the South Coast Air Basin of California, which experience weaker winds and higher emissions.

2.4.4 Emission Effect

In order to study the effects of emissions in the Valley, a simulation was performed in which all of the emissions in the modeling domain were eliminated. With zero emissions one would expect concentrations to approach a level determined strictly by inflow conditions. In Arvin the zero emissions run leads to a reduction by more than 50% in maximum daytime ozone concentration (**Figure 10**). The comparison of **Figures 10 and 7** (the case with zero

boundary conditions) gives insight into the sources of ozone in Arvin. **Figure 10** shows that the background ozone mixing ratio of approximately 50 ppb is the result of the boundary conditions, while **Figure 7** shows the daytime peaks are due to emissions transported from locations farther upwind in the Valley.

Fresno also shows a greatly decreased daytime ozone peak under zero emissions, partially a result of eliminated local emissions, and partially due to the removal of influx emissions. A point of interest in Fresno is an increase in nighttime ozone when there are no emissions. This occurs in many populated areas of the Valley. In the populated areas when emissions are present, NO provides a significant sink for ozone at night. With the decreased level of NO in the zero emissions case, nighttime ozone can accumulate.

Changes in Livermore ozone from zero emissions are strikingly small, with only slightly lower daytime peaks, and slightly higher nighttime lows. This, together with the zero boundary condition diagnostics suggest that the majority of ozone in Livermore is predicted to originate from the upwind regions, while only a small fraction is the result of local emissions.

2.4.5 Dry Deposition Effect

A simulation in which the dry deposition for all species is set to zero allows one to determine the influence of dry deposition on predicted species levels. Relative to the base case, an airmass with zero dry deposition will have a progressively higher concentration of species as it moves downwind. It is therefore expected that sites that are farthest downwind will be most sensitive to perturbations of deposition velocities. This behavior can be seen in **Figure 11**. Although there is a general increase in ozone concentration everywhere in the Valley, the sensitivity of Livermore ozone to zero dry deposition is significantly smaller than that of Arvin or Fresno, which are farther downwind. Increase of ozone with zero dry deposition is also a result of higher levels of NO_x, but this effect is significantly smaller than the direct loss of ozone itself by dry deposition.

One can also see that the greatest sensitivity to dry deposition in Arvin and Fresno is at nighttime, as is the case in most areas of the Valley. This demonstrates that dry deposition represents an important nighttime ozone sink in the San Joaquin Valley. The increased rate of deposition at night

is likely a result of the increased nighttime wind speed, as wind speed and deposition rate are generally correlated. As mentioned earlier, NO is also a major nighttime ozone sink in the more populated areas of the valley. This explains the low nighttime ozone levels in Fresno, where both sinks are significant.

2.4.6 Initial Condition Effect

Comparison of zero initial conditions predictions with those of the base case reveal the significance of the initial state of the model. The closer the predictions of the zero initial conditions run are to those of the base case, the greater the effect of emissions or boundary conditions during the episode. One would expect little residual effects from the initial conditions when the modeling domain is sufficiently flushed out towards the end of the period. In Livermore, Fresno and most sites in the Valley, essentially identical predictions result from the base case and the zero initial condition case after the spin-up time. The only exceptions are Arvin and other sites in the southeastern portion of the Valley, which become identical to the base case after an additional 24 hours.

2.5 Conclusion

Several aspects of the dynamics of air quality in the San Joaquin Valley of central California have been revealed from systematic diagnostic runs of the SARMAP Air Quality Model. Air quality in the San Joaquin Valley contains a complex combination of local and transported emissions.

Relatively high winds through the San Francisco area and the inflow to the Valley impose a strong dependence of local ozone concentrations in Valley locations near inflow regions on imported levels of ozone and precursors. Without any emissions in the modeling region, the boundary conditions produce a relatively constant ozone mixing ratio of approximately 50 ppb in most places in the Valley. Local emissions are then primarily responsible for daytime peaks in ozone.

Specific balances between boundary concentrations and local emissions vary within the Valley according to location and population density. Not

surprisingly, ozone sources in rural sites, such as Arvin, have little dependence on emissions from that site, while ozone sources in larger cities, such as Fresno, are dependent on both local and non-local emissions. Effects of boundary conditions are greater near the inflow to the Valley, and weaker at the end of the Valley.

Ozone sinks are also varied throughout the Valley. In areas with a higher population density NO is usually the major nighttime ozone sink. For downwind sites in the Valley, especially sites away from major cities, dry deposition is the major nighttime ozone sink.

Table 2.1: Discretization of the grid using σ-coordinates.

Level Index	σ-Index	Standard Pressure (hPa)	Standard Height (m)
15	0.000	100	16170
14	0.156	240	10540
13	0.326	393	7210
12	0.464	518	5210
11	0.600	640	3610
10	0.740	766	2190
9	0.814	833	1510
8	0.866	879	1070
7	0.902	912	770
6	0.918	926	640
5	0.934	941	510
4	0.950	955	390
3	0.966	969	260
2	0.980	982	150
1	0.992	993	60
b	0.996	996	30
a	0.9985	999	10
0	1.000	1000	0

Table 2.2: Differential species defined in the chemical mechanism.

Species code	Species name	Species code	Species name
SO2	Sulfur dioxide	SULF	Sulfuric acid
NO2	Nitrogen dioxide	NO	Nitric oxide
O3	Ozone	HNO3	Nitric acid
H2O2	Hydrogen peroxide	ALD	Acetaldehyde
HCHO	Formaldehyde	OPEN	High MW aromatic
PAR	Paraffins	ETH	Ethane
OLE	Olefins	ISO	Isoprene
NH3	Ammonia	N2O5	Dinitrogen pentoxide
NO3	Nitrate radical	PAN	Peroxyacetylnitrate
TOL	Toluene	XYL	Xylene
CRES	Cresol	MGLY	Methylglyoxal
CO	Carbon monoxide	C2O3	Peroxyacyl radical
HONO	Nitrous acid	HNO4	Pernitric acid
CH4	Methane	HO	Hydroxyl radical
HO2	Hydroperoxyl radical		

Table 2.3: Boundary mixing ratios for the lowest level of the SAQM used in the August 3-5, 1990 episode.

Species code	Mixing Ratio (ppb)	Species code	Mixing Ratio (ppb)
SO2	10.0	SULF	0.1
NO2	2.5	NO	0.5
O3	40.0	HNO3	0.01
H2O2	0.01	ALD	1.52
HCHO	5.78	OPEN	0.01
PAR	41.1	ETH	1.4
OLE	0.828	ISO	0.1
NH3	0.1E-06	N2O5	0.1
NO3	0.1	PAN	0.1
TOL	0.492	XYL	0.27
CRES	0.1	MGLY	0.1
CO	200	C2O3	0.1E-06
HONO	0.1	HNO4	0.1
CH4	1700	HO	0.1E-06
HO2	0.1E-06		

Table 2.4: Measures of model error in ozone predictions.

	With SLS	Without SLS
Paired Peak Avg Error	14.13%	25.16%
Mean Gross Error (cutoff = 40 ppb)	18.24	19.34
Mean Gross Error (cutoff = 1 ppb)	20.18	25.21

Table 2.5: Summary of the SAQM computational profile for a base case episode.

Process	% of CPU time
Gas-phase chemistry	71.34
Vertical Advection & Diffusion	12.83
Horizontal Advection & Diffusion	8.74
Other	7.09

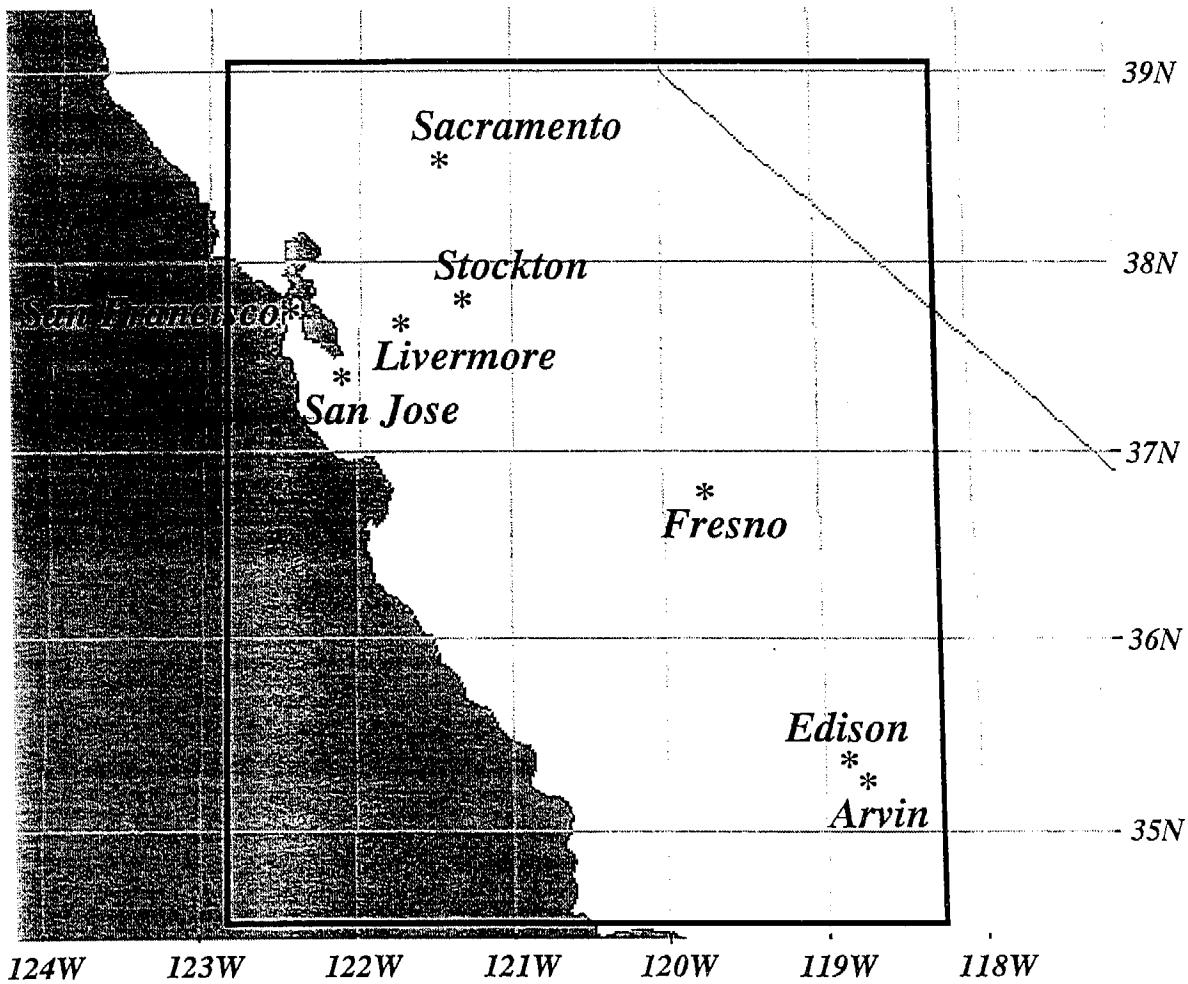

Figure 2-1. SAQM model domain.

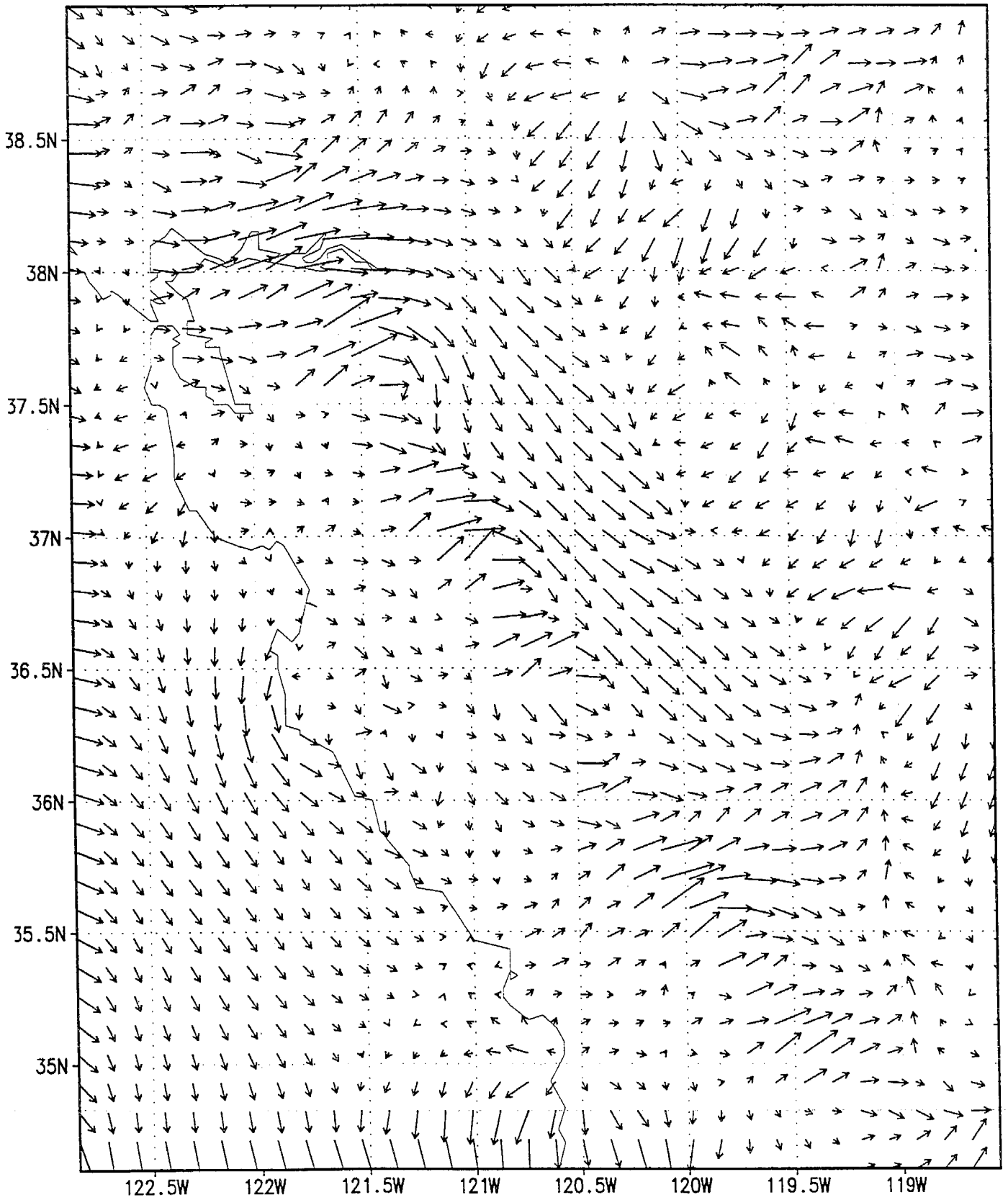

Figure 2-2. Low level MM5 wind field from noon August 4, 1990. 10 m/s

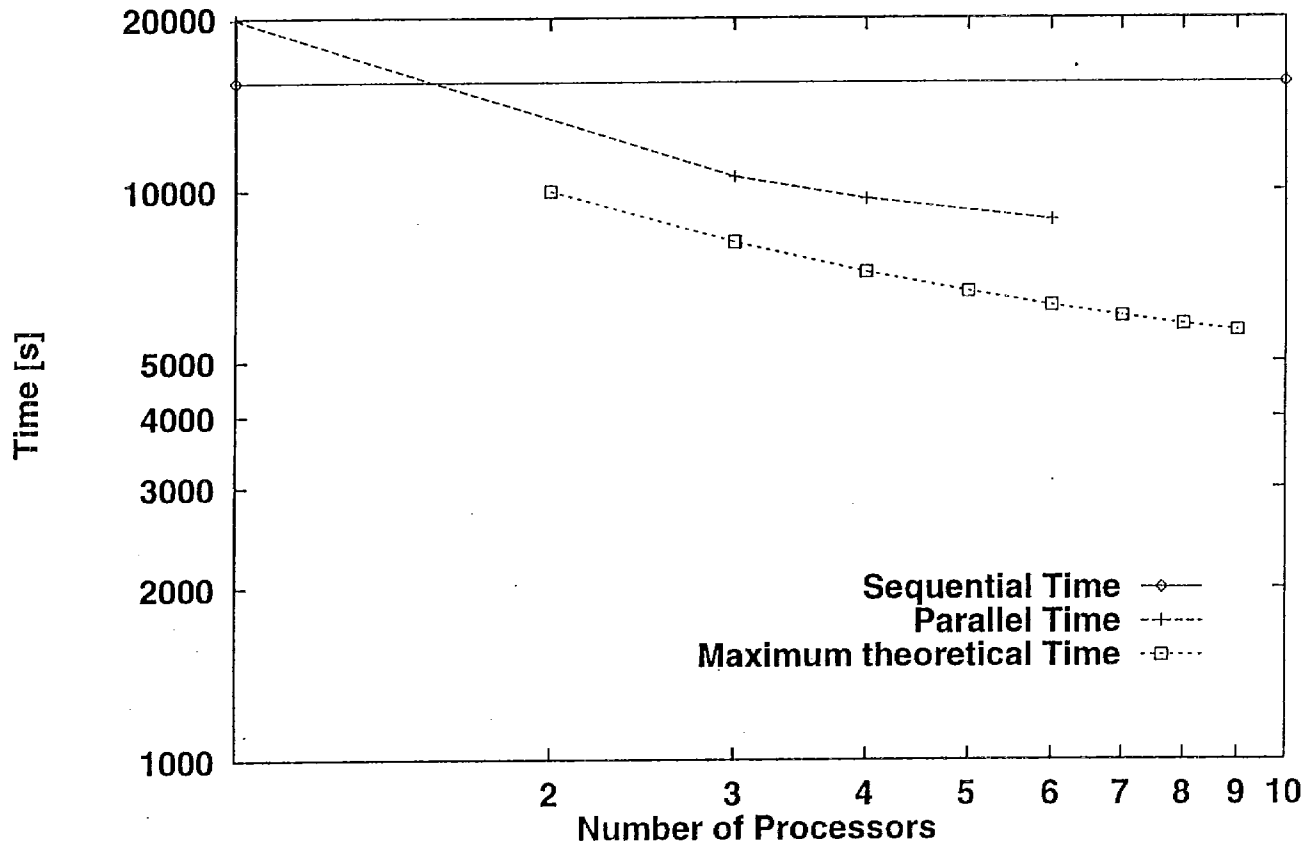

Figure 2-3. Execution time as a function of number of nodes when parallelizing the chemistry loop of the SAQM. Theoretical time presented is calculated from Amdahl's law. Time reported corresponds to a 24 hour standard simulation of the San Joaquin Valley of California.

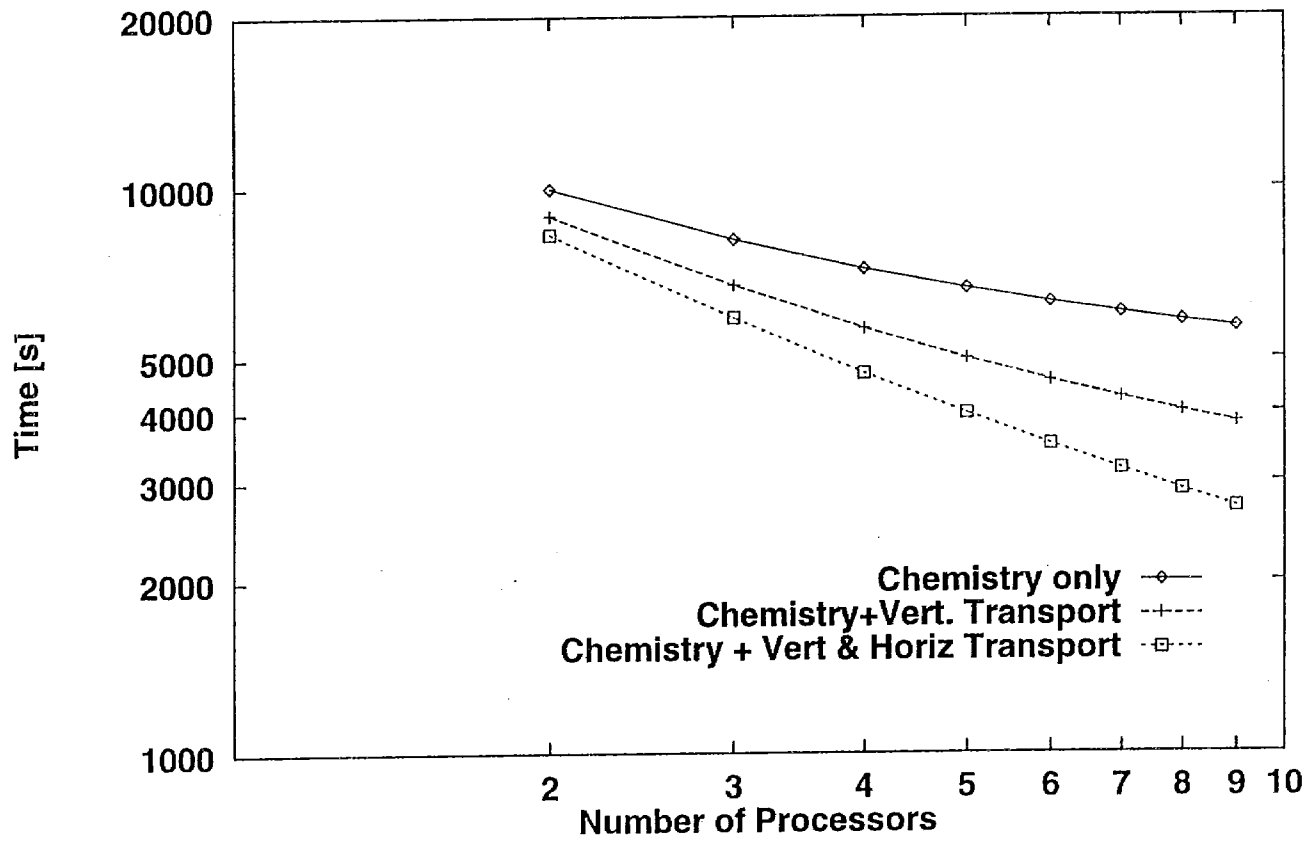

Figure 2-4. Execution time as a function of number of nodes when parallelizing various operators of the SAQM. Theoretical time presented is calculated from Amdahl's law. Time reported corresponds to a 24 hour standard simulation of the San Joaquin Valley of California.

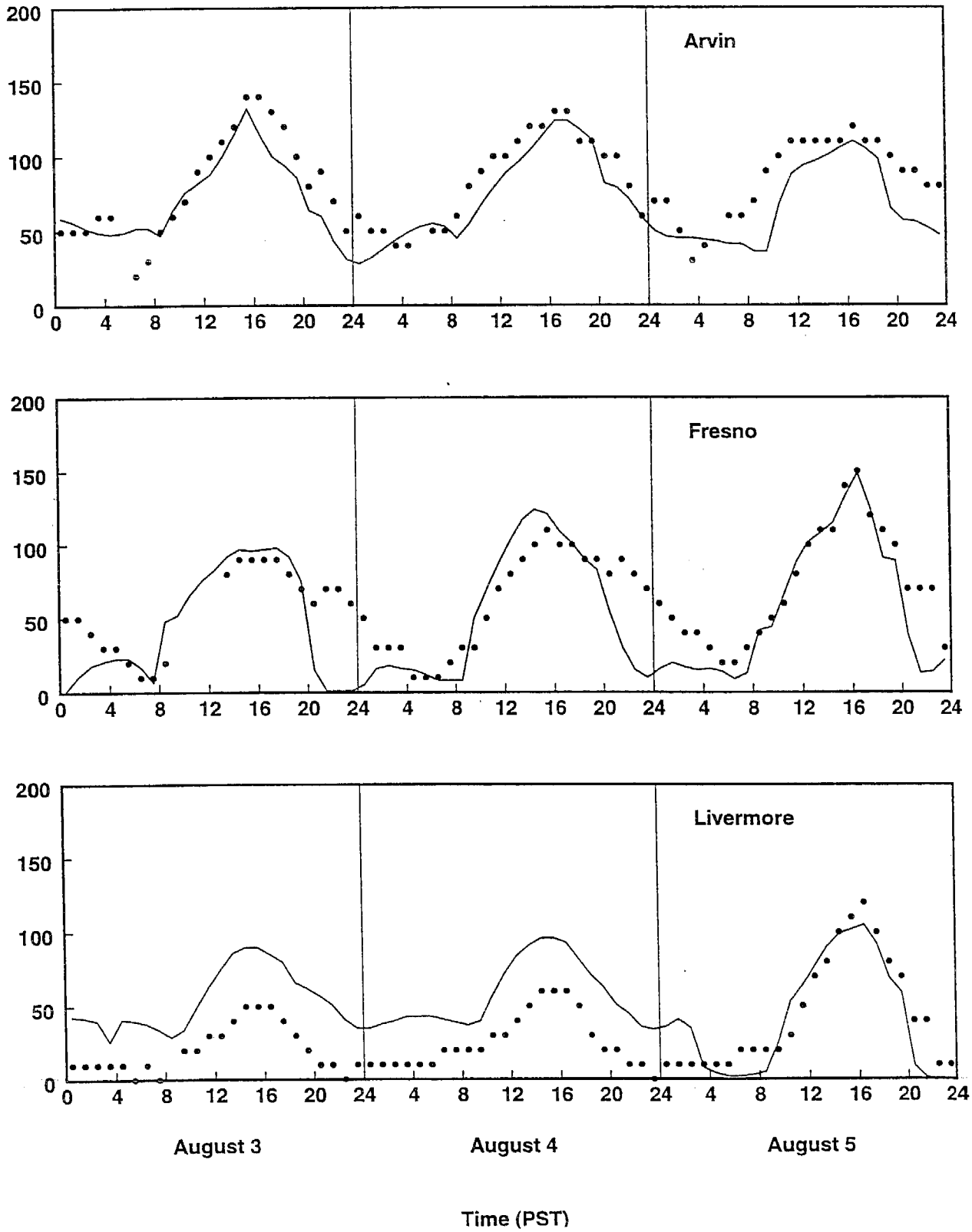

Figure 2-5. Ozone mixing ratio from observations (dotted) and model base case (solid).

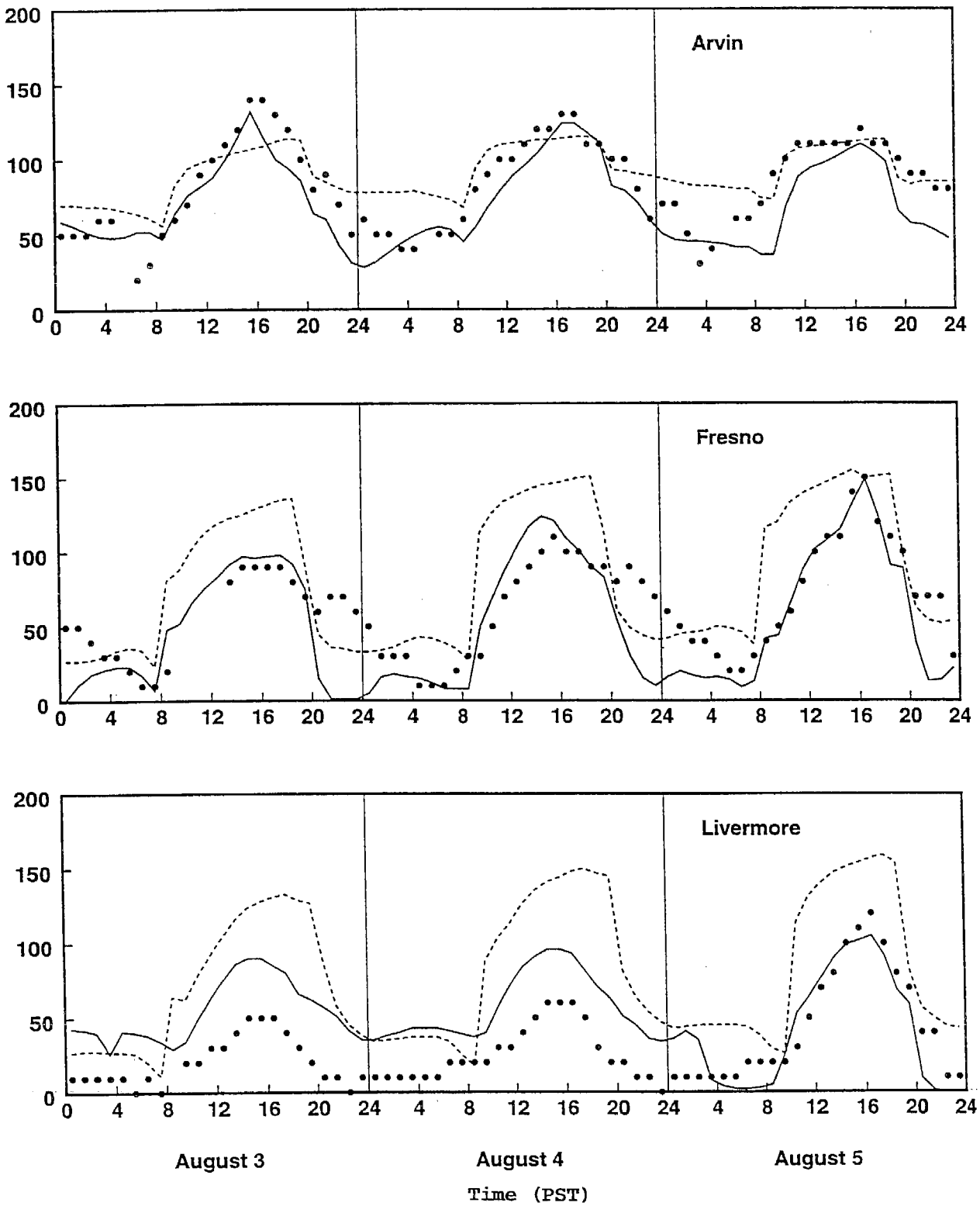

Figure 2-6. Ozone mixing ratio from observations (dotted), model base case (solid), and the model with zero wind (dashed).

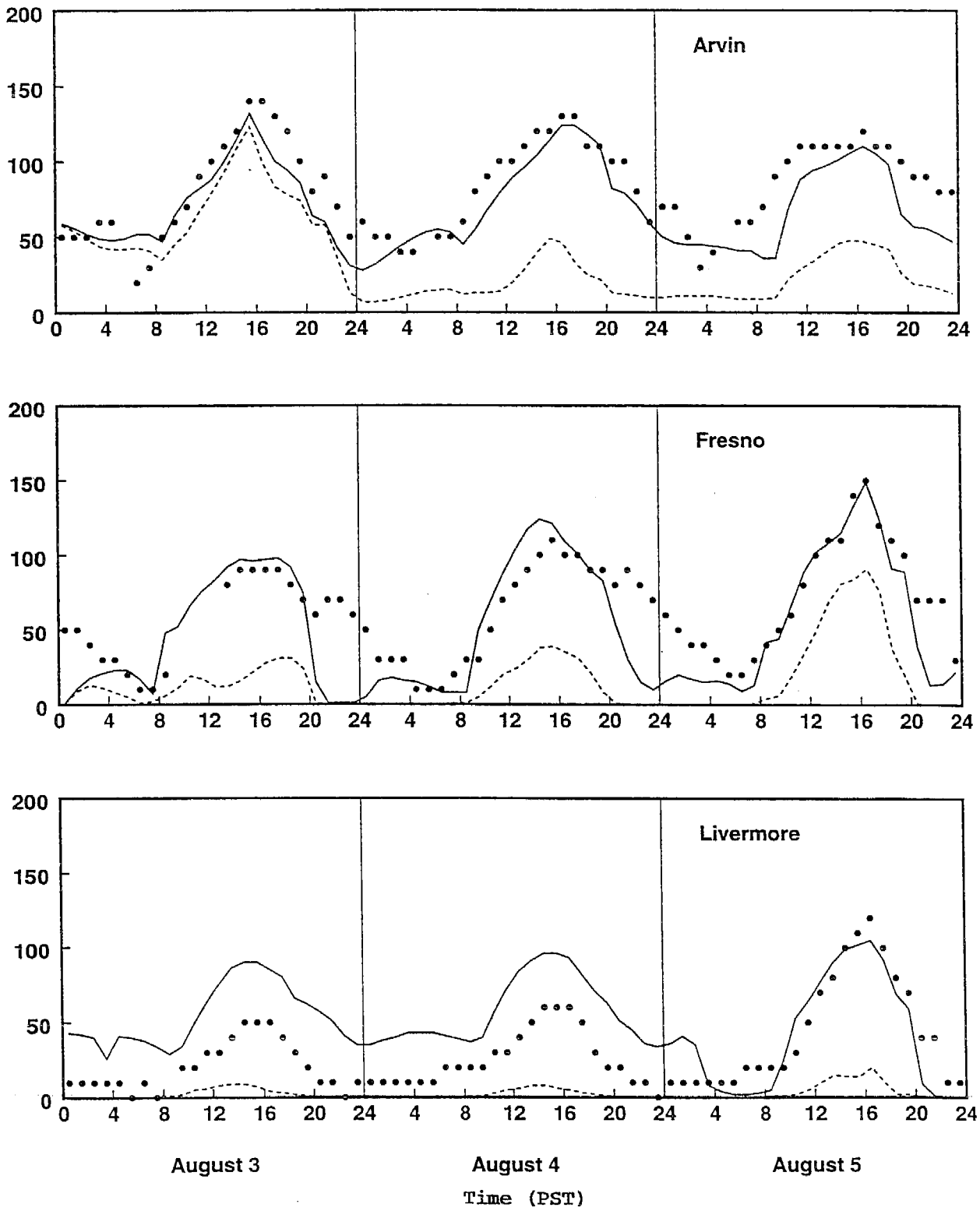

Figure 2-7. Ozone mixing ratio from observations (dotted), model base case (solid), and the model with zero boundary conditions (dashed).

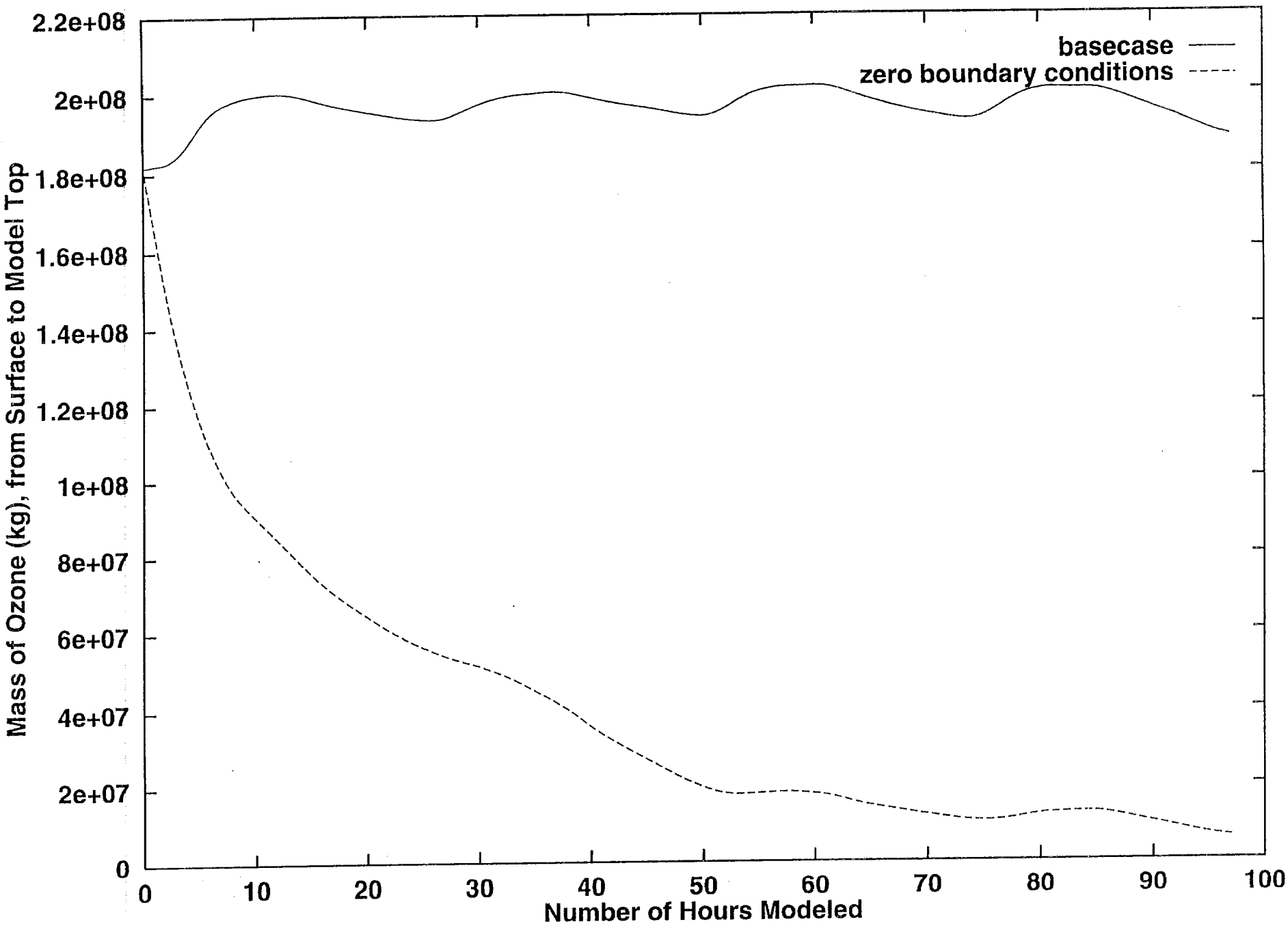

Figure 2-8. Vertically integrated, area average ozone mixing ratio from the model base case (solid), and the model with zero boundary conditions (dashed).

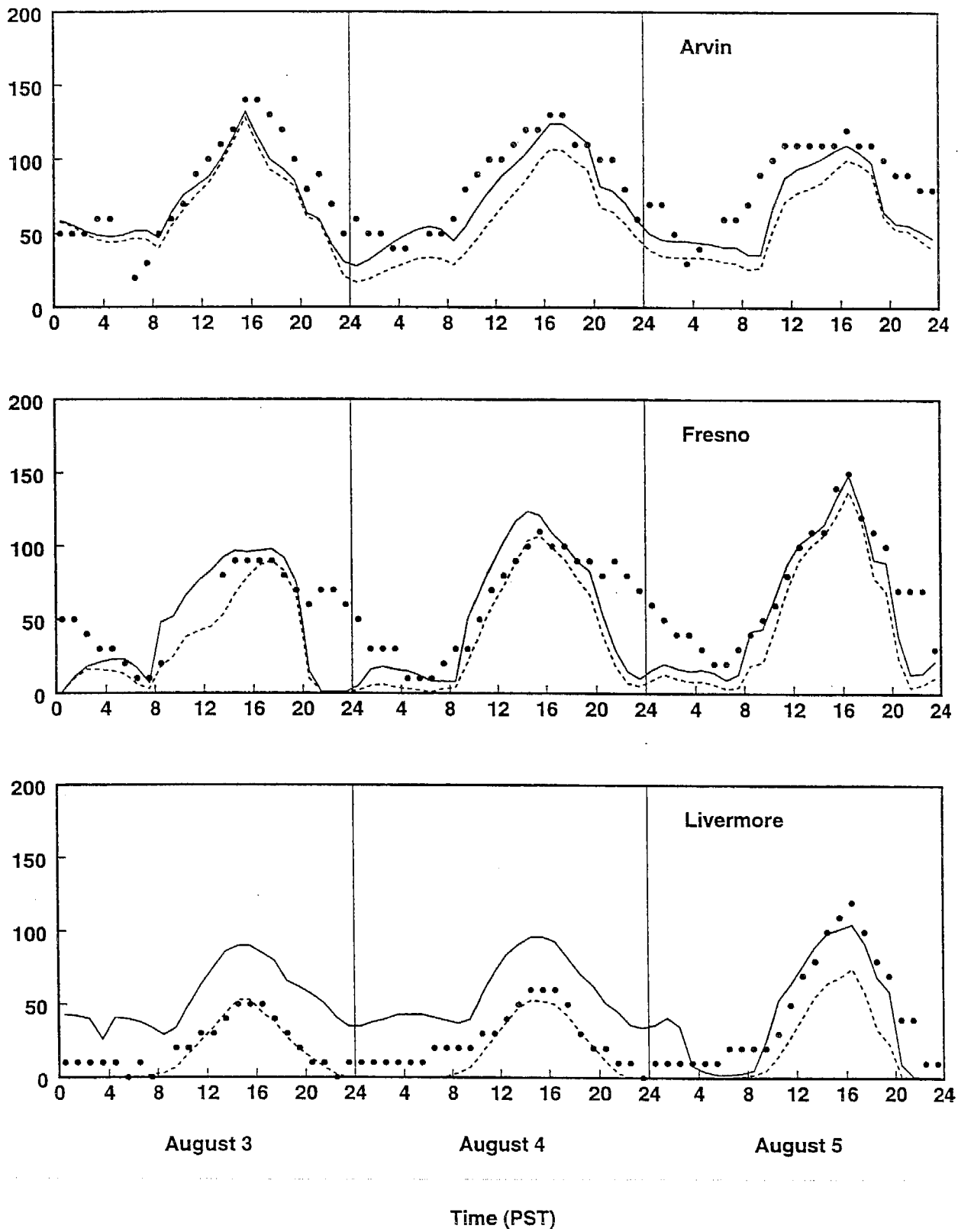

Figure 2-9. Ozone mixing ratio from observations (dotted), model base case (solid), and the model with zero ozone boundary conditions (dashed).

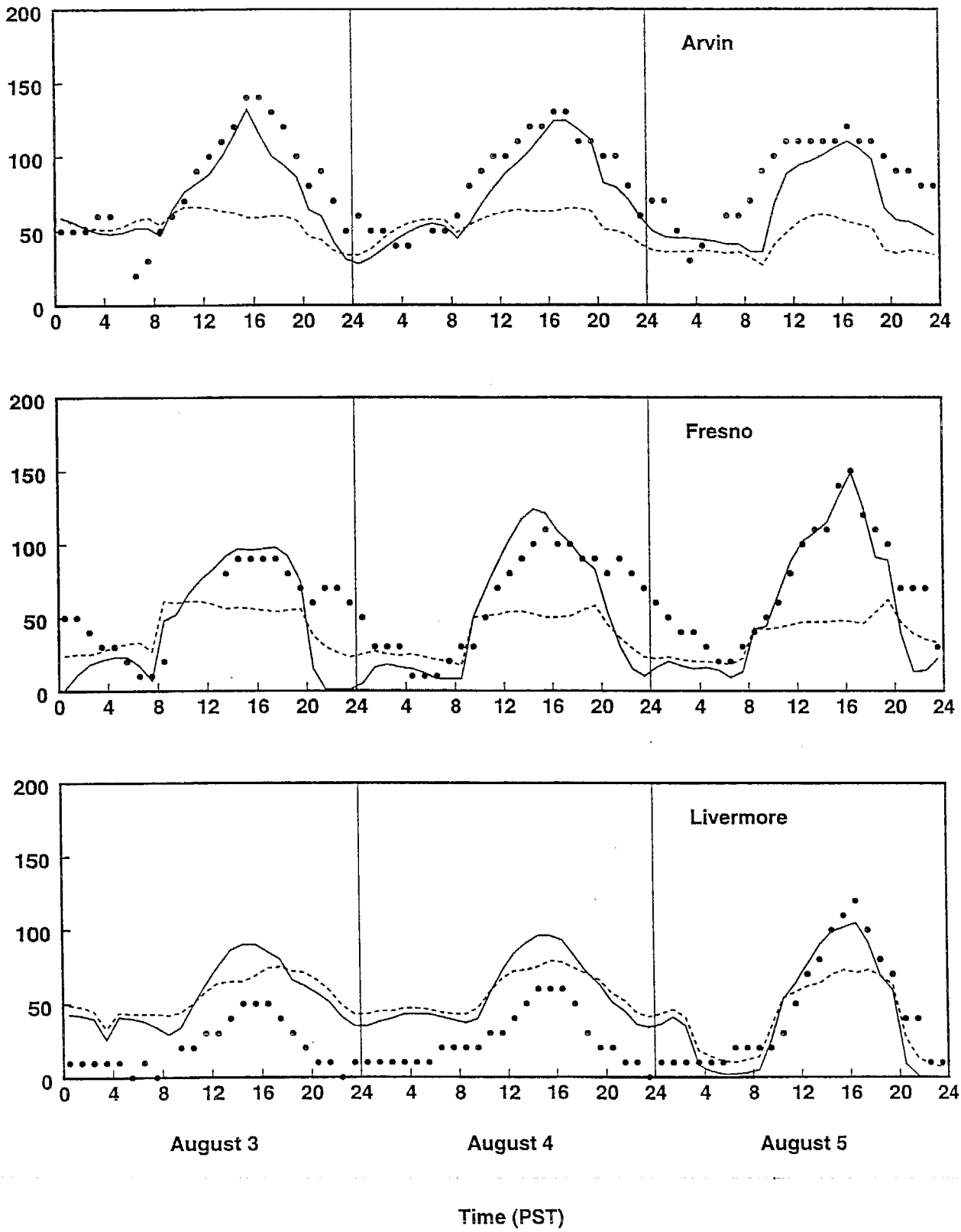

Figure 2-10. Ozone mixing ratio from observations (dotted), model base case (solid), and the model with zero emissions (dashed).

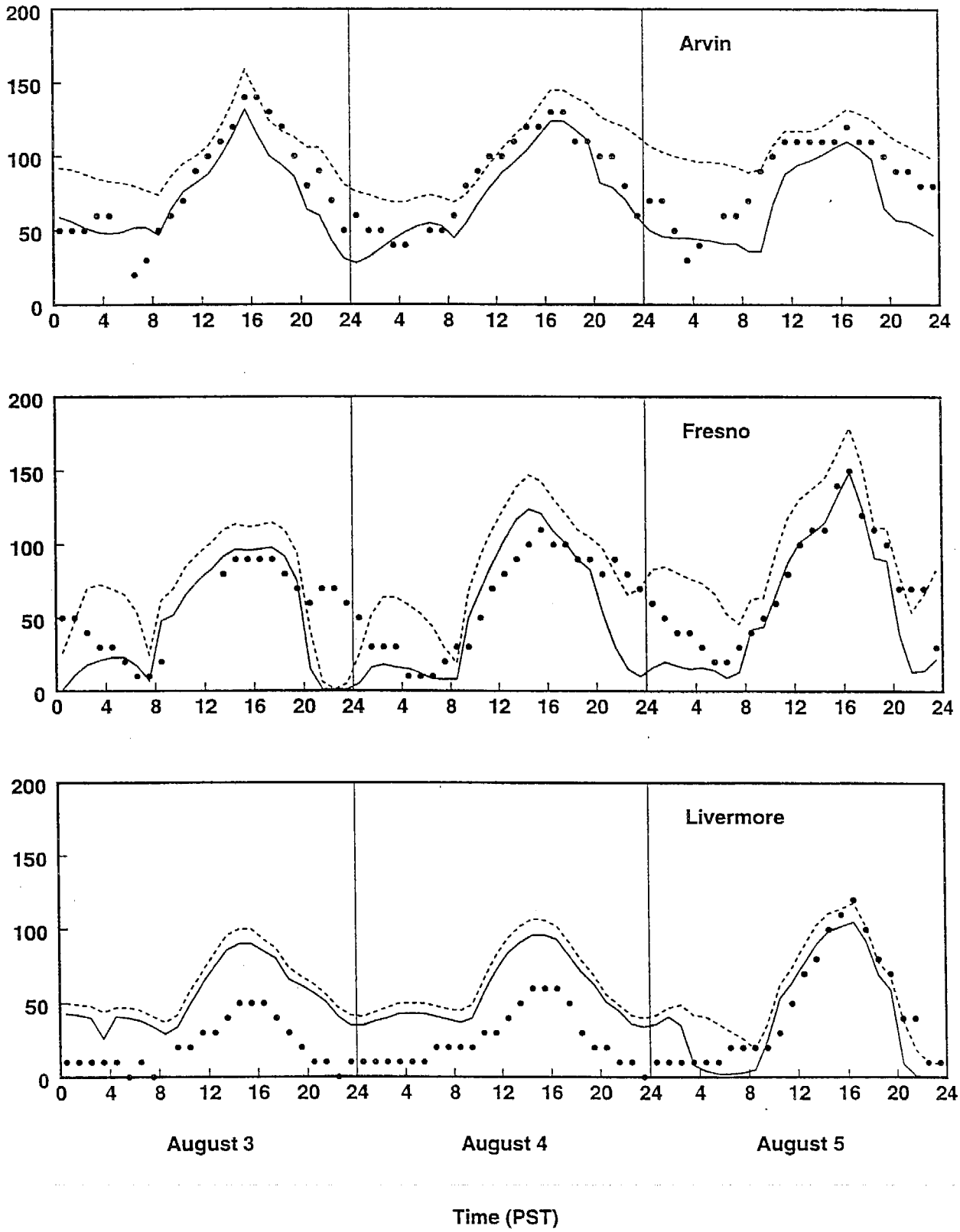

Figure 2-11. Ozone mixing ratio from observations (dotted), model base case (solid), and the model with zero deposition (dashed).

3. IMPLEMENTATION OF A NEW GAS-PHASE CHEMISTRY SOLVER

The photochemical mechanisms used in gridded air quality models include fairly detailed treatment of the inorganic reactions and fairly condensed representations of the organic reactions of importance in the atmospheric chemistry of the NO_x,/VOC/O_3,/SO_2/HNO_3 chemical system. Periodically, the photochemical mechanisms need to be updated to incorporate more recent chemical kinetic and mechanistic data. Likewise, there is a need to implement alternate chemical mechanisms to assess the sensitivity of model results to the choice of chemical mechanism. The original SARMAP air quality model (SAQM) was set up with the chemical mechanisms implemented in a "hardwired" fashion. Implementation of alternate chemical mechanisms in this format is time-consuming and prone to error because all of the reactions are hand-coded. Numerous modern air quality models (RPM, CAMx, UAM/FCM, etc.) have chemical compilers and flexible chemical mechanism interfaces to facilitate incorporation of the new reactions and/or alternate mechanisms. Hence, one of the objectives was to change the chemical mechanism interface so that the chemistry could more easily be updated.

Another objective was to evaluate the numerical methods used to integrate the gas-phase chemical kinetic rate equations. Integrating the system of 30 to 50 ordinary differential equations (ODEs) that describe the gas-phase chemistry takes a large amount of computer time. The chemical kinetic equations are complex, nonlinear, and numerically stiff. The most accurate method for solving stiff systems of ODEs is the Gear method (Gear, 1971; Hindmarsh, 1980). For gridded air quality models, where the equations need to be solved at thousands of grid points, the Gear method is inefficient and time consuming. Various fast chemical kinetic solvers have been developed for use in air quality models that are significantly faster than the Gear solver. The numerical method used in the SAQM is based on the algorithm used in the Regional and Acid Deposition Model (RADM) (Chang et al., 1987). In the last decade significant advancements have been made towards developing faster and more accurate numerical methods. Hence, it was desirable to replace the original SAQM solver with a new generation solver. Furthermore, the implementation of a more flexible chemical mechanism interface could be more readily accomplished if the model's numerical solver was more robust and required less mechanism-specific hardwired coding.

The remainder of this section presents a review of the SAQM's original chemical solver and a comparison of the SAQM's solver with a modern implicit-explicit hybrid (IEH) chemistry solver (Sun et al., 1994; Kumar et al., 1995). Based on the review, the IEH solver was implemented in the SAQM and tested against the original model. Its implementation in the SAQM is described in this section as well.

3.1 REVIEW OF THE SAQM CHEMICAL SOLVER

The SAQM primarily uses the Carbon Bond IV (CB-IV) chemical mechanism to simulate the chemical reactions in the atmosphere (Gery et al., 1988). The Statewide Air Pollution Research Center (SAPRC-90) chemical mechanism was also implemented into the

SAQM, however, it has received little use. In SAQM, the chemical rate equations are numerically integrated using the methods used by Hesstwedt et al. (1978) and Lamb (1982). The chemical rate equations are of the form:

$$\frac{\partial C_i}{\partial t} = a_i - b_i C_i \tag{3-1}$$

where C_i is the concentration of the species i, a_i is the production rate, and b_i is the loss rate of species i. For simplicity, the subscripts i will be omitted in subsequent references to these terms. If a and b are assumed constant during a time step Δt (which is only an approximation for the nonlinear equations), the solution to Equation 3-1 is

$$C^{n+1} = \frac{a}{b} + \left(C^n - \frac{a}{b}\right)\exp(-b\Delta t) \tag{3-2}$$

where C^n is the concentration at time t and C^{n+1} is the concentration at time $t+\Delta t$. The SAQM model uses this equation to solve the chemical rate equations for the stiffest species. Another approximation of Equation 3-1, which is valid only for extremely small time steps, is obtained as a simple difference equation:

$$\frac{C^{n+1} - C^n}{\Delta t} = a - b\left(\frac{C^n + C^{n+1}}{2}\right) \tag{3-3}$$

Equation 3-3 can be rewritten as:

$$C^{n+1} = \frac{a\Delta t + (1 - b\,\Delta t/2)C^n}{1 + b\Delta t/2} \tag{3-4}$$

The SAQM model uses this equation to solve most of the chemical rate equations. This method is computationally fast for each step, however, it is not able to handle significant numerical stiffness and it is only accurate with small time steps. This method is among the simplest used in any gridded air quality model.

The SAQM chemical solver (SCS) incorporates approximations to speed up the integrations of the gas-phase chemistry. The approximations are hardwired for specific chemical mechanisms. Instead of using Equation 3-2 or 3-4 to solve for all of the species concentrations, several pairs of interacting species are grouped together in order to reduce the stiffness of the equations. That is, the model integrates the equations for the sum of these species, which have significantly less stiffness than the equations for the individual species. For the CB-IV mechanism, [NO and NO_2], [NO_3 and N_2O_5], [OH and HO_2], and [PAN and C_2O_3] are grouped together to form four sets of coupled species. The SCS integrates the differential equation for the time-rate of change of the sum of the species pairs and then calculates individual species concentrations from the updated group concentration and

steady-state approximation. While the grouping of species is an effective and accurate means of reducing stiffness in the system of equations, it is problematic because its implementation is hardwired for specific chemical mechanisms. The SCS uses Equation 3-2 to solve for H_2O_2 and HO_x (coupled OH and HO_2), and Equation 3-4 for all other species except the fast-reacting radical species. The concentrations of the fast reacting radical species OH, ROR, TO2, CRO, XO2, XO2N, O1D, and O3P are calculated from the steady-state approximation as is done in most gridded air quality models. Accuracy of the solution depends on the time step used to integrate the equations. SAQM uses particularly small integration time steps in order to maintain accuracy with this simplistic integration method.

In order to test the numerical performance of the solver, the SCS was extracted from the SAQM and implemented as a standalone box model. Initial testing was performed on a numerically stiff problem with conditions similar to those encountered in urban model applications. The integration was started at 9 a.m. under clear sky conditions for 34 degrees latitude in midsummer. **Table 3-1** shows the initial conditions used in the test simulation. Examination of the time steps used in the simulation showed that the SCS mostly used the minimum time step (3 s) input to the model. Using such a small time step can be computationally demanding. Alternate schemes that use more complex solution procedures can take must larger time steps than possible with Equations 3-2 or 3-4. For example, Kumar et al. (1995) reviewed alternate chemical kinetics solvers used in air quality models and found that the IEH solver (Sun et al., 1994; Kumar et al., 1995) was accurate and reasonably fast. In addition, the numerical robustness of the IEH method made it well suited to use with a flexible chemical mechanism (FCM) interface. In fact, it was selected for use in the UAM/FCM model. Hence, a comparison of the SCS and the IEH solver was carried out to evaluate their accuracy and speed.

Table 3-1. Initial concentrations of species for the box model test problem.

Species	Concentration (ppm)	Species	Concentration (ppm)
NO	0.09	CO	2.0
NO2	0.01	FORM	0.01
O3	0.0	ALD2	0.005
PAR	0.2	CH4	1.7
ETH	0.005	HNO3	0.1
OLE	0.2	PAN	0.06
TOL	0.0001	H2O2	0.007
XYL	0.1	MGLY	0.0002
ISOP	0.005	NO3	0.00005
OPEN	0.000008	N2O5	0.00008

3.2 IEH SOLVER

The IEH solver was originally developed by Sun et al. (1994) and modified by Kumar et al. (1995) to make the solver independent of the chemical mechanism used. The IEH solver uses the Gear method to solve for the fast-reacting species and an explicit scheme to solve for the slow-reacting species. Sun et al. (1994) describe the IEH method in detail. A summary of the method is presented here. If the system of stiff ODEs is written as:

$$\frac{dC}{dt} = f(C,t) \tag{3-5}$$

where $C(t)$ is the concentration vector at time t, the system of equations can be written as:

$$\frac{dC_F}{dt} = f_F(C_F, C_S, t) \tag{3-6}$$

$$\frac{dC_S}{dt} = f_S(C_F, C_S, t) \tag{3-7}$$

where C_F and C_S are the concentrations of the fast-reacting and the slow-reacting species, respectively.

Given initial conditions at t_0, the initial time step (h_0) is estimated by the Gear solver for the fast species. $C_S(t_1)$ is determined using h_0 and using a first-order explicit scheme. The result is then used in the implicit step to calculate $C_F(t_1)$ and estimate h_1. If h_0 needs to be readjusted, then $C_S(t_1)$ is redetermined. Otherwise, $C_S(t_2)$ is calculated using the following second-order Adams-Bashforth explicit scheme for $C_S(t_{n+1})$:

$$C_S(t_{n+1}) = C_S(t_n) + h_n\left[\frac{h_n}{2h_{n-1}}(f_S(t_n) - f_S(t_{n-1})) + f_S(t_n)\right] \tag{3-8}$$

The same time step is used for both the fast and the slow species. The solution for the slow species ($C_S(t_{n+1})$) is then used in determining the new fast-species concentrations ($C_F(t_{n+1})$) in the implicit step.

3.3 COMPARISON OF THE SCS AND THE IEH SOLVERS

The SCS and the IEH solvers were tested to assess the accuracy and speed of the two solvers compared to the Gear solver. The Gear solution was obtained by treating all species as fast-reacting species in the IEH solver. The test problem used was the same as described above. Both the SCS and the IEH solvers used the same chemistry with the same rate

constants. The assignment of species as fast or slow reacting in the IEH solver was determined by running the IEH solver with different assignments to get the optimum assignments. The optimum assignments are shown in **Table 3-2**. For the Gear solution an absolute tolerance error (ATE) of 10^{-8} ppm and a relative tolerance error (RTE) of 0.001 were used. For simulation using a combination of fast and slow species, ATE was set to 10^{-6} ppm and RTE was set to 0.01. Prior experience has shown that these tolerance parameters give reasonably accurate solutions.

Figures 3-1 through 3-3 show the concentrations of key species predicted using the three techniques in the test simulations. The results show that the solutions from the SCS and the IEH solvers track the Gear solution closely, but the IEH solver results are closer to the Gear solution. The differences between the two solvers are more prominent when comparing the concentrations of radical species. Most radical species are treated as fast-reacting species in the IEH solver and the results show the predictions for radical species from the IEH solver agree more closely with those from the full Gear solver than do the predictions from the SCS. In short, both the SCS and the IEH solvers give reasonably accurate solutions, though the IEH solver is more accurate. There is a large difference in the predicted XO2N concentrations for the two solvers. This is due to the fact that XO2N is treated differently in the two solvers. The SAQM treats XO2N as a steady-state species even though the only destruction mechanism for XO2N is the reaction with NO. This can cause erroneous results for XO2N when NO concentrations are close to zero, as there will be no loss mechanism for XO2N, which violates the necessary condition for treating a species as a steady-state species. For the IEH solver, a new first-order reaction for dissociation of XO2N was added with the equivalent rate as the XO2 dissociation reaction.

A comparison of the CPU times used by the three solvers for the test problem is presented in **Table 3-3**. The CPU time taken by the SCS is 2.4 times higher than that taken by the IEH solver. The Gear solver is the slowest of all, with a CPU time which is 3.2 times the CPU time taken by the IEH solver. Thus, the results from the test problem suggest that the IEH solver is more accurate and faster than the current solver used in the SAQM. Based on these results and the fact that the IEH solver has been used in designing FCM interface for the UAM-IV (Kumar et al., 1995), it was decided to implement the IEH solver in the SAQM model. This would also make it easier to design a flexible chemical mechanism interface for the SAQM in the future.

3.4 IMPLEMENTATION OF THE IEH SOLVER IN THE SAQM

Currently, the CB-IV chemical mechanism is hardwired in the SAQM. There are seven mechanism-specific routines with nearly 2000 lines of FORTRAN code. The only chemistry parameters that can be changed are the reaction rate constants (this can be done by changing a FORTRAN include file); the form of the reactions cannot be altered and additional reactions cannot be added. The hand-coded, internally hardwired approach is outdated and not suitable for a state-of-the-science air quality model. The chemical mechanisms used in air quality models are continuously updated as the understanding of atmospheric chemistry improves.

Table 3-2. The slow reacting, fasting reacting, and steady-state species assignments for CB-IV in the SAQM-IEH solver.

Species	Molecular Weight	Assignment
HNO4	135.08	Slow
HNO3	63.02	Slow
HONO	47.02	Slow
PAN	121.05	Slow
H2O2	34.02	Slow
PAR	14.00	Slow
ETH	28.05	Slow
OLE	28.00	Slow
OLE2	28.00	Slow
TOL	92.00	Slow
XYL	106.00	Slow
ISO	68.00	Slow
CO	28.01	Slow
HCHO	30.03	Slow
ALD	44.05	Slow
MGLY	72.07	Slow
OPEN	100.00	Slow
SO2	64.00	Slow
SULF	96.00	Slow
COC	75.00	Slow
CH4	16.00	Slow
NTR	12.00	Slow
NH3	17.00	Slow
HCL	36.50	Slow
O3	48.00	Fast
NO	30.01	Fast
C2O3	72.05	Fast
HO2	33.01	Fast
NO3	62.01	Fast
NO2	46.01	Fast
XO2	75.00	Fast
N2O5	108.02	Fast
ROR	75.00	Fast
CRES	108.14	Fast
CRO	33.00	Fast
HO	17.00	Fast
O	NA	Steady-state
O1D	NA	Steady-state
TO2	NA	Steady-state
XO2N	NA	Steady-state

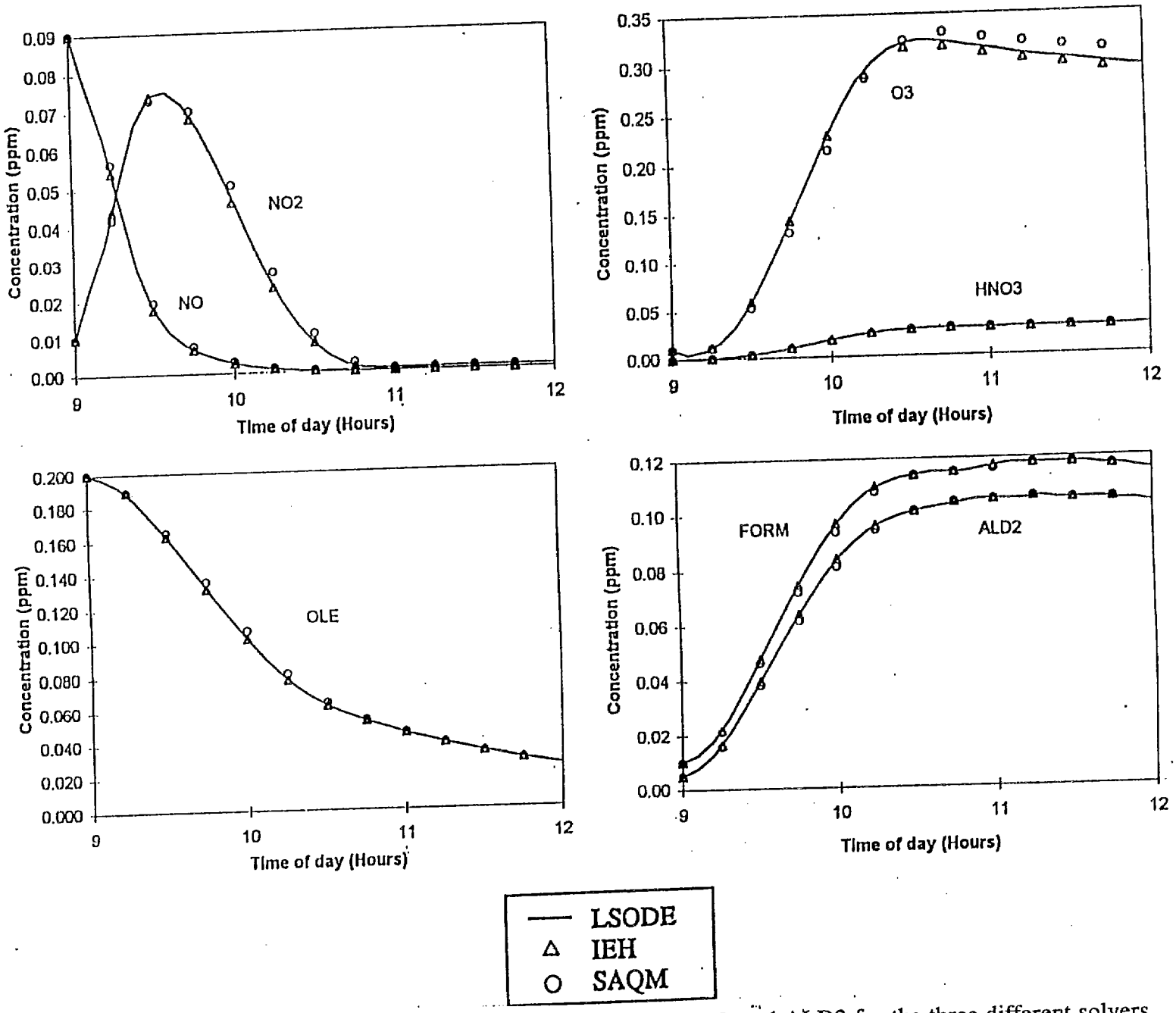

Figure 3-1. Predicted concentrations of NO, NO_2, O_3, HNO_3, OLE, FORM, and ALD2 for the three different solvers.

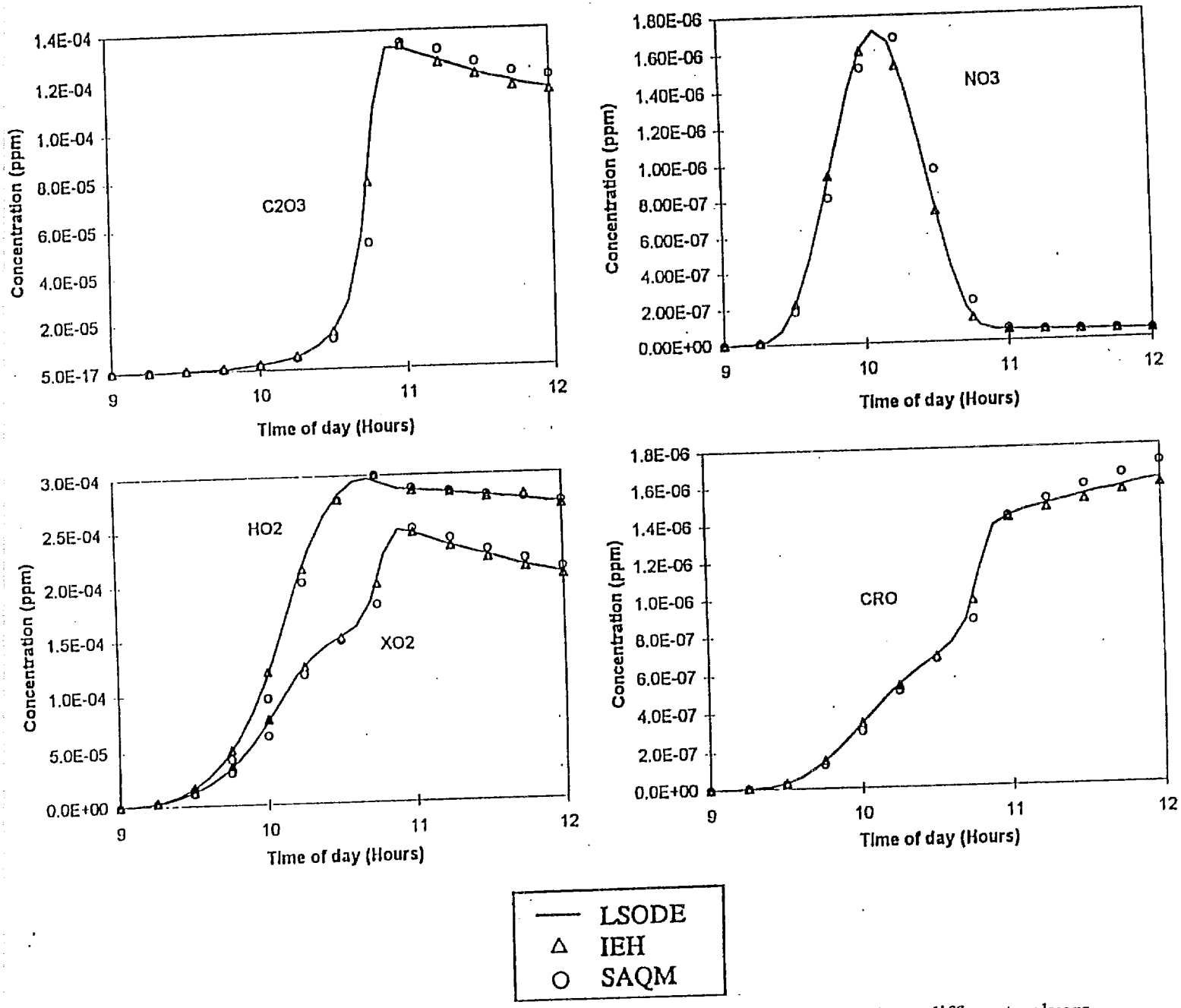

Figure 3-2. Predicted concentrations of C2O3, NO_3, HO_2, XO2, and CRO for the three different solvers.

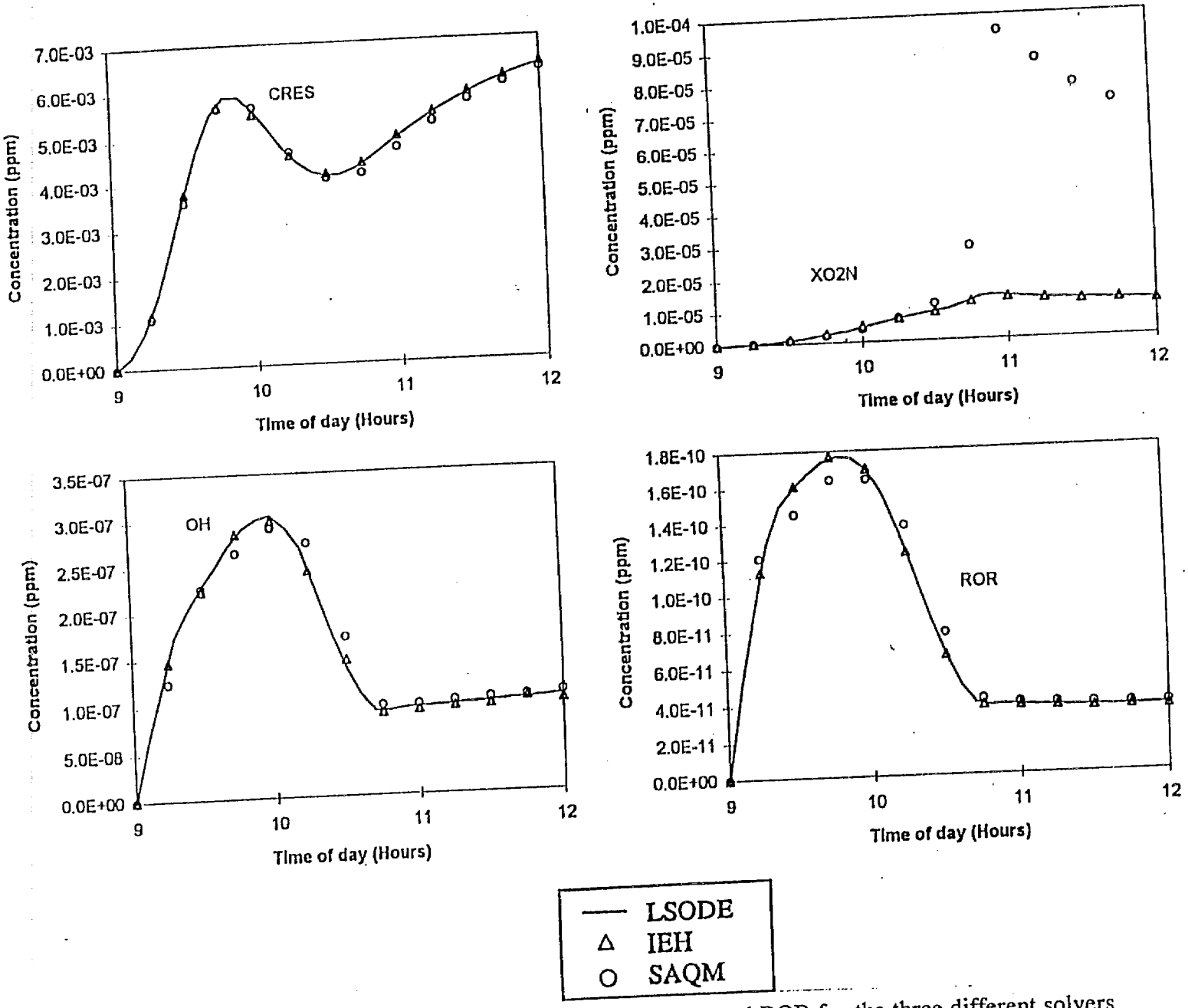

Figure 3-3. Predicted concentrations of CRES, XO2N, OH, and ROR for the three different solvers.

Table 3-3. CPU times taken by different solvers for the test problem.

Solver	CPU Time*
IEH	1.0
Gear	3.2
SAQM	2.4

*Normalized to CPU time for the IEH solver.

Changing or updating a chemical mechanism is prone to errors when a hand-coded approach is used; it is also expensive. On the other hand, a flexible procedure for specification of the chemical mechanisms makes it easier and more cost-effective to change chemical mechanisms in air quality models. Thus, it was decided to use the procedures developed in the design of FCM interface for UAM-IV (Kumar et al., 1995) to implement the IEH solver in the SAQM model. It was beyond the scope of this project to fully design an FCM interface specific to the SAQM, but using procedures similar to those used in the design of the FCM interface for UAM-IV will make it easier to design a similar approach for the SAQM in the future.

In the new version of the SAQM (referred to as SAQM-IEH) the chemical mechanism is described in an ASCII input file (the CHEMPARAM file). This file provides the input parameters for the mechanism, and a FORTRAN include file "CHPARM.COM" which contains common blocks that describe chemistry parameters used in the model. In addition, there is a FORTRAN subroutine, SPRATE, which was written specifically to match some hardwired reaction rates in the chemical mechanism used in the SAQM because those hardwired rates could not be implemented using the existing procedures for FCM for the UAM-IV.

The FORTRAN code for the IEH solver includes subroutines LSODEF1, LSFUN, and STODEF1, which are independent of the chemical mechanism used. Subroutines LSODEF1 and STODEF1 contain the main code for the IEH solver, whereas LSFUN contains various utility routines that are called by both LSODEF1 and STODEF1. There are four more mechanism-specific FORTRAN subroutines in the SAQM-IEH. Subroutine CHREAD reads the CHEMPARAM file; subroutine CHEMI performs the actual integration (this subroutine is produced using the FCM interface); subroutine NITBAL forces the nitrogen balance, if desired; and subroutine PHOT (same as the one used in the SAQM) calculates the photolytic rates. There is an additional FORTRAN BLOCK DATA file, BLK_DAT2, which contains the names and molecular weights of the gas-phase species used in the chemical mechanism. A detailed description of the coding changes made during implementation of the IEH solver in the SAQM is given in Appendix A.

3.4.1 CHEMPARAM File

The CHEMPARAM file is an ASCII file that provides input parameters pertaining to the gas-phase chemical mechanism. The contents and format of the CHEMPARAM file are described in **Table 3-4** and a sample CHEMPARAM file for the CB-IV mechanism used in the SAQM is shown in **Figure 3-4**. The file shown in Figure 3-4 and described below is the one used for the aerosol version of the SAQM (see Section 4).

The first record in the CHEMPARAM file identifies the file header and labels the contents. This is a dummy record and is not read by the model. The second group of records contains data that describe the size of the gas-phase mechanism and the aerosol-size sections. Here, the number of fast and slow species correspond to the fast-reacting and slow-reacting species in the IEH chemical solver used for chemical kinetics integration (Sun et al., 1994; Kumar et al., 1995). The number of aerosol and droplet sections refer to the number of aerosol size-sections for particles with diameters below and above 10μm, respectively. There must be at least one aerosol section. The lower and upper particle diameters in each section are specified here as well.

The next record is the nitrogen balance flag, LNITBAL, which is useful for mechanisms that track all of the nitrogenous products. It is a logical variable (Group 3) that, when input as "T", forces a perfect nitrogen balance after each time slice by assigning the lost or gained nitrogen mass to HNO_3 and NO_2. If all of the nitrogen species are integrated as fast-reacting species, this option is not needed because the IEH solver conserves nitrogen within about 0.01 percent per day. If only the fastest reacting nitrogen are treated as fast species (NO, NO_2, NO_3, and N_2O_5), the IEH solver conserves nitrogen mass within about 1 percent per day without forcing the nitrogen balance (Kumar et al., 1995). Thus, LNITBAL should be set to "T" if a more accurate nitrogen balance is desired. Forcing the nitrogen balance does not effect the computational speed and is recommended provided that the mechanism is written to conserve nitrogen.

The next record(s) contain the reaction rate data. The reaction rate data are provided using two or more records per reaction. The first record contains the reaction rate (RK) at 298 K, reaction type (NRXTYP), and number of reaction parameters (NRXPAR). There are two types of reactions used in the chemical mechanism. A value of 1 for NRXTYP means that the reaction has a constant rate, and only one parameter (A) is required for that reaction. A value of 4 for NRXTYP means that the reaction rate is a function of temperature, and three parameters are required. If the three parameters are A, B, and C, then the reaction rate is given by:

$$k = A\left(\frac{T}{T_{ref}}\right)^{C} e^{\left(\frac{-B}{RT}\right)} \tag{3-9}$$

where T is the temperature (K) of the cell, T_{ref} is the reference temperature (298 K), and R is the gas constant (0.0019872 Kcal/K). Following the reaction kinetic rate data, the constant

Table 3-4. Structure of data on the CHEMPARAM file.

Group	Variables	Format	No. of Records	Variables or Description
1	Dummy	-	1	A two-line header which is ignored by the model
2	NOSPEC, NFAST, NSLOW, NRXN, NCONST, NSC, INDH2O, INDM, INDO2, ISECT, IDROP, (DPB(n), n=1,nsect +ndrop+1)	///, 5(41X,I3/), 6(41X,I2/), 41X,10f9.0	17	One blank line, followed by: number of gas-phase species (NOSPEC); number of fast-reacting gas-phase species (NFAST); number of slow-reacting gas-phase species (NSLOW); number of gas-phase chemical reactions (NRXN); number of constant coefficients in the gas-phase chemical mechanism (NCONST); number of constant concentration gas-phase species (NSC); species indices for the water vapor (INDH2O); species indices for nitrogen (INDM); species indices for the oxygen (INDO2); number of aerosol-size sections (ISECT); number of fog droplet sections (IDROP); diameter cut points for all aerosol and fog-size sections (DPB, nsect+ndrop+1 values in μm ordered from smallest lower cut point to largest upper cut point)
3	LNITBAL	/,42X, L1	2	A blank line and a logical variable for nitrogen balance (LNITBAL)
4		//	2	Two blank lines
Records 5 and 6 are input together for each reaction (i.e., for I=1,NRXN)				
5	RK, NRXTYP, NRXPAR	6X,F14.0, 2I4	1 per reaction	Reaction rate constant at 298 K in ppm-min units (RK(I)); reaction type (NRXTYP(I)); and number of reaction parameters (NRXPAR(I))
6	RXNPAR	11E12.4	1 or more per reaction	The reaction parameters RXNPAR(J,I), J=1, NRXPAR(I)) are read
7		//,6F13.0	(NCONST)/ 6 +2	Two blank lines and the values of the constant coefficients (COEF(I), I=1, NCONST)

```
CHEMPARAM        CHEMISTRY PARAMETERS        CB4_SMP.MOD
09/23/95 (13:17)CARBON BOND MECHANISM.   SAQM VERSION.

     NO OF SPECIES                          =  36
     NO OF FAST SPECIES                     =  12
     NO OF SLOW SPECIES                     =  24
     NO OF REACTIONS                        =  90
     NO OF CONSTANT COEFFICIENTS            =  53
     NO OF CONSTANT SPECIES                 =  3
     INDEX FOR CONCENTRATION OF H2O         =  1
     INDEX FOR CONCENTRATION OF M           =  2
     INDEX FOR CONCENTRATION OF O2          =  3
     NUMBER OF AEROSOL SECTIONS             =  1
     NUMBER OF FOG DROPLETS                 =  0
     DIAMETER CUT POINTS (micro-meter)      =   .039062  10.0

LOGICAL VARIABLE FOR NITROGEN BALANCE IS: T

REACTION MECHANISM PARAMETERS

   1        .0000E+00    4    3
   .0000E+00    .0000E+00    .0000E+00
   2        .0000E+00    4    3
   .0000E+00    .0000E+00    .0000E+00
   3        .1814E-13    4    3
   .1800E-11    .1370E+04    .0000E+00
   4        .9300E-11    4    3
   .9300E-11    .0000E+00    .0000E+00
   5        .0000E+00    4    3
   .0000E+00    .0000E+00    .0000E+00
   6        .0000E+00    4    3
   .0000E+00    .0000E+00    .0000E+00
   7        .3226E-16    4    3
   .1200E-12    .2450E+04    .0000E+00
   8        .0000E+00    4    3
   .0000E+00    .0000E+00    .0000E+00
   9        .0000E+00    4    3
   .0000E+00    .0000E+00    .0000E+00
  10        .2872E-10    4    3
   .7760E-11   -.3900E+03    .0000E+00
  11        .2200E-09    4    3
   .2200E-09    .0000E+00    .0000E+00
  12        .6826E-13    4    3
   .1600E-11    .9400E+03    .0000E+00
```

Figure 3-4. An example of the CHEMPARAM file used in the SAQM.

Page 1 of 5

```
13          .1999E-14    4    3
 .1400E-13    .5800E+03    .0000E+00
14          .0000E+00    4    3
 .0000E+00    .0000E+00    .0000E+00
15          .3008E-10    4    3
 .1300E-10   -.2500E+03    .0000E+00
16          .4031E-15    4    3
 .2500E-13    .1230E+04    .0000E+00
17          .0000E+00    4    3
 .0000E+00    .0000E+00    .0000E+00
18          .1300E-20    4    3
 .1300E-20    .0000E+00    .0000E+00
19          .3666E+11    4    3
 .6580E+27    .1115E+05    .0000E+00
20          .1954E-17    4    3
 .3300E-18   -.5300E+03    .0000E+00
21          .4400E-19    4    3
 .4400E-19    .0000E+00    .0000E+00
22          .0000E+00    4    3
 .0000E+00    .0000E+00    .0000E+00
23          .0000E+00    4    3
 .0000E+00    .0000E+00    .0000E+00
24          .6600E-11    4    3
 .6600E-11    .0000E+00    .0000E+00
25          .1000E-19    4    3
 .1000E-19    .0000E+00    .0000E+00
26          .0000E+00    4    3
 .0000E+00    .0000E+00    .0000E+00
27          .0000E+00    4    3
 .0000E+00    .0000E+00    .0000E+00
28          .8279E-11    4    3
 .3700E-11   -.2400E+03    .0000E+00
29          .0000E+00    4    3
 .0000E+00    .0000E+00    .0000E+00
30          .6179E+11    4    3
 .4290E+27    .1087E+05    .0000E+00
31          .4653E-11    4    3
 .1300E-11   -.3800E+03    .0000E+00
32          .2798E-11    4    3
 .5900E-13   -.1150E+04    .0000E+00
33          .6239E-09    4    3
 .2200E-17   -.5800E+04    .0000E+00
34          .0000E+00    4    3
 .0000E+00    .0000E+00    .0000E+00
```

Figure 3-4. An example of the CHEMPARAM file used in the SAQM.

```
35        .1655E-11    4    3
 .3100E-11    .1870E+03    .0000E+00
36        .0000E+00    4    3
 .0000E+00    .0000E+00    .0000E+00
37        .0000E+00    4    3
 .0000E+00    .0000E+00    .0000E+00
38        .1000E-10    4    3
 .1000E-10    .0000E+00    .0000E+00
39        .0000E+00    4    3
 .0000E+00    .0000E+00    .0000E+00
40        .0000E+00    4    3
 .0000E+00    .0000E+00    .0000E+00
41        .1653E-12    4    3
 .3000E-10    .1550E+04    .0000E+00
42        .6300E-15    4    3
 .6300E-15    .0000E+00    .0000E+00
43        .4388E-12    4    3
 .1200E-10    .9860E+03    .0000E+00
44        .1620E-10    4    3
 .7000E-11   -.2500E+03    .0000E+00
45        .2500E-14    4    3
 .2500E-14    .0000E+00    .0000E+00
46        .0000E+00    4    3
 .0000E+00    .0000E+00    .0000E+00
47        .1902E-10    4    3
 .3480E-10    .1800E+03    .0000E+00
48        .9306E-11    4    3
 .2600E-11   -.3800E+03    .0000E+00
49        .4233E-03    4    3
 .2000E+17    .1350E+05    .0000E+00
50        .2000E-11    4    3
 .2000E-11    .0000E+00    .0000E+00
51        .6500E-11    4    3
 .6500E-11    .0000E+00    .0000E+00
52        .7729E-14    4    3
 .2400E-11    .1710E+04    .0000E+00
53        .8100E-12    4    3
 .8100E-12    .0000E+00    .0000E+00
54        .2193E+04    4    3
 .1000E+16    .8000E+04    .0000E+00
55        .1600E+04    4    3
 .1600E+04    .0000E+00    .0000E+00
56        .1500E-10    4    3
 .1500E-10    .0000E+00    .0000E+00
```

Figure 3-4. An example of the CHEMPARAM file used in the SAQM.

Page 3 of 5

```
57          .4046E-11    4    3
 .1200E-10    .3240E+03    .0000E+00
58          .3184E-10    4    3
 .5200E-11   -.5400E+03    .0000E+00
59          .1198E-16    4    3
 .1400E-13    .2105E+04    .0000E+00
60          .7700E-14    4    3
 .7700E-14    .0000E+00    .0000E+00
61          .7011E-12    4    3
 .1000E-10    .7920E+03    .0000E+00
62          .7943E-11    4    3
 .2000E-11   -.4110E+03    .0000E+00
63          .1891E-17    4    3
 .1300E-13    .2633E+04    .0000E+00
64          .6187E-11    4    3
 .2100E-11   -.3220E+03    .0000E+00
65          .8100E-11    4    3
 .8100E-11    .0000E+00    .0000E+00
66          .4200E+01    4    3
 .4200E+01    .0000E+00    .0000E+00
67          .4100E-10    4    3
 .4100E-10    .0000E+00    .0000E+00
68          .2200E-10    4    3
 .2200E-10    .0000E+00    .0000E+00
69          .1400E-10    4    3
 .1400E-10    .0000E+00    .0000E+00
70          .0000E+00    4    3
 .0000E+00    .0000E+00    .0000E+00
71          .3000E-10    4    3
 .3000E-10    .0000E+00    .0000E+00
72          .1009E-16    4    3
 .5400E-16    .5000E+03    .0000E+00
73          .2509E-10    4    3
 .1700E-10   -.1160E+03    .0000E+00
74          .1700E-10    4    3
 .1700E-10    .0000E+00    .0000E+00
75          .0000E+00    4    3
 .0000E+00    .0000E+00    .0000E+00
76          .1800E-10    4    3
 .1800E-10    .0000E+00    .0000E+00
77          .9600E-10    4    3
 .9600E-10    .0000E+00    .0000E+00
78          .1200E-16    4    3
 .1200E-16    .0000E+00    .0000E+00
```

Figure 3-4. An example of the CHEMPARAM file used in the SAQM.

Page 4 of 5

```
 79        .3200E-12    4    3
  .3200E-12    .0000E+00    .0000E+00
 80        .8100E-11    4    3
  .8100E-11    .0000E+00    .0000E+00
 81        .1334E-11    4    3
  .1700E-13   -.1300E+04    .0000E+00
 82        .6800E-12    4    3
  .6800E-12    .0000E+00    .0000E+00
 83        .6017E-11    4    3
  .7670E-13   -.1300E+04    .0000E+00
 84        .1990E-02    4    3
  .1990E-02    .0000E+00    .0000E+00
 85        .4046E-11    4    3
  .1200E-10    .3240E+03    .0000E+00
 86        .3184E-10    4    3
  .5200E-11   -.5400E+03    .0000E+00
 87        .1198E-16    4    3
  .1400E-13    .2105E+04    .0000E+00
 88        .7700E-14    4    3
  .7700E-14    .0000E+00    .0000E+00
 89        .1000E-14    4    3
  .1000E-14    .0000E+00    .0000E+00
 90        .1000E-14    4    3
  .1000E-14    .0000E+00    .0000E+00

 CONSTANT COEFICIENTS
  .200000E+01  .890000E+00  .110000E+00  .790000E+00  .870000E+00
.130000E+00
  .760000E+00 -.110000E+00  .800000E+01  .110000E+01  .960000E+00
.940000E+00
 -.210000E+01  .400000E-01  .200000E-01  .630000E+00  .380000E+00
.280000E+00
  .300000E+00  .200000E+00  .220000E+00  .200000E+02 -.100000E+01
.500000E+00
  .740000E+00  .330000E+00  .440000E+00  .100000E+00  .910000E+00
.900000E-01
  .700000E+00  .170000E+01  .156000E+01  .420000E+00  .120000E+00
.800000E-01
  .360000E+00  .560000E+00  .402000E+03  .900000E+00  .400000E+00
.600000E+00
  .221000E+03  .300000E-01  .620000E+00  .690000E+00  .800000E+00
.416000E+03
  .550000E+00  .450000E+00  .670000E+00  .600000E-01  .740000E+03
```

Figure 3-4. An example of the CHEMPARAM file used in the SAQM.

Page 5 of 5

coefficients (mostly product stoichiometric coefficients) are input. These constant coefficients are an integral part of the procedures used to prepare the CHEMPARAM file utilizing the FCM interface. For a detailed explanation of these inputs, see Kumar et al. (1995).

3.4.2 Other Mechanism-Specific Files in SAQM-IEH

CHPARM.COM is a FORTRAN include file that contains the parameter statements and common blocks that describe the chemistry parameters used in the model. **Figure 3-5** shows the CHPARM.COM file used in SAQM-IEH. LSPEC is the number of advected gas-phase species used in the model; NREAC is the number of chemical reactions; NCMAX is the maximum number of constant coefficients; MAXKON is the maximum number of constant species; MAXFST is the maximum number of fast species; and MAXSLO is the maximum number of slow species. The parameter MSPEC defines the maximum number of species including both the gas-phase and the aerosol-phase species. NSECT and NDROP are defined in the FORTRAN include file, NSECT.INC (see Section 4), and refer to the number of size-sections and the number of droplets used in the aerosol module, respectively. The file NSECT.INC must always be included before the file CHPARM.COM in any subroutine. The integer array LDUM refers to pointers for different species, and common block KCHNM defines those pointers.

Figure 3-6 shows the BLK_DAT2 block data file used in SAQM-IEH. The array SPNAM defines the advected gas-phase species used in the model. The array MAPSP maps the species names to the order of species occurring in the emissions input file. A value of "-1" for MAPSP means that species is not included in the emissions input file. The array WTM defines the molecular weights of the advected species used in the model.

3.5 EVALUATION OF THE IEH SOLVER IN THE SAQM

An evaluation of the SAQM-IEH was performed to check if the implementation of the IEH solver in the SAQM was done correctly. The approach followed was to simulate the August 3-6, 1990 San Joaquin Valley (SJV) ozone episode using the original SAQM (SAQM-STD) and the SAQM-IEH and compare the results. The SAQM-IEH was also run with all of the advected species treated as fast-reacting species, which provided a full Gear solution to use as reference for the other solvers (i.e., gold standard equivalent to using the standard Gear solver for integration of chemistry). This simulation is referred to as SAQM-LSODE. The simulations were started at 4 a.m. on August 2 and continued for 120 hours. All the input data files for the August 3-6, 1990 SJV ozone episode were obtained from the ARB staff. The air quality model grid spacing was approximately 12 km throughout the domain. It is important to note that all of the simulations presented here were performed using the original single surface layer model, rather than the new version, which includes three surface sublayer models. A surface sublayer module was made available later and was subsequently implemented in the SAQM-IEH along with the aerosol module (see Section 4).

```
C     CHPARM INCLUDE FILE
C-----------------------------------------------------------------------
C
C     *** /CHPARM/ CONTAINS CHEMISTRY PARAMETERS
C
      PARAMETER (LSPEC = 36,NREAC = 90,NCMAX = 53)
      PARAMETER (MAXKON=  3,MAXFST= 12,MAXSLO= 24)
      PARAMETER (LSSS = LSPEC + 1)
      PARAMETER (MSPEC = LSPEC + (NSECT+NDROP)*NASPEC)
      INTEGER LDUM(LSPEC+2)
C
      EQUIVALENCE (KHNO4,LDUM(1))
C
      COMMON /KCHNM/ KHNO4,KHNO3,KHONO,KPAN ,KH2O2,KPAR ,
     &               KETH ,KOLE ,KOLE2,KTOL ,KXYL ,KISO ,
     &               KCO  ,KHCHO,KALD ,KMGLY,KOPEN,KSO2 ,
     &               KSULF,KCOC ,KCH4 ,KNTR ,KNH3 ,KHCL ,
     &               KO3  ,KNO  ,KC2O3,KHO2 ,KNO3 ,KNO2 ,
     &               KXO2 ,KN2O5,KROR ,KCRES,KCRO ,KHO  ,
     &               KCHJ1,
     &               KCHJ2
```

Figure 3-5. The CHPARM.COM include file used in SAQM-IEH.

```
BLOCK DATA
      include "fpdc.h"
      include "fpdt.h"
      include "a_params.com"
      include "nsect.inc"
      include "chparm.com"
      include "a_cmmns.com"
C
      DATA SPNAM / "(HNO4)","(HNO3)","(HONO)","(PAN )","(H2O2)",
     &             "(PAR )","(ETH )","(OLE )","(OLE2)","(TOL )",
     &             "(XYL )","(ISO )","(CO  )","(HCHO)","(ALD )",
     &             "(MGLY)","(OPEN)","(SO2 )","(SULF)","(COC )",
     &             "(CH4 )","(NTR )","(NH3 )","(HCL )","(O3  )",
     &             "(NO  )","(C2O3)","(HO2 )","(NO3 )","(NO2 )",
     &             "(XO2 )","(N2O5)","(ROR )","(CRES)","(CRO )",
     &             "(HO  )" /
C
      DATA MAPSP / -1,-1,14,-1,-1, 7, 8, 9,15,11,12,10,13, 6, 5,
     &             -1,-1, 1, 2,-1,-1,-1,16,-1,-1, 4,-1,-1,-1, 3,
     &             -1,-1,-1,-1,-1,
     &             -1 /
C
      DATA WTM   / 135.1, 63.0, 47.0,121.1, 34.0, 14.0, 28.0, 28.0,
     &              28.0, 92.0,106.0, 68.0, 28.0, 30.0, 44.0, 72.1,
     &             100.0, 64.0, 96.0, 75.0, 16.0, 12.0, 17.0, 36.5,
     &              48.0, 30.0, 72.1, 33.0, 62.0, 46.0, 75.0,108.0,
     &              75.0,108.1, 33.0,
     &              17.0 /
C
      END
```

Figure 3-6. BLK_DAT2 FORTRAN block data file used in SAQM-IEH.

3.5.1 Comparison of SAQM-STD and SAQM-IEH Results

Figures 3-7 and 3-8 show the time-series plots of O_3 and NO_2, respectively, comparing the results from the SAQM-STD and SAQM-IEH simulations against the observations. It can be seen that results from the SAQM-STD and SAQM-IEH simulations are similar to each other, with minor differences. SAQM-IEH predicts a slightly higher ozone peak at Fresno, Kern Refuge, Livermore (day 3), Oildale (day 4), Citrus Heights, Academy, Arvin (days 3 and 4), and Corcoran. Differences in predicted NO_2 are more pronounced than the differences in predicted ozone for the two simulations. Both SAQM-STD and SAQM-IEH severely underestimate the observed NO_2 concentrations at most stations. At Kern Refuge, NO_2 concentrations predicted by the SAQM-IEH are significantly higher than those predicted by the SAQM-STD and closer to the observed values.

Another comparison was made where ozone concentrations predicted by the SAQM-STD and SAQM-IEH at high ozone (greater than 120 ppb) stations were compared. **Table 3-5** shows the observed ozone at those stations and the corresponding ozone concentrations predicted by the SAQM-IEH and SAQM-STD. It can be seen that at most stations SAQM-IEH predicts the peak ozone concentration better than the SAQM-STD. For example, highest observed ozone for this episode was 160 ppb at Mouth of Kern River, and SAQM-IEH predicted 108.7 ppb compared to 90.7 ppb predicted by the SAQM-STD. On average, the SAQM-IEH predicted 111 ppb of ozone at the high ozone stations compared to 106 ppb predicted by the SAQM-STD against the observed average of 131 ppb.

Figure 3-9 compares the ozone concentrations predicted by the SAQM-IEH and SAQM-LSODE. It can be seen that the ozone concentrations predicted by the two simulations exactly match each other. This test illustrates the high accuracy of the solution provided by the IEH solver. **Table 3-6** compares the high ozone concentrations predicted by SAQM-LSODE against those predicted by the SAQM-STD and SAQM-IEH at the same grid locations. Again, it can be seen that ozone concentrations predicted by the Gear solver and the IEH solver are extremely close to one another, whereas those predicted by the SAQM-STD are different by up to 30 ppb.

Table 3-7 compares the CPU time taken by the SAQM-STD and the SAQM-IEH simulations. It can be seen that SAQM-IEH is slower by a factor of 1.3 compared to SAQM-STD. This is in direct contrast to what was seen in the box model simulation where the IEH solver was 2.4 times faster than the SCS. The reason for this discrepancy is that in the box model the IEH solver can take large time steps (without sacrificing accuracy), whereas in the SAQM-IEH the time step is limited by the maximum chemistry operator time step which is 300 seconds. The SAQM uses a small operator time step because there is no Courant stability check performed to select the time step and a conservative approach is followed by using a reasonably small time step to ensure that stability criteria is never violated. (It is shown in Section 4 that using a time step of 300 seconds actually violates the stability criteria.) Strength of the IEH solver lies in its ability to take larger time steps without sacrificing accuracy. A test simulation was performed where the transport operator time step was kept at 150 seconds (there are two transport steps for each chemistry step) and the chemistry operator

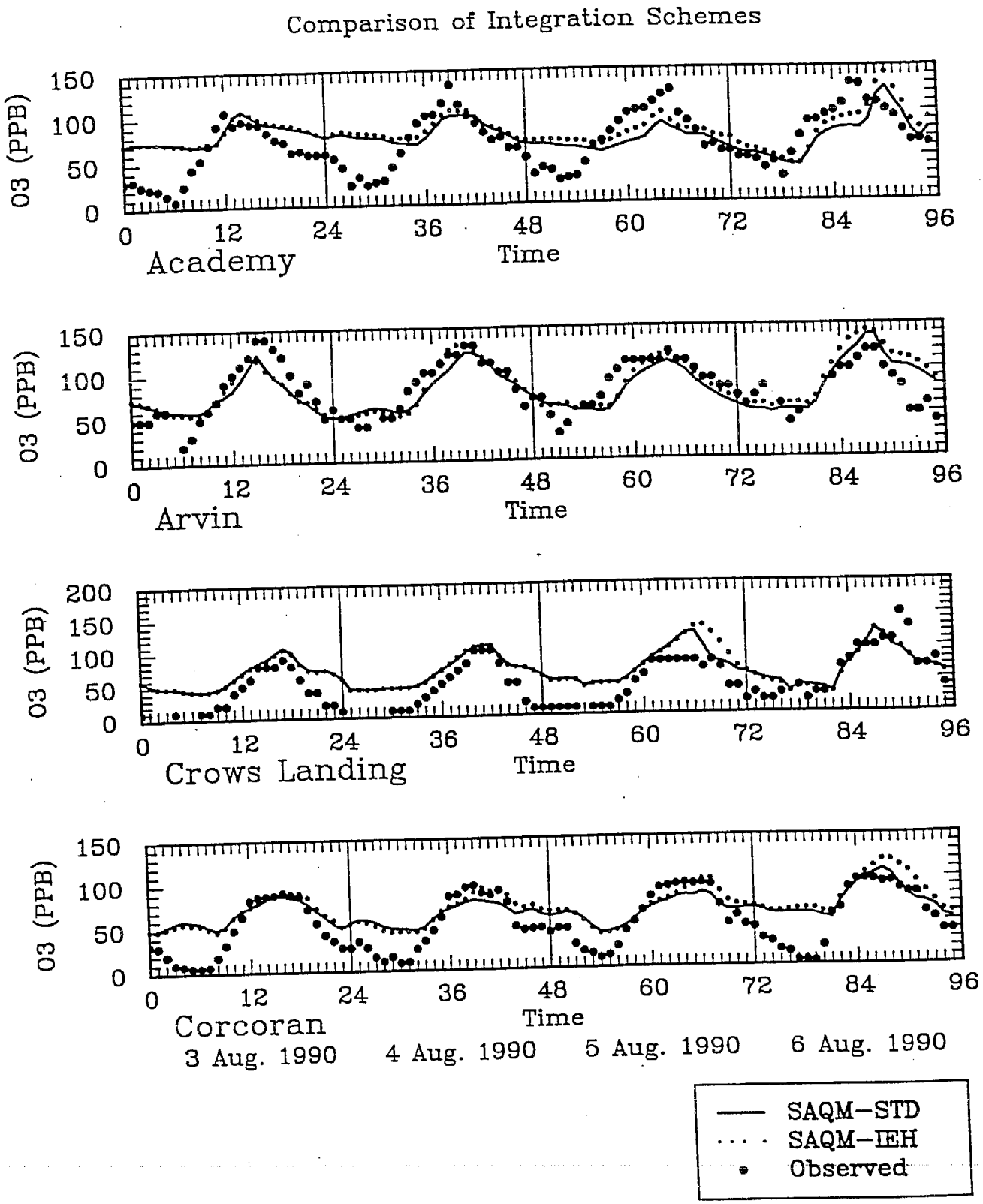

Figure 3-7. Time-series plots of O_3 comparing results from SAQM-IEH and SAQM-STD.

Page 1 of 3

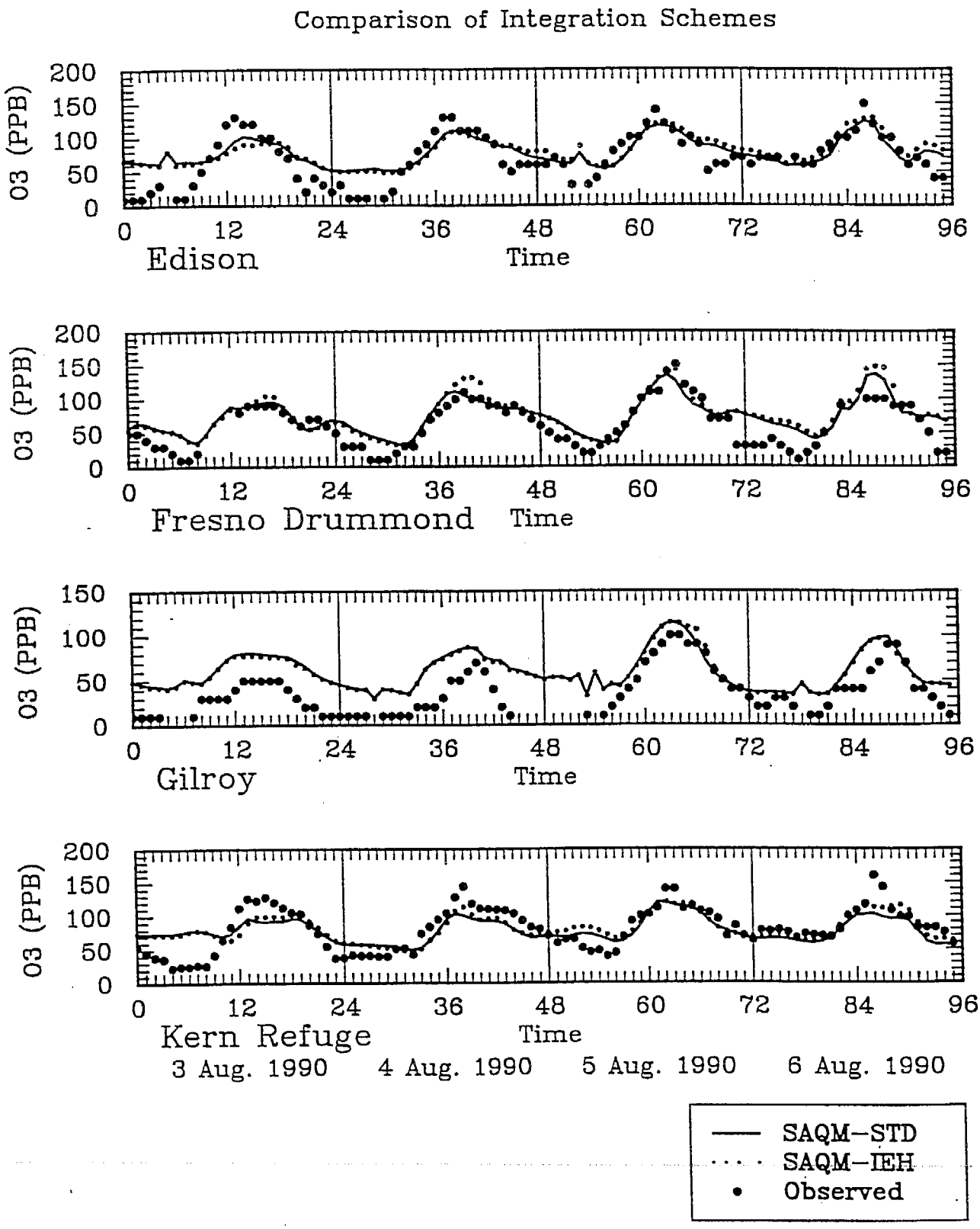

Figure 3-7. Time-series plots of O_3 comparing results from SAQM-IEH and SAQM-STD.

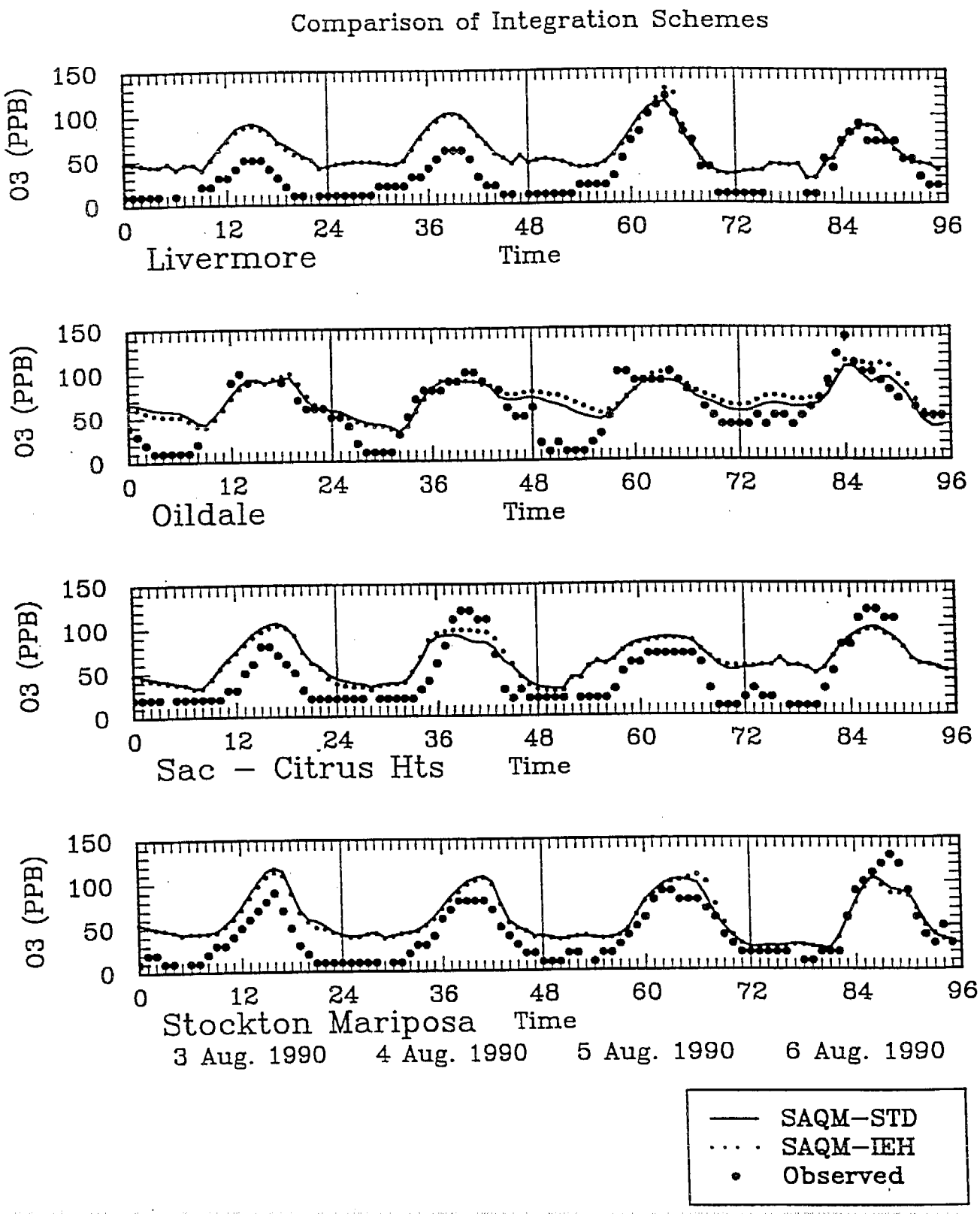

Figure 3-7. Time-series plots of O_3 comparing results from SAQM-IEH and SAQM-STD.

Page 3 of 3

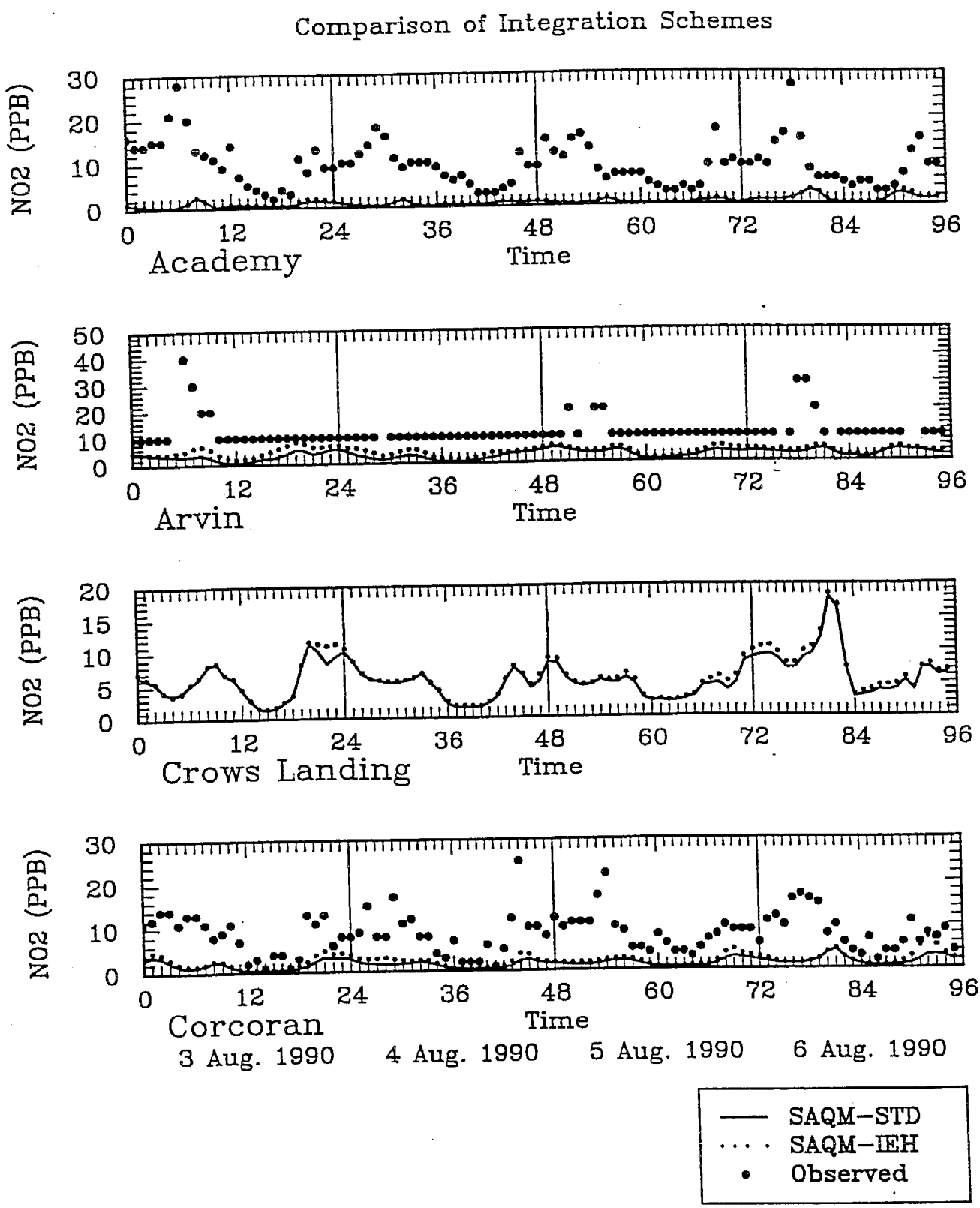

Figure 3-8. Time-series plots of NO_2 comparing results from SAQM-IEH and SAQM-STD.
Page 1 of 3

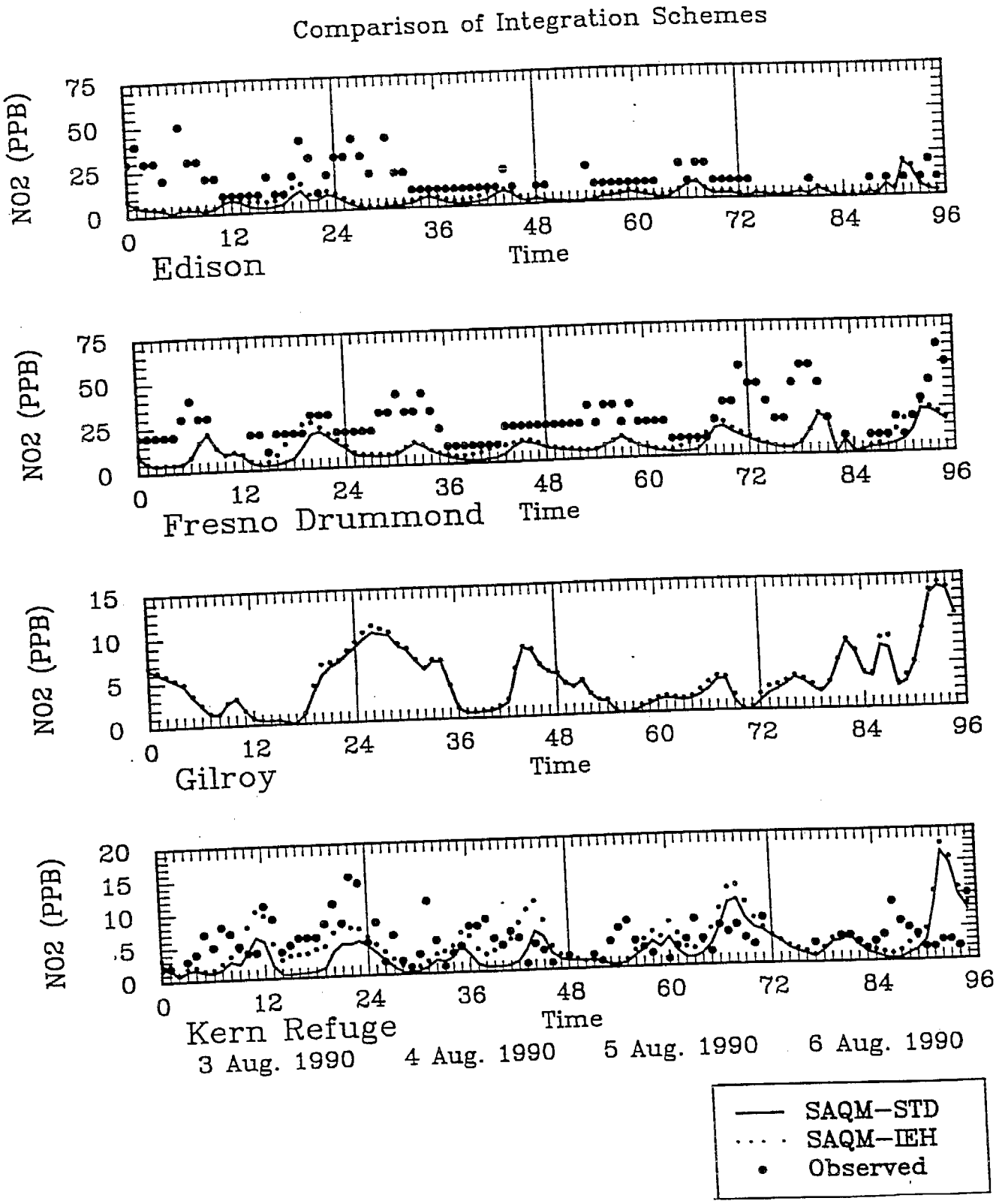

Figure 3-8. Time-series plots of NO_2 comparing results from SAQM-IEH and SAQM-STD.

Page 2 of 3

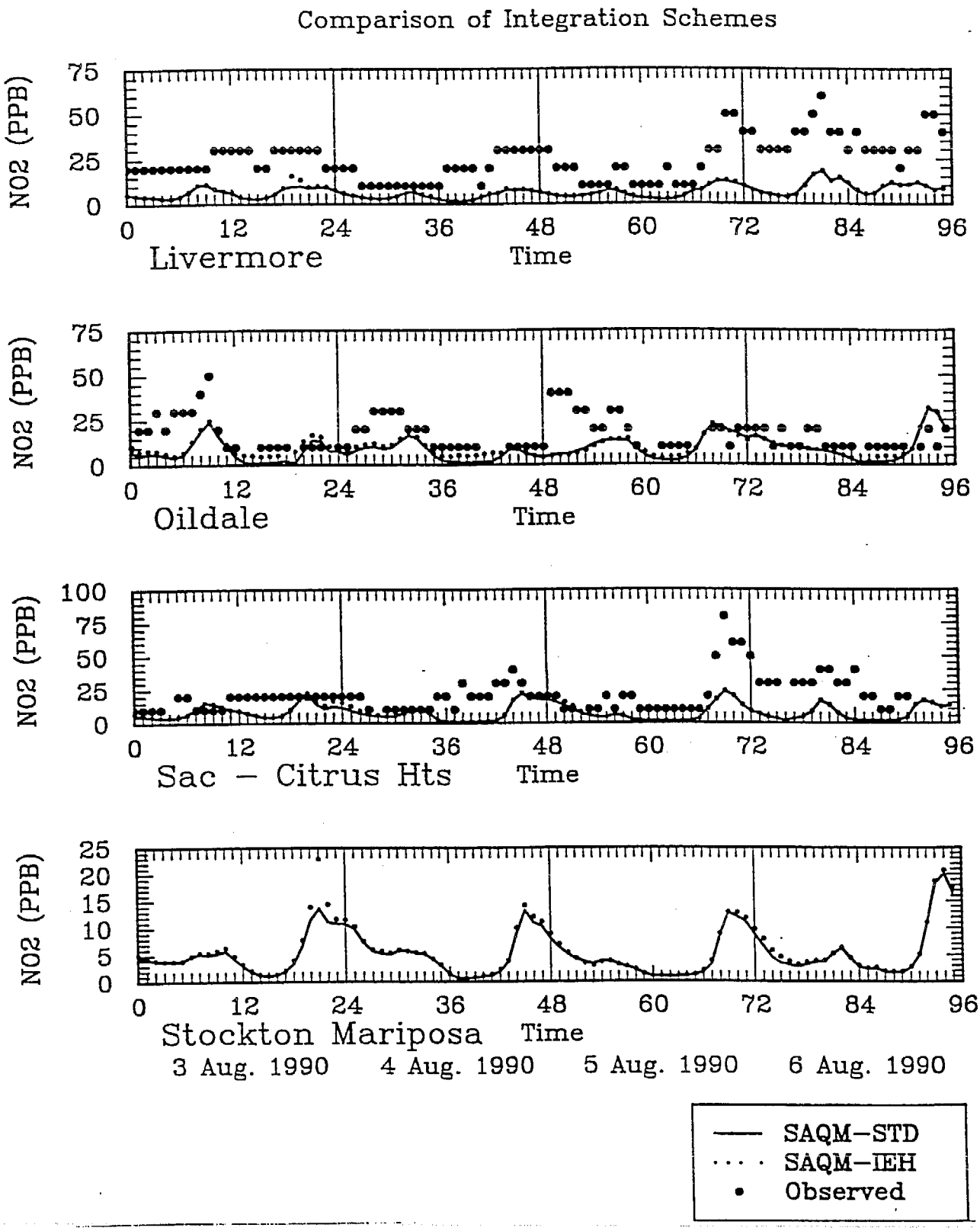

Figure 3-8. Time-series plots of NO_2 comparing results from SAQM-IEH and SAQM-STD.

Page 3 of 3

Table 3-5. Comparison of SAQM ozone predictions at high ozone station with the IEH and standard chemistry solvers.

Station	Hour	Observed (ppb)	SAQM IEH Solver	SAQM STD Solver
Mouth of Kern River	1500	160	108.7	90.7
Edison (ARB's site)	1500	150	120.1	106.3
Edison-Hwy 58	1500	141	120.1	106.3
Auburn-Dewitt	1600	140	81.5	82.3
Oildale-3311 Manor	1300	140	110.2	100.1
Mariposa	1800	136	120.4	124.5
Academy	1500	131	162.0	149.6
Slough House Rd.	1600	131	110.3	113.5
Stockton	1700	130	81.4	84.5
Maricopa	1400	129	94.0	78.5
Taft	1300	127	137.0	131.7
Pardee Reservoir	1400	124	124.1	125.5
Friant	1400	121	138.3	127.7
Arvin	1600	120	126.1	117.6
Bethel Island Rd.	1600	120	72.0	74.4
Sacramento-Del Paso	1400	120	95.9	100.0
Stockton Lodi	1600	120	82.0	83.9
Turlock-Monte Vista	1600	120	109.1	110.2
Average		131	111	106

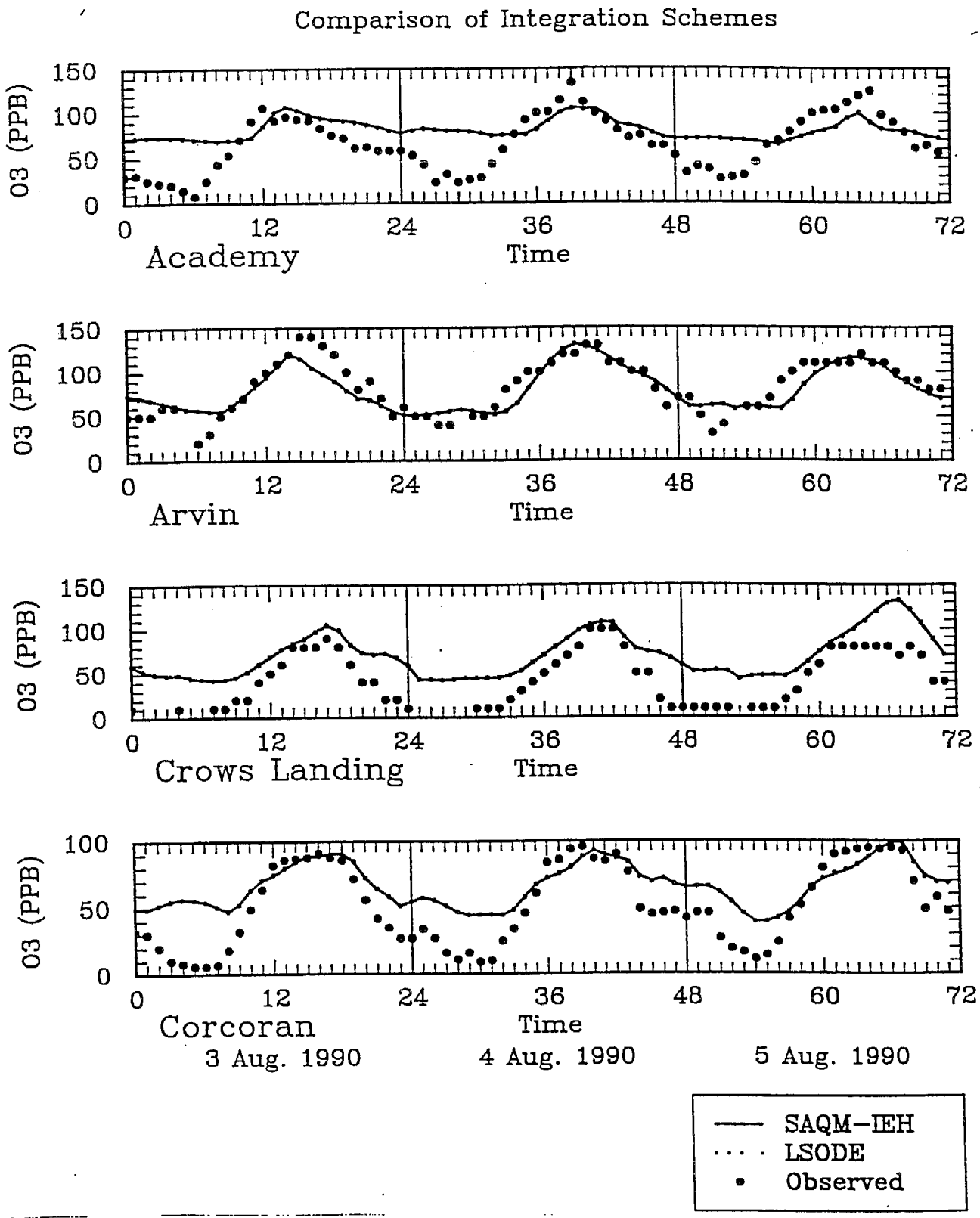

Figure 3-9. Time-series plots of O_3 comparing results from SAQM-IEH and LSODE.

Page 1 of 3

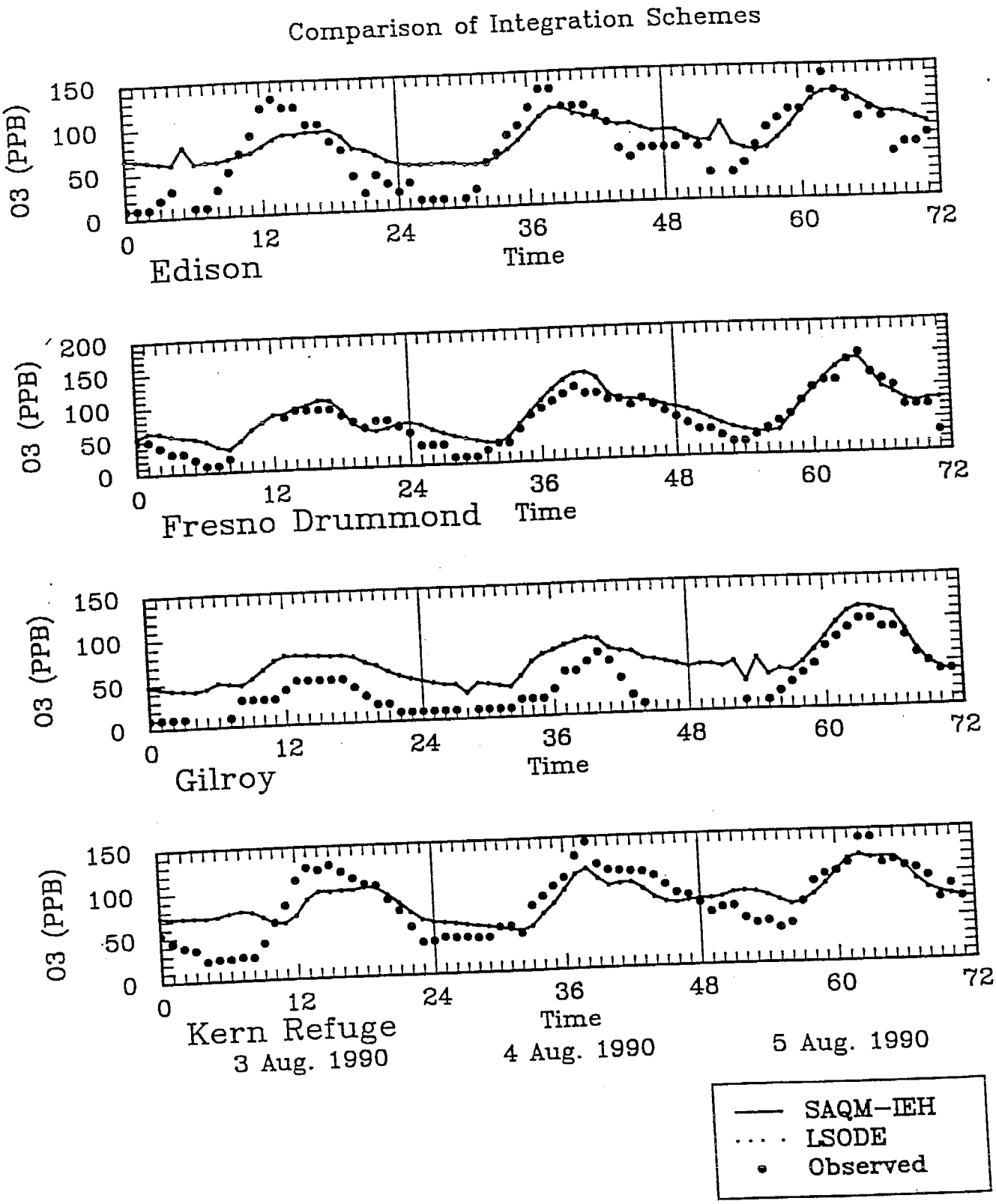

Figure 3-9. Time-series plots of O_3 comparing results from SAQM-IEH and LSODE.
Page 2 of 3

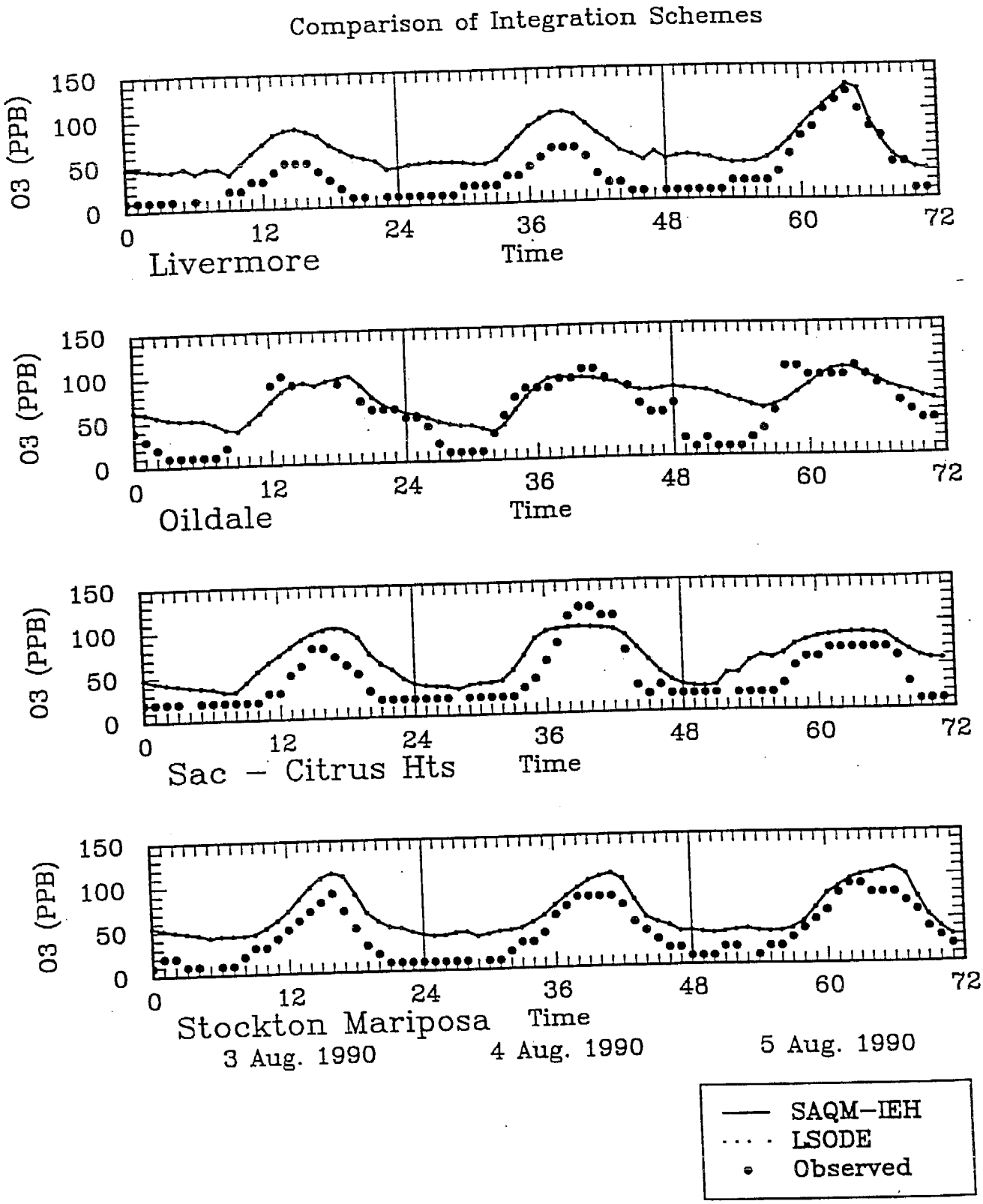

Figure 3-9. Time-series plots of O_3 comparing results from SAQM-IEH and LSODE.

Page 3 of 3

Table 3-6. Comparison of SAQM ozone predictions with different chemistry solvers.

X-Coord	Y-Coord	Hour	Gear Solver	SAQM IEH Solver	SAQM STD Solver
25	17	1700	167.2	168.2	142.6
24	18	1600	163.7	164.6	137.3
26	18	1700	148.3	148.9	132.6
27	17	1800	143.7	144.4	133.4
9	29	1500	139.9	139.9	124.7
26	16	1700	137.3	138.3	125.4
14	25	1800	136.2	136.4	113.5
13	27	1700	132.9	133.3	120.7
16	19	2100	132.5	132.7	96.4
13	23	1900	130.5	130.9	90.5
18	15	200	126.4	126.5	95.1
31	2	2100	120.7	121.3	104.1
17	17	2300	118.5	118.7	94.5
13	33	1800	117.3	117.8	100.5
18	22	1800	117.2	118.2	117.1
15	21	2000	116.7	116.8	84.4
32	4	1700	116	116	102.3
32	8	1800	115.9	117.2	108.6
29	2	2000	115.8	116.2	98.2
17	19	2200	114.6	114.7	85.1

Table 3-7. Comparison of CPU time used by the SAQM-STD and SAQM-IEH.

SAQM Model	Total CPU (mins)	Chemistry % of CPU	Transport % of CPU	Misc. % of CPU
SAQM-STD	439	66.4	26.7	6.9
SAQM-IEH	572	73.5	20.6	5.9

time step was increased to 1200 seconds. Thus, there were four transport steps performed before the chemistry calculation and four transport steps performed after the chemistry calculation. This reduced the CPU time per day of simulation to 424 minutes, which is slightly faster than the SAQM-STD and significantly faster than the SAQM-IEH simulation with the 300 seconds chemistry step. **Figure 3-10** compares the ozone concentrations predicted by the two SAQM-IEH simulations (with 300 and 1200 seconds chemistry operator time steps). Results from the two simulations are similar, though the peak ozone concentration predicted using a 1200 seconds chemistry time step is slightly lower than the one predicted using a 300 seconds chemistry time step at some stations.

3.6 SUMMARY

The IEH solver was successfully implemented in the SAQM using the procedures developed for the FCM interface for UAM-IV. The evaluation of the SAQM-IEH showed that it was more accurate than the SAQM-STD. The SAQM-IEH took 1.3 times more CPU time compared to the CPU time taken by the SAQM-STD. In general, SAQM-IEH will be faster when larger operator time steps can be used. For this particular simulation, small time steps are used because the model extends to 15 km and the horizontal velocities in the top layer are in the 20 to 30 m/s range. Moreover, the vertical velocities at some locations and times are as high as 1 m/s, which significantly limits the extent to which the numerical operators can be time split. The greatest speed improvements with SAQM-IEH are likely to be for applications with lower vertical velocities and horizontal velocities aloft than occurred in the August 3-6, 1990 episode in the SJV.

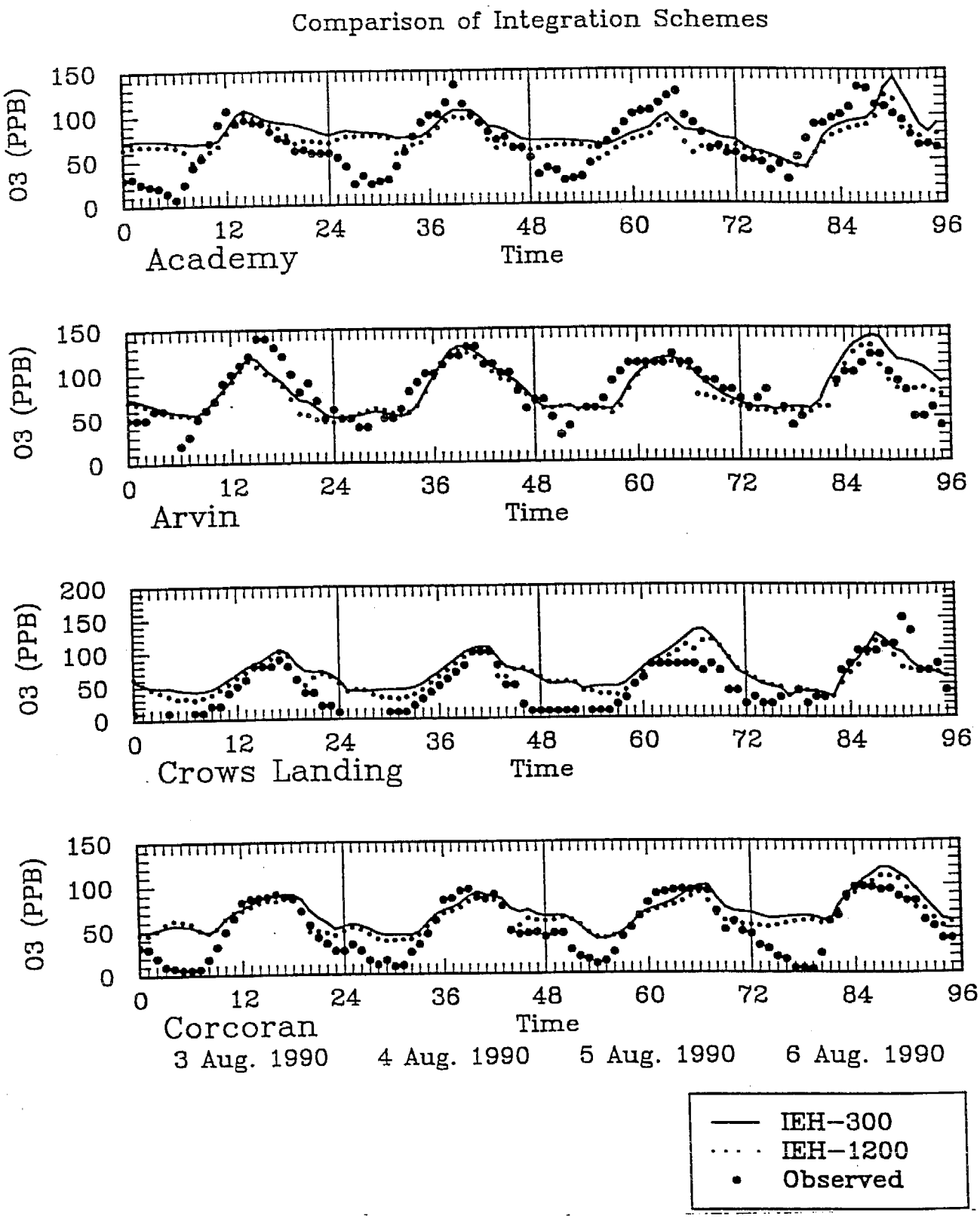

Figure 3-10. Time-series plots of O_3 comparing results from SAQM-300 and SAQM-1200.

Page 1 of 3

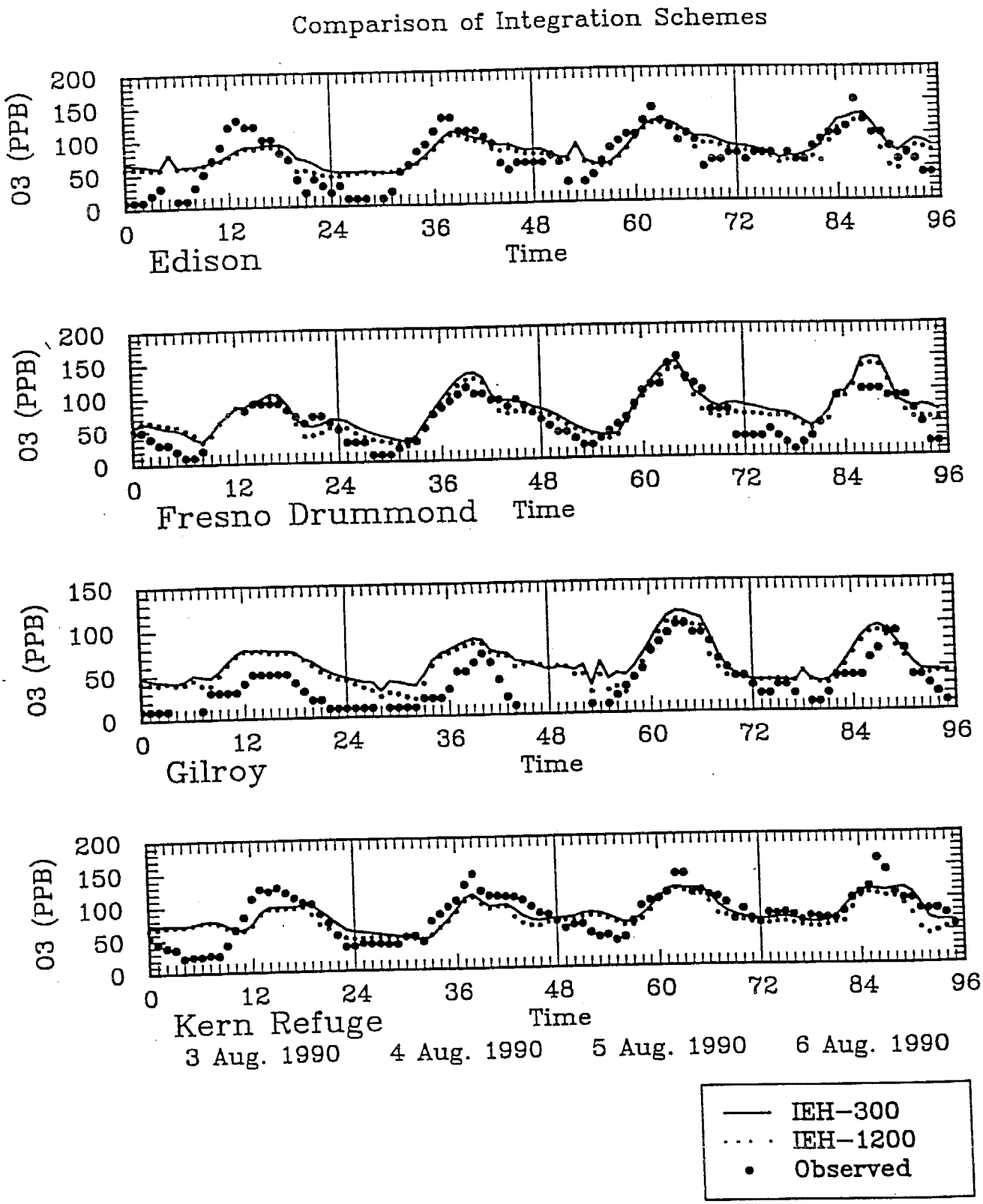

Figure 3-10. Time-series plots of O_3 comparing results from SAQM-300 and SAQM-1200.
Page 2 of 3

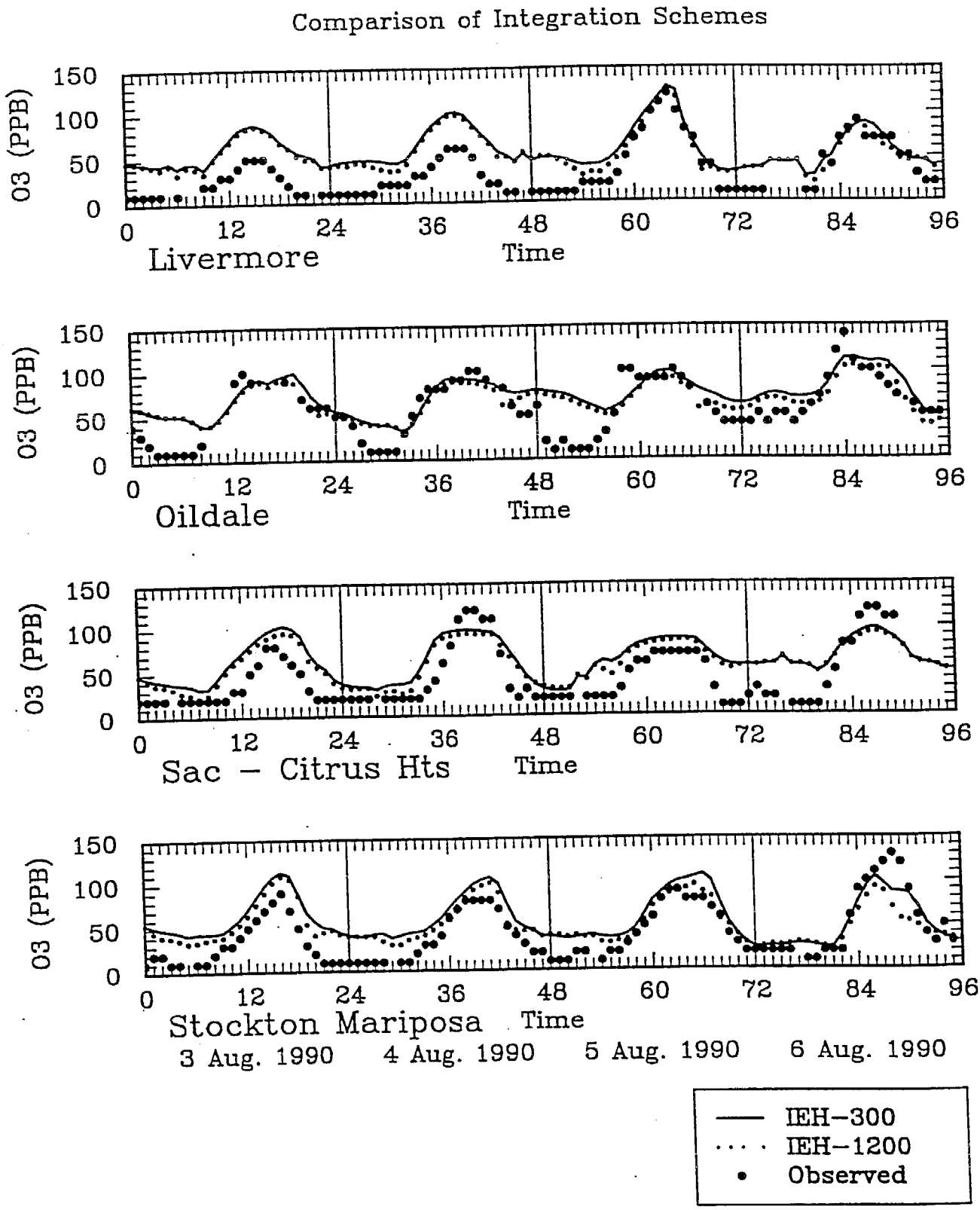

Figure 3-10. Time-series plots of O_3 comparing results from SAQM-300 and SAQM-1200.

Page 3 of 3

4. INCORPORATION OF AEROSOL SPECIES IN SAQM

4.1 OVERVIEW

The incorporation of aerosol species in acid deposition models is essential because the wet and dry deposition of particles containing sulfate, nitrate, and ammonium can affect the acidity of deposited materials. In this study, the SAQM model was extended to treat aerosol species of importance in California. The extension involved adding an aerosol module to simulate the gas-aerosol partitioning of relevant species, the evolution of the aerosol size distribution (optionally), the production of secondary organic aerosol species, and the dry deposition of particles. The version of the model with aerosol species is referred to as SAQM-AERO.

The approach used for the extension was to implement the aerosol module developed for the UAM-AERO model (Lurmann et al., 1997; Kumar et al., 1996) into the SAQM model. This approach is computationally efficient (at least when it is run with a single aerosol size section) and incorporates a level of physical and chemical detail that is appropriate for grid models. The major features of this aerosol module are:

- Simulation of the aerosol concentrations of all the major primary and secondary components of atmospheric particulate matter (PM), including sulfate, nitrate, ammonium, chloride, sodium, elemental carbon, organic carbon, water, and other crustal material.
- A sectional approach for characterization of the continuous aerosol size distribution, typically extending from 0.01 to 10 μm for aerosols and from 0.01 to 30 μm when fog droplets are present, with user-specified size bins. The model can also be applied with a single aerosol size bin.
- The internally mixed aerosol assumption, where all particles in a specific size range are assumed to have the same chemical composition.
- An algorithm to simulate the mass transfer occurring between the gaseous and aerosol species during condensation and evaporation. The effects of nucleation and coagulation are ignored in the algorithm.
- An algorithm to simulate the distribution of aerosol species concentrations based on the thermodynamics of the sulfate/nitrate/chloride/ammonium/sodium/water chemical system encoded in the SEQUILIB aerosol module (Pilinis and Seinfeld, 1987; Pandis, 1996).
- Production of condensable organic species from oxidation of gaseous organic compounds based on the organic aerosol yields reported by Pandis et al. (1992).
- An algorithm to approximate effects of fogwater condensation and evaporation on the growth and shrinkage of the aerosol/fog droplet-size distribution.

- An algorithm to simulate particle deposition and gravitational settling for particles of various sizes.
- Incorporation of ammonia (NH_3) and hydrochloric acid (HCl) as gas-phase species in the model. These species only interact with the aerosol phase because the gas-phase reactions of ammonia and HCl are of negligible importance relative to their interactions with the aerosol phase.

4.1.1 Aerosol Thermodynamics

The inorganic and organic aerosol species are distributed among the aerosol and gas phases by assuming that thermodynamic equilibrium is established over time scales smaller than the 5- to 15-minute operator-splitting time step used in the model. Stelson et al. (1979) postulated that ammonium nitrate aerosol constituents should be in thermodynamic equilibrium with the local gas phase. Hildemann et al. (1984) found that particulate and gaseous concentrations at some inland sites in the Los Angeles Basin agreed with the thermodynamic equilibrium assumption. Wexler and Seinfeld (1990) predicted that the more volatile inorganic components of atmospheric aerosols may not be in equilibrium with their gas-phase counterparts due to mass transfer limitations under some atmospheric conditions (e.g., low temperatures and low particle number concentrations) and found support for their predictions in some of the Southern California Air Quality Study (SCAQS) data (Wexler and Seinfeld, 1992). Testing was performed to determine the practicality of including detailed mass transfer calculations in the aerosol module and the results suggested the computational burden for simulating the detailed mass transfer calculation was large and impractical (Wexler et al., 1994). Thus, the gas-aerosol equilibrium assumption is employed in the model, despite the potential error introduced in certain cases.

The inorganic multicomponent atmospheric aerosol equilibrium model, SEQUILIB, of Pilinis and Seinfeld (1987) with recent updates (Pandis, 1996) is used for the calculation of the total quantities of ammonium, chloride, nitrate, and water contained in atmospheric particles. The model predicts the gas-phase concentrations of NH_3, HCl, HNO_3, and the aerosol-phase concentrations of H_2O, NH_4^+, $SO_4^=$, NO_3^-, Na^+, Cl^-, HSO_4^-, H_2SO_4, Na_2SO_4, $NaHSO_4$, NaCl, $NaNO_3$, NH_4Cl, NH_4NO_3, $(NH_4)_2SO_4$, NH_4HSO_4, and $(NH_4)_3H(SO_4)_2$ using the equilibrium relationships shown in **Table 4-1**. It uses the Bromley method to obtain multicomponent activity coefficients (Bromley, 1973) and the Pitzer method to obtain the binary activity coefficients (Pitzer, 1979). Kim et al. (1993a, 1993b) suggest that the Pitzer method is more accurate than the Bromley method for multicomponent activity coefficients and that the K-M method (Kusik and Meissner, 1978) may be more accurate than the Pitzer method for binary activity coefficients. Given the paucity of high-concentration laboratory data on which to evaluate their performance, the activity coefficient calculation methods originally coded in SEQUILIB were used. The water activity coefficients are obtained using the ZSR method (Stokes and Robinson, 1966). The equilibrium code has been relatively successful in predicting the concentrations of the various aerosol species in the Southern California Air Basin (SoCAB) (Pilinis and Seinfeld, 1987, 1988) and elsewhere (Watson et al., 1994).

Table 4-1. Equilibrium relations in the SEQUILIB aerosol module.

Reaction	Equilibrium Constant
$NaCl(s) + HNO_3(g) \leftrightarrow NaNO_3(s) + HCl(s)$	$3.96 \exp\left[5.50\left(\frac{T_o}{T}-1\right) - 2.180\left(1+\ln\left(\frac{T_o}{T}\right)-\frac{T_o}{T}\right)\right]$
$NH_3(g) + HNO_3(g) \leftrightarrow NH_4^+ + NO_3^-$	$3.99 \times 10^{17} \exp\left[64.7\left(\frac{T_o}{T}-1\right) + 11.51\left(1+\ln\left(\frac{T_o}{T}\right)-\frac{T_o}{T}\right)\right] mol^2Kg^{-2}atm^{-2}$
$HCl(g) \leftrightarrow H^+ + Cl^-$	$2.03 \times 10^{6} \exp\left[30.21\left(\frac{T_o}{T}-1\right) + 19.91\left(1+\ln\left(\frac{T_o}{T}\right)-\frac{T_o}{T}\right)\right] mol^2Kg^{-2}atm^{-1}$
$NH_3(g) + HCl(g) \leftrightarrow NH_4^+ + Cl^-$	$2.12 \times 10^{17} \exp\left[65.08\left(\frac{T_o}{T}-1\right) + 14.51\left(1+\ln\left(\frac{T_o}{T}\right)-\frac{T_o}{T}\right)\right] mol^2Kg^{-2}atm^{-2}$
$Na_2SO_4(s) \leftrightarrow 2Na^+ + SO_4^{2-}$	$0.4805 \exp\left[0.98\left(\frac{T_o}{T}-1\right) + 39.57\left(1+\ln\left(\frac{T_o}{T}\right)-\frac{T_o}{T}\right)\right] mol^3Kg^{-3}$
$(NH_4)_2SO_4(s) \leftrightarrow 2NH_4^+ + SO_4^{2-}$	$1.425 \exp\left[-2.65\left(\frac{T_o}{T}-1\right) + 38.55\left(1+\ln\left(\frac{T_o}{T}\right)-\frac{T_o}{T}\right)\right] mol^3Kg^{-3}$
$HSO_4^- \leftrightarrow H^+ + SO_4^{2-}$	$1.031 \times 10^{-2} \exp\left[7.59\left(\frac{T_o}{T}-1\right) + 18.83\left(1+\ln\left(\frac{T_o}{T}\right)-\frac{T_o}{T}\right)\right] mol\,Kg^{-1}$
$HNO_3(g) \leftrightarrow H^+NO_3^-$	$3.638 \times 10^{6} \exp\left[29.47\left(\frac{T_o}{T}-1\right) + 16.84\left(1+\ln\left(\frac{T_o}{T}\right)-\frac{T_o}{T}\right)\right] mol^2Kg^{-2}atm^{-1}$
$NH_4Cl(s) \leftrightarrow NH_3(g) + HCl(g)$	$1.039 \times 10^{-16} \exp\left[-71.04\left(\frac{T_o}{T}-1\right) + 2.40\left(1+\ln\left(\frac{T_o}{T}\right)-\frac{T_o}{T}\right)\right] atm^{-2}$
$NH_3(g) + HNO_3(g) \leftrightarrow NH_4NO_3(s)$	$3.349 \times 10^{16} \exp\left[75.11\left(\frac{T_o}{T}-1\right) - 13.46\left(1+\ln\left(\frac{T_o}{T}\right)-\frac{T_o}{T}\right)\right] atm^{-2}$
$NaNO_3(s) \leftrightarrow Na^+ + NO_3^-$	$11.971 \exp\left[-8.22\left(\frac{T_o}{T}-1\right) + 16.01\left(1+\ln\left(\frac{T_o}{T}\right)-\frac{T_o}{T}\right)\right] mol^2Kg^{-2}$
$NaCl(s) \leftrightarrow Na^+ + Cl^-$	$37.743 \exp\left[-1.57\left(\frac{T_o}{T}-1\right) + 16.89\left(1+\ln\left(\frac{T_o}{T}\right)-\frac{T_o}{T}\right)\right] mol^2Kg^{-2}$
$NaHSO_4(s) \leftrightarrow Na^+ + HSO_4^-$	$2.44 \times 10^{4} \exp\left[0.79\left(\frac{T_o}{T}-1\right) + 4.53\left(1+\ln\left(\frac{T_o}{T}\right)-\frac{T_o}{T}\right)\right] mol^2Kg^{-2}$

Thermodynamic equilibrium is also assumed for the condensable organic vapors. When their gas-phase concentrations exceed their vapor pressure, the vapors condense to the aerosol phase in an effort to establish equilibrium. Evaporation occurs when the gas phase is subsaturated. Following Pandis et al. (1992), the aerosol module assumes a negligibly small saturation vapor pressure (0.1 ppt), which essentially places all of the condensable organic material in the aerosol phase. Due to the physical and chemical uncertainties in the secondary organic aerosol species, no attempt is made to estimate the amount of water absorbed or desorbed by the organic particles. Saxena et al. (1995) have shown that condensed organic species can alter the hygroscopic behavior of atmospheric particles, and alterations may be positive or negative depending on the location (nonurban or urban). These differential water absorption effects are not included in the model.

4.1.2 Modeling the Aerosol Size Distribution

The model can be applied using one or more size bins. In theory, simulation of the aerosol size distribution is necessary to accurately simulate the physical and chemical evolution of the aerosol, and the aerosol removal by deposition. When the model is applied to simulate the aerosol size distribution, it is generally recommended that the model be run with at least eight sections below 10 μm and one section above 10 μm if fogs occur in the simulation period. Usually these sections are logarithmically spaced as in the sample distribution shown below, however, the aerosol model algorithm can accommodate arbitrarily spaced size bins.

Bin No.	Lower Limit D_p (μm)	Mean Diameter (μm)	Upper Limit D_p (μm)	Surface Area ($cm^2/\mu gm$)
1	0.0390625	0.055	0.078125	0.905
2	0.0781250	0.110	0.156250	0.453
3	0.1562500	0.220	0.312500	0.226
4	0.3125000	0.441	0.625000	0.113
5	0.6250000	0.883	1.250000	0.057
6	1.2500000	1.767	2.500000	0.028
7	2.5000000	3.535	5.000000	0.014
8	5.0000000	7.071	10.00000	0.007
9	10.000000	17.32	30.00000	0.003

Using more than eight or nine sections is highly desirable, but the user should expect proportional increases in the CPU times for simulations. With the numerical methods incorporated into the model, using fewer than eight aerosol size sections can lead to excessive pseudo-diffusion of particles between size bins. For ambient PM modeling, it is important to include size sections to represent the dominant aerosol modes: the nuclei mode, the accumulation mode, and the coarse mode. The nuclei mode corresponds to particles below 0.1 μm in diameter and is associated with fresh combustion emissions. The accumulation mode corresponds to particles approximately 0.1 to 2 μm in diameter and is associated with particles originating from aged combustion sources, photochemical processes, and smaller fog or cloud droplets. The coarse mode corresponds to particles above 2 μm and is associated with wind

blown dust, mechanically generated aerosols, and larger fog and cloud droplets. Note, most of the surface area of ambient particles occurs in the particles with diameters below 0.2 or 0.3 μm and it is important to include sufficient size resolution to represent these particles.

In SAQM-AERO, the size bins are always ordered by increasing size and the output concentration file contains all of the species in the first section followed by all of the species in the second section, etc. The user specifies the number of aerosol sections, the number of fog droplet sections, the lower limit diameter for the first aerosol size section, and the upper limit diameters for all of the sections. Note, the lower limit on the first size section is artificial. All particles with diameters smaller than the first upper limit diameter are represented in the first size section. The first lower limit diameter is needed to calculate a representative mean diameter for the first size section. The mass mean diameter of each section is calculated as the square root of the product of the lower limit and upper limit diameters.

There is a significant computational burden associated with simulation of the aerosol size distribution. For example, increasing the number of aerosol size sections from one to nine increases the overall model execution time by a factor of 5 to 10. This large increase in CPU time occurs not only because the number of transported species increases (10 transported species for each size bin), which affects all operators except the gas-phase chemistry, but also because the number of aerosol thermodynamic calculations increases in proportion to the number of size bins. We have found in applications of the UAM-AERO model to the SoCAB that the PM_{10} response to regional changes in VOC, NO_x, SO_2, NH_3, and particle emissions is quite similar in one and nine section simulations (Lurmann and Kumar, 1997). Thus, for PM_{10} analyses, one can run the model with a single aerosol size section to explore various emission control options (i.e., screening runs) and then perform refined simulations that include size resolution for the most important emission control strategies. Incorporation of aerosol size resolution is recommended for $PM_{2.5}$ and visibility analyses.

The aerosol module implemented in SAQM uses the internally mixed assumption for aerosol composition. The aerosol size composition is discretized in size sections and all particles in each section are assumed to have the same chemical composition (Gelbard et al., 1980; Seigneur et al., 1986). The movement of these sections in the size coordinate, as a result of particle growth and shrinkage (i.e., by gas-to-particle conversion, condensation, or evaporation), is initially calculated using the moving section technique (Gelbard, 1990; Kim and Seinfeld, 1990). With the moving section technique, the number of particles in each size bin is constant during the aerosol transport step and the changes in mass due to condensation or evaporation are reflected in new mass mean diameters for the sections. In some situations where a large amount of mass is being transported between the gas and aerosol phases, multiple aerosol transport steps are taken to assure numerical stability. However, because the three-dimensional air quality model requires fixed aerosol size bins for the advection and diffusion steps, the mass in the new size distribution is reallocated to the original size bins using a mass-conserving cubic spline-fitting procedure.

The gas-aerosol transport is calculated as follows. The single particle flux (J_i) of condensate or evaporate is

$$J_i = \frac{2\pi D_p D_i (C_{ai} - C_{ei})}{1 + \beta} \tag{4-1}$$

where D_p is the particle diameter, D_i is the molecular diffusivity of the condensing or evaporating compound i, and C_{ai} - C_{ei} is the difference between the ambient concentration (C_{ai}) and the equilibrium particle surface concentration (C_{ei}). Beta is defined as

$$\beta = \frac{2\lambda}{\alpha D_p} \tag{4-2}$$

where λ is the mean free path of air and α is the accommodation coefficient. In the model, gases are transported to particles of diameter D_p at a rate given by Equation 4-1. The overall transport rate to a size section (nJ_i) depends on the number of particles in the section, $n(D_p)$, and the single-particle transport rate. The fraction of condensate that appears in each size section, f, is given by

$$f = \frac{2n\pi D_p D_i (C_{ai} - C_{ei}) / (1 + \beta)}{\int_0^\infty 2n\pi D_p D_i (C_{ai} - C_{ei}) / (1 + \beta) d D_p} \tag{4-3}$$

In general, C_{ei} depends on chemical composition of the aerosol in each size section, but in the aerosol module used in the UAM-AERO model C_{ei} is determined from an aerosol equilibrium calculation for the total aerosol chemical composition. When the concentration difference (C_{ai} - C_{ei}) is independent of particle size, the transport factor expression reduces to

$$f = \frac{n D_p / (1 + \beta)}{\int_0^\infty n D_p / (1 + \beta) d D_p} \tag{4-4}$$

where β depends on the particle size and accommodation coefficient. The accommodation coefficient has been estimated to range from near unity, for water molecules condensing on water, to 10^{-4}. Changes in accommodation coefficient independent of particle size alter the size distribution of the condensate. Smaller values of the accommodation coefficient favor condensation on larger particles. Based on the work of Pandis et al. (1993), an accommodation coefficient of one is used for water and all other aerosol species in the aerosol module.

To predict the size distribution of the condensable compounds, the model first calculates the gas-phase concentrations of these compounds resulting from transport and chemical reactions. For the inorganic compounds, the equilibrium concentrations of the total aerosol and

vapors are determined from SEQUILIB. The amount condensed or evaporated is partitioned among the sections in accordance with Equation 4-3. SEQUILIB is then used again to obtain improved estimates of the water content of each aerosol section. As a result of the condensation or evaporation, the aerosol size sections grow or shrink. Then, the mass in the new size distribution is reallocated to the original size bins using a mass-conserving cubic spline-fitting procedure. The cubic spline reallocation procedure is numerically robust, however, it introduces some pseudo dispersion into the size distributions. That is, the predicted size distributions are somewhat smoother or broader than may exist in the ambient atmosphere. During periods of rapidly increasing or decreasing moisture, the gas-aerosol transfer and resizing is performed using small time steps to ensure the size distribution evolves in a stable manner.

The individual steps and logic in the aerosol module are shown schematically in **Figure 4-1**. The aerosol module performs the following nine steps each time it is called:

1. Each size section of the aerosol is neutralized.
2. The number density for each size section is calculated.
3. The thermodynamic routine is called to calculate the equilibrium composition.
4. The transport factors are calculated, which apportion mass according to the product of diffusional resistance and number of particles for each section.
5. The species are transported using the previously calculated transport factors and the difference between the equilibrium values and the initial values.
6. Each size section is neutralized a second time.
7. The equilibrium routine is called to calculate the water content for each section.
8. New section mean diameters and cut point diameters are calculated.
9. The new size distribution is fitted to a cubic spline for each aerosol component and the distribution is reapportioned to the initial size sections using numerical integration.

If the thermodynamic routine predicts that a significant amount of mass should be transported between the phases, there is the possibility that the change in size of one section could overtake the size of the next higher section. In these situations, the transport factors are reduced and a smaller amount of mass is transported in multiple time steps. This same reduction is also applied to the fraction of water transported to achieve equilibrium. If this step is successful without sectional overlap, then the resulting distribution is fitted to a cubic spline and the aerosol mass is reapportioned to the original size sections. The transport factors are then increased and the number density for the new distribution is calculated. Then the transport step is repeated. Under extreme situations where concentrations are far from equilibrium, up to five gas-aerosol transport steps (about 2 minutes each) are needed to transport the material in a numerically stable manner.

When the model is run with aerosol size resolution, the aerosol module is called at each time step (which is 5 minutes in the summer SJV application using 12 x 12 km grids). It needs to be called frequently in order to integrate the growth and shrinkage of the size distribution properly. When the model is run with a single aerosol size section (0-10 μm), the aerosol module can be called less frequently (the frequency is a user-selected input). Comparable

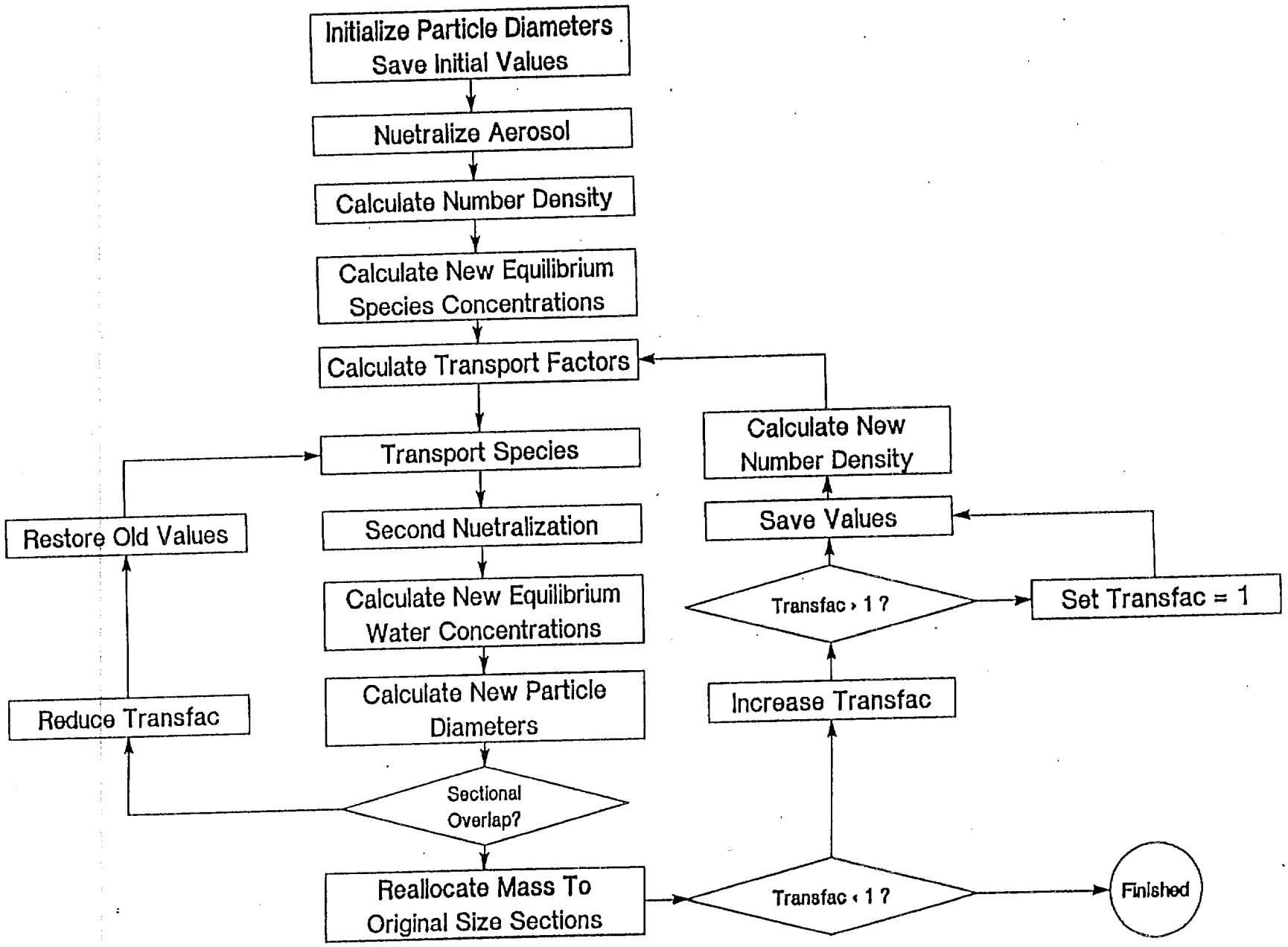

Figure 4-1. Schematic of the individual steps and logic in the aerosol module.

results were obtained when the aerosol module was called at 5 and 20 minute intervals in the summer SJV simulations.

4.1.3 Secondary Organic Aerosol Production

For this application, the CB-IV chemical mechanism was extended to include production of condensable organic species from higher molecular weight (C5+) gaseous VOCs. The condensable organic compound (COC) yields for the lumped organic compounds are obtained from the database of individual compound yields reported by Pandis et al. (1992) and the composition of the regional VOC emission inventories. The knowledge of the chemical composition of most condensable vapor products and the exact chemical pathways leading to their formation, including the stoichiometry and rate constants, remains incomplete. Therefore, the mechanistic description of the production of low-volatility products follows the condensed gas-phase mechanisms used in regional photochemical models. The atmospheric oxidant of a hydrocarbon, HC, by an oxidant like OH, O_3, or NO_3 is described by a single reaction that incorporates all the individual mechanistic steps

$$\text{HC} + \text{Oxidant} \longrightarrow aA + bB + \ldots + gG \qquad \textbf{(4-2)}$$

where A, B, etc., are the regular gaseous products, G is a generic condensable gas that forms secondary organic aerosol, and g is the corresponding stoichiometric coefficient. The stoichiometric coefficient g is approximately equivalent to the fractional aerosol yield, Y, of the hydrocarbon. Experimental measurements of the aerosol yields, Y, are available from the literature for numerous hydrocarbons and estimates of the yields of the remaining hydrocarbons are provided by Grosjean and Seinfeld (1989) and Pandis et al. (1992). The aerosol yields from the lumped organics included in the CB-IV chemical mechanism were developed for the 1987 SCAQS Volatile Organic Carbon (VOC) and are shown in **Table 4-2**. These data indicate that toluene, xylene, cresols, and monoterpenes have the highest secondary organic aerosol yields.

The organic species lumping scheme in the CB-IV mechanism was selected to model ozone with the fewest possible organic species (Gery et al., 1988). It was designed to distinguish the major differences in photochemical reactivity of organic compounds rather than differences in aerosol production rates. Although there is often little relationship between the secondary aerosol yields and photochemical reactivity, the representation of aromatic species in the CB-IV mechanism is adequate for modeling secondary aerosol production from these species. The treatment of paraffinic compounds is not ideal, yet probably acceptable because the yields from these compounds are not large. The CB-IV mechanism's highly condensed representation of olefins is not adequate because the C_{10} monoterpenes, which produce large amounts of aerosol, are lumped with other small olefins (e.g., propylene) that do not produce aerosols. Thus, a second class of olefins (OLE2) was added to the chemical mechanism to represent monoterpenes. The reactions for the OLE2 class have a large aerosol yield (740 $\mu g/m^3/ppm$) compared to the anthropogenic olefins (OLE), which have a small aerosol yield (20 $\mu g/m^3/ppm$). Rather than implementing a gas-phase mechanism specifically for

monoterpenes, the existing reaction scheme for OLE was duplicated for the second class of olefins, which provides consistency with the original treatment of monoterpenes. The individual monoterpene species assignments to CB-IV species, shown in **Table 4-3**, is identical to the original assignments with the exception that OLE2 is substituted for OLE. Note, virtually all of the aerosol yield from the monoterpene is associated with the OLE2 species even though it only has two carbons. The specific aerosol producing reactions included in the model are shown in **Table 4-4**.

Table 4-2. Secondary organic aerosol yields for the CB-IV chemical mechanism organic classes.

Species	Description	Numbers of Carbons	Aerosol Yield[a]
PAR	Paraffinic bonds	1	8
TOL	Toluene	7	402
XYL	Xylene	8	416
CRES	Cresols and other alkyl phenols	7	221
OLE	Anthropogenic olefinic bonds	2	20
OLE2	Biogenic C10 monoterpenes	2	740
FORM	Formaldehyde	1	0
ALD	Acetaldehyde	2	0
ETH	Ethene	2	0
ISOP	Isoprene	5	0

[a] Aerosol yields are in $\mu g\ m^{-3}\ ppm^{-1}$ of aerosol mass, including carbon, hydrogen, oxygen, etc. (not just carbon). The individual component yields are from Pandis et al. (1992). The lumped compound yields are based on the VOC composition of the 1987 regional emissions inventory for the South Coast Air Basin.

Table 4-3. Assignment of C10 biogenic species emissions to CB-IV compound classes.

Species	SAROAD	OLE2	ALD	PAR
Terpenes	43123	1	0	8
Beta-Pinene	98026	1	0	8
D-limonene	98027	1	2	4
Alpha-Pinene	98025	0.5	1.5	6
Terpinene	98079	0.5	1.5	6
3-Carene	99021	0.5	1.5	6

Table 4-4. Aerosol production reactions for the CB-IV mechanism.

PAR + OH	---> .87XO2 + .13XO2N + .11HO2 + .11ALD2 + .76ROR -.11PAR + 8.COC
OLE + O	---> .63ALD2 + .38HO2 + .28XO2 + .30CO + .2FORM +.02XO2N + .22PAR + .2OH + 20.COC
OLE + OH	---> FORM + ALD2 + HO2 + XO2 - PAR + 20.COC
OLE + O3	---> .5ALD2 + .74FORM + .33CO - PAR + .1OH + .44HO2 + .22XO2 + 20.COC
OLE + NO3	---> NO2 + FORM ALD2 + .91XO2 + .09XO2N -PAR + 20.C0C
OLE2 + OH	---> FORM + ALD2 + HO2 + XO2 - PAR + 740.COC
OLE2 + O3	---> .5ALD2 + .74FORM + .33CO - PAR + .1OH + .44HO2 + .22XO2 + 740.COC
OLE2 + NO3	---> NO2 + FORM ALD2 + .91XO2 + .09XO2N -PAR + 740.C0C
TOL + OH	---> .08XO2 + .36CRES + .44HO2 + .56TO2 + 402.COC
CRES + OH	---> .4CRO + .6XO2 + .6HO2 + .3OPEN +221.COC
XYL + OH	---> .7HO2 + .5XO2 + .2CRES + .8MGLY + PAR + .3TO2 +416.COC

The vapor pressures of the secondary organic aerosol (SOA) species are not well known and, for simplicity, we assume they are negligibly small. With this assumption, the gaseous condensable organic species (COC) is transferred to the organic material (OM) aerosol species each time the aerosol module is called. The model could be set up to track the primary and secondary OM separately, however, currently it aggregates them as a single OM species.

4.1.4 Dry Deposition of Particles

The dry deposition of particles to surfaces may occur from diffusion, impaction, and/or gravitational settling. The dominant mechanism for particle deposition varies with the particle size. In the aerosol module, particle deposition velocities are calculated from the following equation recommended by Slinn and Slinn (1980)

$$v_d^i = \frac{1}{r_a + r_d^i + r_a\, r_d^i\, v_g} + v_g^i \qquad \textbf{(4-6)}$$

where
v_d^i = deposition velocity (m/s) of particles of the ith size bin
r_a = aerodynamic resistance (s/m)
r_d^i = deposition layer resistance (s/m) of particles of the ith size bin
v_g^i = gravitational settling velocity (m/s) of particles of the ith size bin

Particle diffusion in the thin, quasi-laminar deposition layer just above the surface is principally due to Brownian diffusion and inertial impaction. Particles transported through this layer are assumed to stick to the surface (Voldner et al., 1986). The resistance to diffusion through this layer (r_d) is parameterized in terms of the Schmidt number and the Stokes number. The deposition layer resistance is given by

$$r_d^i = \frac{1}{u_*(Sc^{-2/3} + 10^{-3/St})}$$

$$S_c = \frac{\nu}{D} \quad \textit{(Schmidt number)} \qquad \textbf{(4-7)}$$

$$S_t = \frac{v_g^i u_*^2}{\nu g} \quad \textit{(Stokes number)}$$

where
ν = viscosity of air
D = Brownian diffusivity
v_g^i = gravitational settling velocity (of the ith particle-size bin)
u_* = friction velocity

The gravitational settling velocity is calculated from

$$v_g = \frac{D_p^2 g C(\rho_p - \rho_g)}{18\nu}$$

$$C = 1 + \frac{2\lambda}{D_p}\left[1.257 + 0.4\exp\left(\frac{-0.55 D_p}{\lambda}\right)\right] \qquad \textbf{(4-8)}$$

where
D_p = particle diameter (m), mean diameter of particle-size bin
ρ_p = particle density (g/m^3)
ρ_g = air density (g/m^3)
g = acceleration due to gravity (m/s^2)
C = Cunningham correction factor for small particles
λ = mean free path of air (m)
ν = viscosity in g/m-s

Deposition in the constant-flux, surface layer, which is the next 10 to 20 m above the deposition layer, is a function of the atmospheric turbulence (or stability) and the surface characteristics. The aerodynamic resistance (r_a) is the same for gases and particles, and is calculated from

$$r_a = \frac{1}{k\,u_*}\left[\ln\left(\frac{z_s}{z_o}\right) - \phi_H(L, z_s)\right] \qquad \textbf{(4-9)}$$

where
z_s = reference height (m)
z_o = surface roughness height (m)

k = von Karman constant (0.4)
ϕ_H = stability correction term
L = Monin-Obukhov length (m)

Figure 4-2 shows experimental data for size dependence of particle deposition velocities. The data indicate that particles with diameters less than 0.015 μm and greater than 2 μm have significant deposition velocities, while particles in the 0.015- to 2-μm range do not. The reason for this behavior is that small particles ($D_p < 0.015$ μm) behave much like gases and are efficiently transported across the deposition layer by Brownian diffusion. Brownian diffusion is not an effective transport mechanism for particles with diameters above 0.05 μm. Moderately large particles in the 2- to 20-μm-diameter range are efficiently transported across the deposition layer by inertial impaction and the deposition of even larger particles ($D_p >$ 20 μm) is principally due to gravitational settling. Since the settling velocity increases with the square of the particle diameter, large particles (and fog droplets) have relatively high deposition velocities. There are no effective transport mechanisms for particles in the 0.015 to 2-μm-diameter range, the size range for most secondary aerosols in the atmosphere. The atmospheric lifetimes of these particles may be many days unless they are scavenged by fog or precipitation. In the aerosol module, the deposition velocities of all particles in a specific size bin are calculated using the geometric mass mean diameter of the size section. The deposition velocities are calculated at each time step of the simulation. If the model is applied using only one size section, the model assumes the aerosol size is log-normally distributed for each component. It uses internally stored geometric-mass mean diameters (D_p^{mean}) and geometric standard deviations (σ_d) for each chemical component to compute a mass-weighted average deposition velocity based on nine calculations of deposition velocities for diameters between $D_p^{mean} - 2\sigma_d$ and $D_p^{mean} + 2\sigma_d$. The size distributions for one-section simulations are spatially and temporally invariant; however, separate size parameters are input for each aerosol component.

4.2 IMPLEMENTATION OF THE AEROSOL MODULE IN THE SAQM

The aerosol module was implemented in the SAQM after the IEH solver had already been implemented (see Section 3). The gas-phase chemical mechanism was slightly modified to add ammonia (NH_3), hydrochloric acid (HCl), condensable organic compounds (COC), and OLE2 as new species. NH_3 and HCl only interact with the aerosol phase and their gas-phase reactions are too slow to be included. After modifying the chemical mechanism in the model, the aerosol module was extracted from the UAM-AERO model and implemented in the SAQM. This process was mostly straightforward as the aerosol module is a stand-alone package. The only other changes required were in implementing the emission and deposition of aerosol species and changing the gas-phase host model (the SAQM-IEH in this case) to account for new variables and to add calls to new subroutines. Additional changes were required in the transport algorithms to account for minor differences in the logic for treating gas-phase and aerosol-phase species. The modifications of the source code are described in detail in Appendix A. A brief overview of the implementation of the main modules is

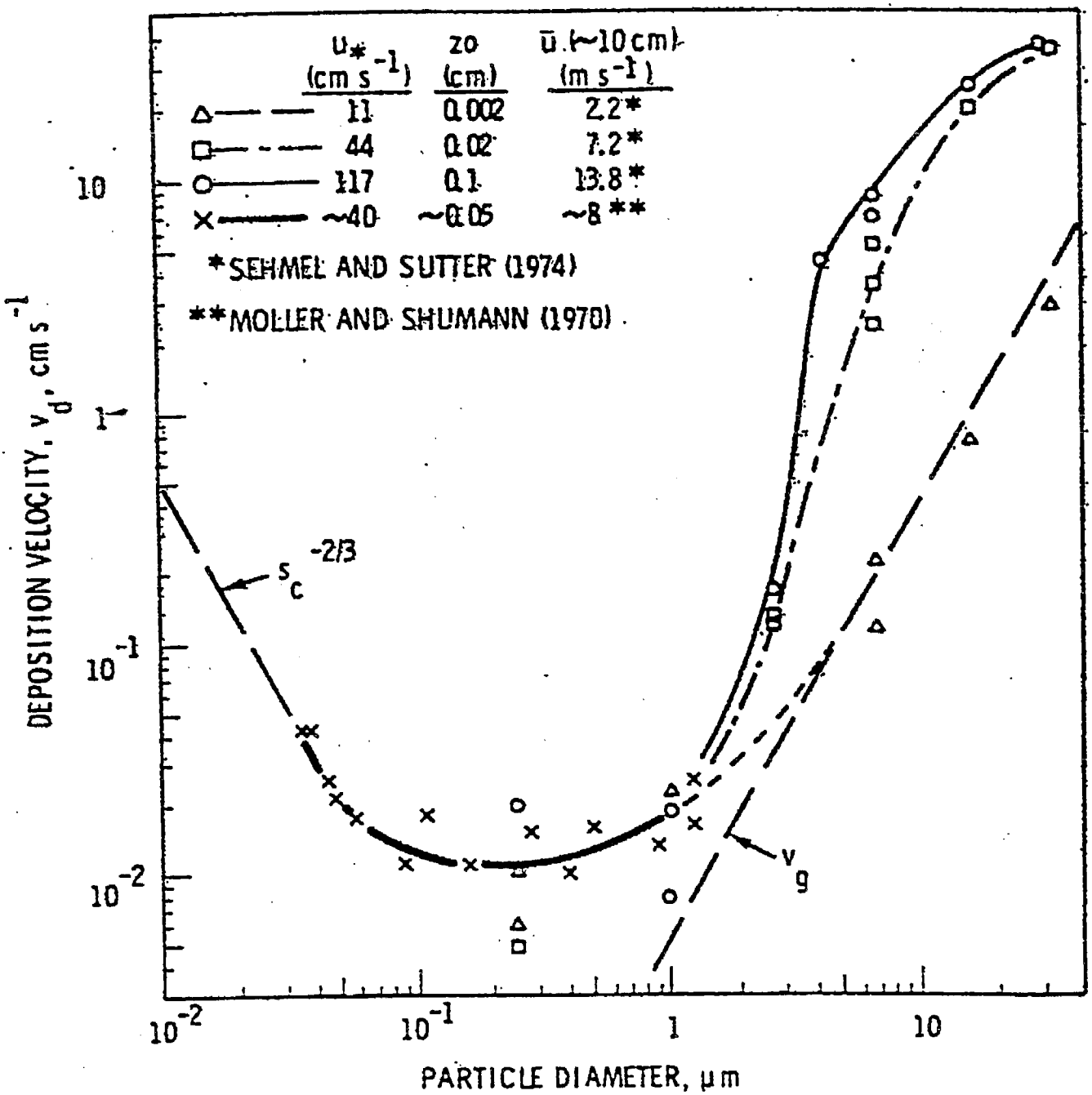

Figure 4-2. Experimental data for size dependence of particle deposition velocities.

presented here. The aerosol module was first implemented in the old single surface layer model. Subsequently, the aerosol module was implemented in the surface sub-layer model.

Subroutine AEROAQ is the main subroutine for the aerosol module which calls other routines. The source code for the aerosol module contains other subroutines which are TEEQ, EQUILIB, SPLINE, and various utility subroutines. TEEQ calculates equilibrium partition between gas and aerosol phases. It calls the subroutine EQUILIB which determines the equilibrium concentrations of the total aerosol and vapors. Subroutine SPLINE is used to reallocate the aerosol mass in new size distribution (calculated in EQUILIB) to the original size bins. Subroutine SPLINE uses a mass-conserving cubic spline-fitting procedure.

The logic to incorporate emission and deposition of aerosol species are not included in subroutine AEROAQ and were implemented separately. Subroutine ADDAEREM was written to add the aerosol emissions to the concentration arrays as a step function increase in the species concentrations. This subroutine is called every time step after the chemistry operator. To model particle deposition, subroutines VDEP and PBLMOD were extracted from the UAM-AERO and implemented in the SAQM. Subroutine PBLMOD calculates the friction velocity, Monin-Obhukov length, and 10 m wind speed. This subroutine is called before deposition velocities for the aerosol species are calculated using the subroutine VDEP. Subroutine ADDDEP was written to simulate the effect of dry deposition on the concentrations at each time step.

Data and logic were incorporated into the model to define the aerosol species and gas-phase species which interact with the aerosol species. The file "blk_dat3.f" contains FORTRAN block data, which define the names of the aerosol species and the names of the condensable gas-phase species, and a subroutine, BLOCK, which is called at the beginning of the simulation. Subroutine BLOCK adds extensions to the names of the aerosol species based on the number of size sections used in a specific simulation. For example, sodium is defined as "NA+" in the block data and subroutine BLOCK assigns the names "NA+1", "NA+2", ... "NA+9" for sodium in sections 1 through 9, where section 1 is the smallest section.

One common block include file and three parameter include files contain much of the interface between the host model and the aerosol routines. The include files are named "a_aero.com", "dep.inc", "nsect.inc", and "param.inc". The file "a_aero.com" contains the main common block statements specific to the aerosol module. The file "dep.inc" contains the common block statements required for particle deposition routines. The file "nsect.inc" contains the parameter statements specifying the number of sections, number of droplet sections, number of aerosol species, number of emitted aerosol species, and common block statements for the aerosol species names. The file "param.inc" contains more parameter statements specific to the aerosol module. **Figure 4-3** shows the files "nsect.inc" and "param.inc" used in the model. **Table 4-5** describes the parameters which are important from the user's point of view.

```
c Sample nsect.inc file
      parameter (nsect = 1, ndrop=0) ! No. aerosol and droplet sections
      parameter (naspec= 10) ! No. aerosol species per section
      parameter (LAEROEM = 6*NSECT)! Number of aerosol emission species
c
      character*10 specnm(naspec),aeroname(naspec*(nsect+ndrop))
      integer mapaemis(NASPEC*NSECT)
c
      common /specname/ specnm, aeroname
      common /aeroem/ mapaemis
```

```
c Sample "param.inc" file
      parameter(ngmax = 50)      ! maximum number of gas-phase species
      parameter(namax = 10)      ! maximum number of aerosol components
      parameter(nsectmax = 9)    ! maximum number of total sections
      parameter (ngspec = 5)     ! number of condensable gas-phase species
c useful constants
      parameter (pi6 = 3.1415927/6.0)    ! pi
      parameter (rhopart    = 1.2e6)          ! particle density [ g/m^3]
c
      common /diameter/ dp(nsectmax),dps(nsectmax),dpb(nsectmax+1),
     1                  dpm(nsectmax+1)
c
c condensable gas-phase components in local arrays
c
      parameter (ngca =  1)       ! ammonia
      parameter (ngcn =  2)       ! nitric acid
      parameter (ngcc =  3)       ! hydrochloric acid
      parameter (ngc4 =  4)       ! gas-phase sulfate
      parameter (ngco =  5)       ! gas-phase organics
      parameter (ngcspec = ngspec)          ! alternative name
c aerosol species addresses
      parameter (kaena  = 1)      ! sodium
      parameter (kaeh   = 2)      ! hydrogen
      parameter (kaenh4 = 3)      ! ammonium
      parameter (kaeno3 = 4)      ! nitrate
      parameter (kaecl  = 5)      ! chloride
      parameter (kaeso4 = 6)      ! sulfate
      parameter (kaewat = 7)      ! water
      parameter (kaeec  = 8)      ! elemental carbon
      parameter (kaeo   = 9)      ! organic carbon
      parameter (kaecr  = 10)     ! crustal
c number of condensable organic gas-phase species
      parameter (norg = 1)
c
c common blocks used by aerosol routines
c
      character*4 gaspecnm(ngspec)
      integer ngindex(ngspec)
      common /gasaddrs/ nga, ngn, ngc, ng4, ngo, kgso4, kgnh3,
     & kgno3, kgcl, kgal, nmgaspec, gaspecnm
      equivalence (ngindex,nga)
      common /aer2gas/ iaer2gas(namax)
      common /gfactors/ factnh4,factno3,factcl,factso4,factoc
      dimension gasfac(ngspec)
      equivalence (gasfac(1),factnh4)
      character*12 cvarrn,cvar0,cvar1,cvar2,cvar3,cvar4,cvar5,
     1 cvar6,cvar7,cvar8,cvar9,cvar10,cvar11,cvar12,cvar13
      common/cvars/cvarrn,cvar0,cvar1,cvar2,cvar3,cvar4,cvar5,
     1 cvar6,cvar7,cvar8,cvar9,cvar10,cvar11,cvar12,cvar13
      logical berror,berror0,binerr,binerr0
      common /binerror/ berror,berror0,binerr(nsectmax),
     1       binerr0(nsectmax)
      common /aerwat/ water0(nsectmax),watereq(nsectmax),
     1 waternew(nsectmax)
```

Figure 4-3. Examples of the "nsect.inc" and "param.inc" include files in the SAQM-AERO model.

Table 4-5. Description of important parameters used in the aerosol module.

Parameter	Description
NSECT	Number of aerosol sections (should match the number of sections in the header of the CHEMPARAM file)
NDROP	Number of droplet (fog) sections (should match the number of droplet sections in the header of the CHEMPARAM file)
NASPEC	Number of aerosol species, which should not be changed as it is fixed in the current version of the aerosol module
LAEROEM	Number of aerosol emission species
NGMAX	Maximum number of gas-phase species, which should be ≥ LSPEC in CHPARM.COM
NAMAX	Maximum number of aerosol components, which should be ≥ NASPEC
NSECTMAX	Maximum number of total aerosol sections, which should be ≥ (NSECT+NDROP)
NGSPEC	Number of condensable gas-phase species, which should not be changed as it is fixed in the current version of the aerosol module
NORG	Number of condensable organic gas-phase species, which should not be changed as it is fixed in the current version of the aerosol module

4.3 TESTING OF THE MODEL FOR AEROSOL SPECIES

A rigorous evaluation of an aerosol model requires a large special study aerometric database that includes meteorological, emissions, and both gas-phase and PM air quality data. The model evaluation should include testing for a variety of atmospheric conditions, including conditions with high atmospheric concentrations of PM. In the SJV, high PM concentrations usually occur in the fall and winter under cool and moist conditions that are favorable for the formation and buildup of secondary PM species, including sulfate, nitrate, and ammonium (Chow et al., 1992). High PM concentrations also occur in the summer in the SJV, however, these high concentrations are often due to local sources of wind blown dust. The summer aerosol contains mostly primary aerosol constituents, such as crustal material, organic material, and elemental carbon.

Regional models like SAQM are better suited to address source-receptor relationships for pollutants where the geographic scale of influence is urban and regional, rather than local. They are well suited to treat ozone, sulfate, and nitrate which have urban and regional scale patterns. Regional models are rarely applied with sufficient horizontal resolution to resolve local effects of primary sources of PM.

A significant problem was encountered in selecting episodes for testing the SAQM model for aerosol species; the only aerometric data suitable for testing the model were collected for a warm summer ozone episode which had little secondary PM. Our preference

was to test the model on fall and winter episodes where the model's ability to estimate secondary PM species could be evaluated. However, setting up the SAQM model inputs for one or more high PM episodes was beyond the scope of this study and the only period with the necessary daily PM data for multiday episodes was the summer AUSPEX sampling period. Hence, the model was tested against the AUSPEX data for August 3-6, 1990 (Chow et al., 1996). A benefit of selecting this episode was that the meteorological and photochemical modeling were already evaluated and refined. A disadvantage of testing against the August 3-6, 1990 period was that the secondary PM concentrations were low, especially those for ammonium nitrate, and that little would be learned regarding the model's performance in the types of episodes for which it was mostly designed to simulate.

The SAQM-AERO version of the model was applied to the August 3-6, 1990 ozone episode using the meteorological inputs derived from the MM5 model and the NO_x, VOC, CO, and SO_2 emission estimates developed for the ozone modeling. Only one aerosol size section (0-10 μm) was used for the aerosol species in order to enhance computational efficiency. A number of new model inputs were prepared for the SAQM-AERO simulations, including additional initial concentrations, boundary conditions, and emissions for other gas-phase and particle-phase species. **Table 4-6** shows the surface layer concentrations of the new gas-phase species and the aerosol-phase species that were added to the initial condition file and the boundary condition file. In contrast to the standard SAQM model file structure, the initial concentrations of all the species were provided in a single initial condition file. The initial and boundary PM_{10} concentrations were set at 15 $\mu g/m^3$, which may have been somewhat high. The composition of the initial and boundary PM_{10} values was assumed to be similar to remote sites in California. The model was applied using 12 x 12 km spatial resolution for the entire modeling domain. It was recognized that finer spatial resolution would be highly desirable for modeling primary PM constituents. However, for purposes of demonstrating the model in a computationally efficient mode, we elected to stay with the 12 x 12 km resolution.

4.3.1 Emissions for Ammonia and Aerosol Species

The SAQM-AERO model requires ammonia emissions to simulate the formation of secondary aerosols (i.e., ammonium sulfate, ammonium nitrate, and ammonium chloride) and PM emissions to simulate the primary aerosol components. It requires chemically-resolved and size-resolved PM emissions data corresponding to the model's chemical components of PM and the size distribution used for a particular simulation. The chemical components for which it expects PM emissions are sulfate, elemental carbon, organic material, crustal material, sodium, and chloride. The ammonium and PM emission inputs need to be time-resolved (hourly) and spatially-resolved for the modeling grid.

Preliminary gridded NH_3 and PM emission estimates were developed for the SJV modeling domain in another study (Lurmann et al., 1996). However, the preliminary gridded emission estimates in that study were believed to be underestimated because numerous categories of emissions were omitted and other types of emissions were not accurately characterized. The preliminary gridded ammonia inventory contained 88 tons per day in the

Table 4-6. Surface layer concentrations of new species in the initial concentration and boundary condition files.

Species	Description	Concentration
CRO	Peroxy radical from reaction of Cresols with OH radical	1.0E-08 ppm
XO2	Peroxy radical for NO to NO_2 conversion	1.0E-08 ppm
ROR	Lumped Peroxy radicals	1.0E-08 ppm
NTR	Other Organic Nitrates	1.0E-15 ppm
HCL	Hydrochloric Acid	1.0E-10 ppm
COC	Condensable Organics (gaseous)	1.0E-10 ppm
OLE2	Monoterpenes with Olefinic Bond	1.0E-08 ppm
NA+1	Sodium	0.27 $\mu g/m^3$
H+1	Proton	1.0E-04 $\mu g/m^3$
NH4+1	Ammonium	0.78 $\mu g/m^3$
NO3-1	Nitrate	1.50 $\mu g/m^3$
CL-1	Chloride	0.35 $\mu g/m^3$
SO4=1	Sulfate	1.00 $\mu g/m^3$
H2O.1	Water	0.10 $\mu g/m^3$
EC.1	Elemental Carbon	0.53 $\mu g/m^3$
OC.1	Organic Material	2.70 $\mu g/m^3$
OTR.1	Crustal	7.77 $\mu g/m^3$

modeling domain. Chinkin et al. (1996) developed an updated gridded ammonia emissions inventory for the same SJV modeling domain. The draft updated ammonia inventory contained 534 tons per day. This difference is large and preliminary simulations made with the Lurmann et al. inventory showed underprediction of ammonia and ammonium. Even though the updated ammonia inventory was not finalized by ARB at the time the emissions data were prepared for the simulations, permission was obtained to use the draft updated ammonia emission inventory since it was probably more accurate (Ranzieri, 1996). Nevertheless the preliminary nature of the ammonia emissions used in the study should be recognized.

Because of the concern for underestimation of emissions, a comparison was made between the preliminary gridded PM inventory and ARB's county-level CEIDARS emissions

data for 1990. The preliminary gridded emission inventory contained 80 tons per day of PM_{10} emissions for the eight counties within the SJV (not the whole modeling domain). The CEIDARS database contained 1096 tons per day of PM_{10} for the eight SJV counties. Again, this difference is extremely large and suggests the preliminary gridded emissions could be grossly underestimated. This comparison points out a critically important need for aerosol modeling: development of accurate PM emission estimates.

Development of a new PM inventory for the region was beyond the scope of this study. An approximate inventory was prepared by scaling the PM emissions in the Lurmann et al. (1996) inventory to account for probable biases. If the CEIDARS PM_{10} emissions are accurate and if the relative difference between the CEIDARS PM_{10} emission estimates and the preliminary gridded inventory in the eight-county SJV domain is characteristic of those for the entire modeling domain, the total PM_{10} emissions for the modeling domain should be about 2000 tons per day. After examining the total emissions for EC, OM, and crustal material in the preliminary gridded emission inventory and comparing it with the composition of the inventory in the SoCAB, it was decided to increase the EC emissions by a factor of 3, OM emissions by a factor of 9, and crustal emissions by a factor of 30. In addition, the sodium emissions were adjusted to stoichiometerically match the chloride emissions. **Table 4-7** shows the daily total emissions used in the simulations. The total PM_{10} emissions for the modeling domain are 1819 tons per day. It must be emphasized that this is an extremely approximate method of estimating the PM_{10} emissions and that it was done in this manner in order to perform the demonstration simulations with hopefully improved PM emission estimates. The performance of the model for primary PM species cannot be seriously evaluated until such time that better gridded PM emissions data are developed.

4.3.2 Model Results

The AUSPEX nitric acid, ammonia, $PM_{2.5}$, and PM_{10} aerosol data were collected at the following nine sites during the August 3-6, 1990 episode: Altamont Pass, Crows Landing, Pacheco Pass, Academy, Edison, Buttonwillow, Sequoia, Yosemite, and Point Reyes. The data were collected for four sampling periods each day: 00-07, 07-12, 12-17, and 17-23 PDT. The chemical components included NH_3, HNO_3, NA^+, Cl^-, NO_3^-, NH_4^+, $SO_4^=$, EC, OM, and PM_{10} mass. HiVol SSI PM_{10} data were also available as a 24-hour average on August 3, 1990. For purposes of comparing the model with the data, the observed OM was estimated as 1.4*OC to account for the oxygen and hydrogen associated with carbon. The data from Point Reyes were excluded from the comparison because this site is close to the upwind boundary and the model predictions for this site are mostly determined by boundary conditions, rather than emissions. In addition, since the model was applied using only one aerosol size section corresponding to PM_{10}, comparisons were only made with the PM_{10} data; the $PM_{2.5}$ data were not used.

Graphical comparison of the model's estimated concentrations and the observed concentration for the four sampling intervals per day are shown in Figures 4-4 through 4-13. These figuresshow the time series of predicted and observed PM_{10} SO_4, PM_{10} NO_3, total

Table 4-7. Total emissions for the modeling domain used in the simulation for Friday August 3, 1990.

Species	Emissions (metric tons/day)
NO_x	992
SO_2	167
PAR	1952
ETH	100
OLE1	56
OLE2	129
TOL	124
XYL	141
FORM	23
ALD	321
ISOP	419
Total VOC	3265
CO	7121
NH_3	534
Sodium PM_{10}	32
Chloride PM_{10}	50
Sulfate PM_{10}	28
EC PM_{10}	147
OM PM_{10}	584
Crustal PM_{10}	978
Total PM_{10}	1819

nitrate (TNO3 = PM_{10} NO_3 + HNO_3), PM_{10} NH_4, total ammonium (TNH4 = PM_{10} NH_4 + NH_3), PM_{10} EC, PM_{10} OM, PM_{10} mass, nitric acid, and ammonia concentrations, respectively, at the eight monitoring stations for August 3-6, 1990. **Table 4-8** shows the mean observed and predicted concentrations, and four statistical measures of model performance: the mean bias, mean normalized bias, mean error, and mean normalized error for the key species on each day of the simulations. Bias is defined here as predicted minus observed, hence positive bias indicates model overprediction. Comparisons are presented for total nitrate and total ammonia because they are useful for diagnosing potential causes of model discrepancies. Examination of the total nitrate predictions are informative because they show the model's ability to produce, transport, and deposit inorganic nitrate (gas and aerosol phases) and are less sensitive to errors in the gas-aerosol partitioning. For example, gross underestimation of the gas-phase production of nitric acid would be more readily detected in TNO3 than HNO3 or NO_3 (which go back and forth between the gas and aerosol phases). Similarly, comparisons are presented for total ammonium which are insensitive to errors in gas-aerosol partitioning and are useful for assessing the performance of all-ammonia related

Table 4-8. Comparison of mean observed and predicted concentrations ($\mu g/m^3$) of aerosol species for August 3-6, 1990.

Species	Day	Mean Observed	Mean Predicted	Normalized Bias (%)	Mean Bias	Normalized Error (%)	Mean Error
PM_{10} SO_4	August 3	3.2	3.3	8	0.1	39	1.3
PM_{10} SO_4	August 4	3.5	2.7	-16	-0.7	29	1.1
PM_{10} SO_4	August 5	3.6	3.2	4	-0.4	44	1.3
PM_{10} SO_4	August 6	3.4	3.1	13	-0.4	60	1.5
PM_{10} NO_3	August 3	2.4	1.4	-37	-1.0	92	2.0
PM_{10} NO_3	August 4	3.2	0.8	-74	-2.4	90	2.7
PM_{10} NO_3	August 5	3.2	0.5	-89	-2.7	89	2.7
PM_{10} NO_3	August 6	2.4	0.1	-95	-2.3	95	2.3
Total NO_3	August 3	5.9	4.8	-5	-1.1	49	2.4
Total NO_3	August 4	6.4	4.6	-21	-1.8	44	2.6
Total NO_3	August 5	7.1	4.2	-38	-2.9	58	3.8
Total NO_3	August 6	10.0	3.7	-60	-6.3	67	6.9
PM_{10} NH_4 #	August 3	1.5	1.3	-9	-0.2	36	0.5
PM_{10} NH_4	August 4	1.6	0.9	-41	-0.7	41	0.7
PM_{10} NH_4	August 5	1.7	1.0	-42	-0.7	42	0.7
PM_{10} NH_4	August 6	1.5	0.8	-48	-0.8	48	0.8
Total NH_4 #	August 3	11.2	7.6	-20	-3.7	41	4.6
Total NH_4	August 4	9.9	7.5	6	-2.3	57	4.4
Total NH_4	August 5	12.7	10.4	10	-2.3	60	6.4
Total NH_4	August 6	13.4	12.0	9	-1.4	54	7.0
PM_{10} OM	August 3	11.9	7.2	-39	-4.7	48	5.9
PM_{10} OM	August 4	11.3	8.0	-25	-3.3	49	5.2
PM_{10} OM	August 5	12.8	9.7	-22	-3.1	45	6.2
PM_{10} OM	August 6	13.6	10.9	-21	-2.8	53	7.8
PM_{10} EC	August 3	2.6	1.5	-40	-1.1	49	1.3
PM_{10} EC	August 4	2.3	1.7	-25	-0.6	44	1.1
PM_{10} EC	August 5	2.3	2.1	-6	-0.3	51	1.2
PM_{10} EC	August 6	2.7	2.4	-2	-0.3	68	1.8
PM_{10} mass	August 3	36.6	25.0	-5	-11.6	57	14.6
PM_{10} mass	August 4	36.1	26.0	-3	-10.2	55	17.4
PM_{10} mass	August 5	39.9	30.5	-5	-9.4	49	16.4
PM_{10} mass	August 6	52.1	30.4	-18	-21.8	46	27.6
HNO_3 *	August 3	1.5	1.4	17	-0.1	58	0.6
HNO_3	August 4	1.6	1.5	2	-0.1	40	0.6
HNO_3	August 5	1.8	1.4	0	-0.4	62	1.0
HNO_3	August 6	3.2	1.4	-33	-1.8	62	2.2
NH_3 * #	August 3	9.4	7.9	4	-1.5	48	3.7
NH_3	August 4	8.1	8.3	58	0.2	91	3.8
NH_3	August 5	10.6	11.7	56	1.1	88	5.8
NH_3	August 6	11.5	13.9	58	2.4	88	6.9

* HNO_3 and NH_3 are in ppb units.
\# The NH_4 and NH_3 statistics exclude the Crows Landing site.

species. Bias in total ammonium is more directly related to bias in emission estimates than either bias in NH_3 or NH_4. Note, however, that the statistics shown in Table 4-8 for NH_3 and TNH4 do not include the values at Crows Landing because the model grossly overestimates NH_3 at that location (see Figure 4-13) and this discrepancy completely dominated the mean bias and error for NH_3 and TNH_4. The statistics with Crows Landing excluded are presented to provide a more representative picture of the model performance.

4.3.2.1 Sulfate

As shown in **Figure 4-4**, the model predicted PM_{10} SO_4 concentrations between 2 and 8 $\mu g/m^3$ at the eight monitoring sites when the observed levels were from 2 and 6 $\mu g/m^3$. The model consistently underestimated the sulfate at Altamont Pass, Crows Landing, and Pacheco Pass by 1 to 3 $\mu g/m^3$, indicating that the sulfate coming into the SJV from the Bay Area was underestimated. Within the SJV, the model estimated the observed sulfate levels within 1 to 2 $\mu g/m^3$ at Buttonwillow, Edison, and Academy. It showed more frequent underpredictions than overpredictions at these sites, and underestimated the maximum concentrations at Academy and Buttonwillow. In the Sierras, the model predicted the sulfate fairly well at Yosemite throughout the simulation and at Sequoia National Park on August 3 and 4. However, the model grossly overestimated sulfate at Sequoia on August 5 and on the morning of August 6, predicting 4 to 6$\mu g/m^3$ when 1 to 2 $\mu g/m^3$ were observed. Overall, the model predicted mean PM_{10} SO_4 concentrations of 3.3, 2.7, 3.2, and 3.1 $\mu g/m^3$ when the mean observed values were 3.2, 3.5, 3.6, and 3.4 $\mu g/m^3$ on August 3, 4, 5, and 6, respectively. The mean normalized bias ranged from -16 percent to +13 percent, and the mean normalized error ranged from ± 29 to ± 60 percent. On an absolute basis, the model predicted the sulfate within ± 1.5 $\mu g/m^3$ on average. The model's ability to simulate the observed diurnal patterns in sulfate was mixed; for example, the model predicted smaller daytime sulfate increases than were observed at Academy, Altamont Pass, and Crows Landing.

4.3.2.2 Nitrate, Nitric Acid, and Total Nitrate

The observed nitrate levels were quite low (1 to 10 $\mu g/m^3$) in this episode compared to the levels of nitrate that occur in winter episodes. The model's estimates of PM_{10} nitrate levels were generally much lower than the observed concentrations, as shown in **Figure 4-5**. On average, the model predicted 1.4, 0.8, 0.5, and 0.1 $\mu g/m^3$ nitrate when 2.4, 3.2, 3.2, and 2.4 $\mu g/m^3$ nitrate were observed on August 3, 4, 5, and 6, respectively, at the eight stations. The mean normalized bias in the model estimates ranged from -37 to -95 percent. On an absolute basis, the model bias ranged from -1.0 to -2.7$\mu g/m^3$. The model formed less than 0.2 $\mu g/m^3$ of nitrate at Academy, Buttonwillow, and Yosemite, and formed small amounts of nitrate (1 to 7 $\mu g/m^3$) in the morning hours at the other stations. The August 3-6, 1990 episode was particularly warm, as shown by the surface temperatures listed in **Table 4-9**. Thermodynamic data for the nitric acid - ammonia - ammonium nitrate system indicates nitric acid and ammonia are favored, rather than ammonium nitrate aerosol, at high temperatures. While the low observed nitrate levels are consistent with the high temperatures, the model does not form enough aerosol nitrate at these warm temperatures. A shortage of ammonia can cause

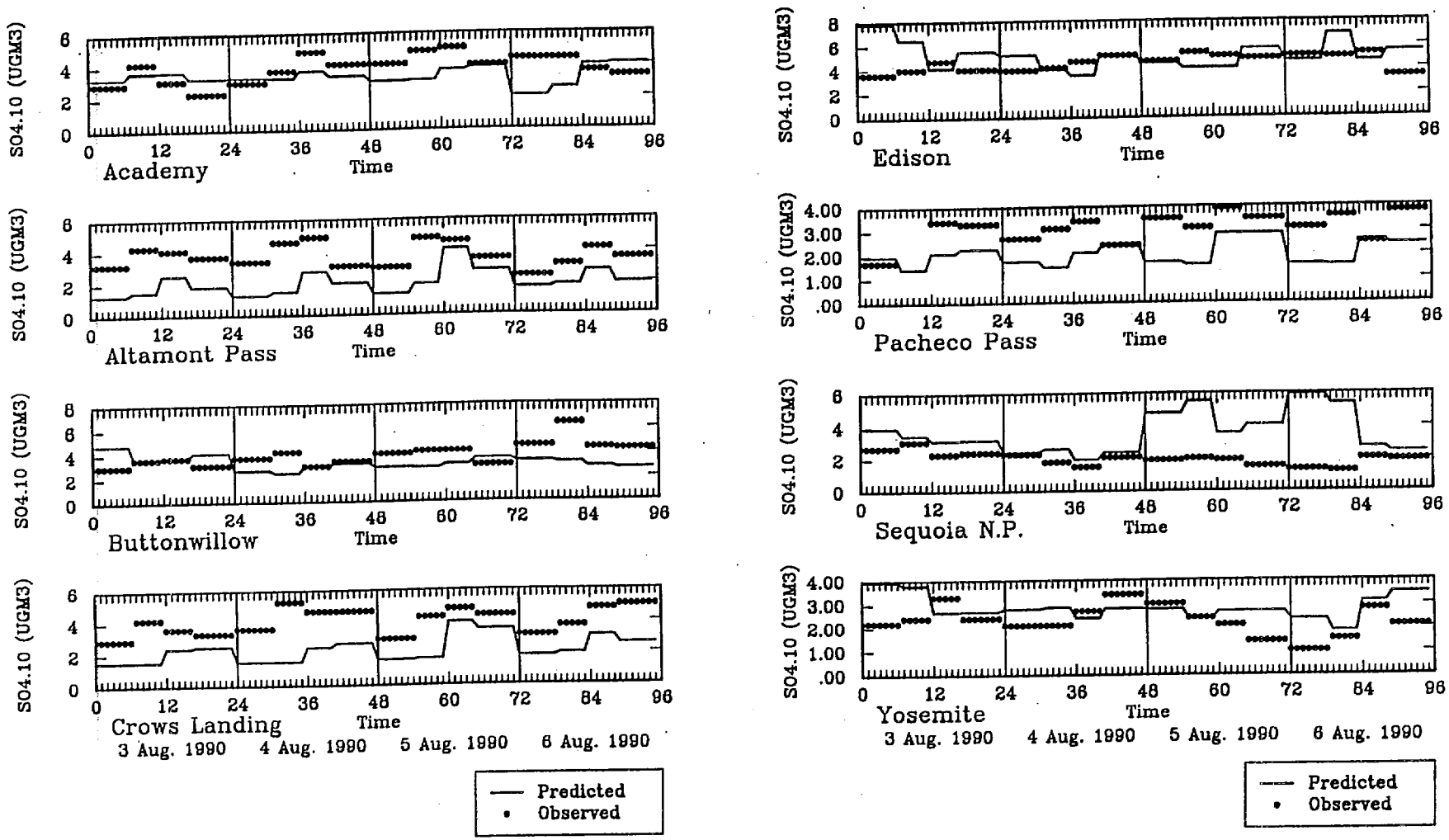

Figure 4-4. Time-series plot of observed (•••) and predicted (—) PM_{10} SO_4 concentrations.

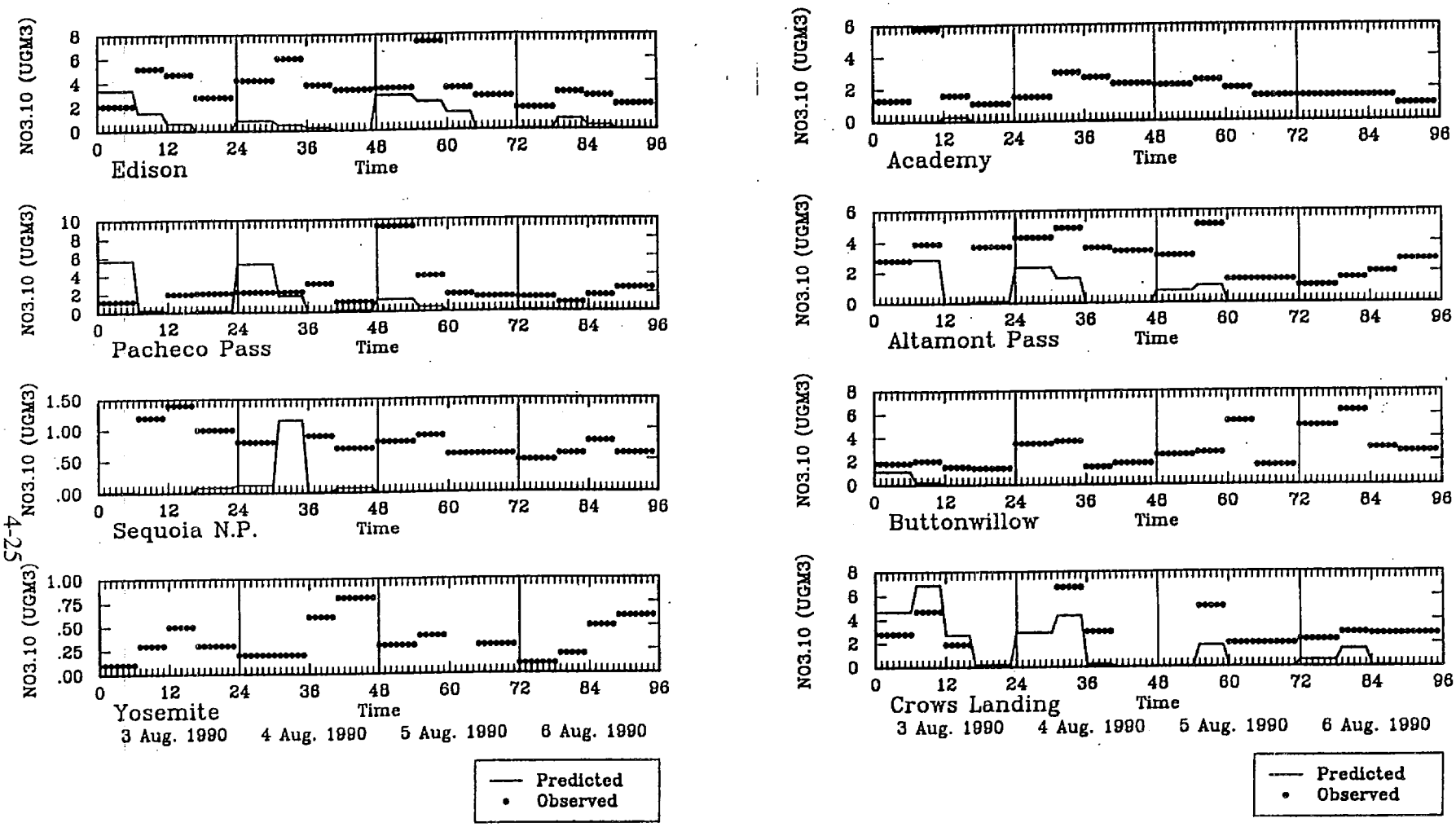

Figure 4-5. Time-series plot of observed (•••) and predicted (—) PM_{10} NO_3 concentrations.

Table 4-9. Surface temperature and relative humidity in the SJV modeling domain on August 3-6, 1990.

Location	Day	Temperature (F)			Relative Humidity (%)		
		Minimum	Maximum	24- hr Avg	Minimum	Maximum	24-hr Avg
Bakerfield	8/03	71	99	85	23	53	-
Bakerfield	8/04	70	99	85	26	62	-
Bakerfield	8/05	74	102	88	21	64	-
Bakerfield	8/06	78	110	94	22	53	-
Fresno	8/03	69	99	84	23	71	-
Fresno	8/04	69	100	85	26	64	-
Fresno	8/05	71	104	88	29	66	-
Fresno	8/06	77	107	92	23	74	-
Stockton	8/03	61	90	76	36	68	-
Stockton	8/04	60	95	78	35	68	-
Stockton	8/05	62	102	82	26	61	-
Stockton	8/06	69	107	88	20	47	-
Davis	8/03	57	92	73	46	89	67
Davis	8/04	58	93	74	45	89	65
Davis	8/05	57	102	80	34	90	54
Davis	8/06	65	107	85	30	71	47
Sacramento	8/03	59	91	75	34	87	-
Sacramento	8/04	59	98	79	29	84	-
Sacramento	8/05	58	106	82	16	87	-
Sacramento	8/06	66	108	87	14	68	-
San Jose	8/03	59	79	68	49	99	74
San Jose	8/04	61	78	68	52	95	77
San Jose	8/05	60	89	72	33	96	66
San Jose	8/06	64	91	76	37	97	66
San Francisco	8/03	58	77	68	52	84	-
San Francisco	8/04	57	71	64	53	87	-
San Francisco	8/05	57	74	66	52	90	-
San Francisco	8/06	56	77	67	52	93	-

underestimation of ammonium nitrate, however, as discussed below, there is plenty of ammonia in the model simulations and observations. The observations do not contain sufficient ammonium to buffer the observed sulfate and nitrate. If one assumes the observed sulfate exists as ammonium sulfate and the remaining observed ammonium exists as ammonium nitrate, then on average there is 1.4 to 2.2 $\mu g/m^3$ of nonvolatile nitrate remaining. The model includes the formation of nonvolatile sodium nitrate, but the modeled and measured sodium concentration are too low (<0.2 $\mu g/m^3$) to fully account for the observations. It is also unlikely that the nitrate measurements are biased high because nitrate is quite volatile and, if there is a sampling bias, it is most likely one that would underestimate nitrate. Thus, the biases in the nitrate predictions may be a result of errors in the partitioning of ammonium nitrate and the omission of nonvolatile nitrate formation pathways.

Figure 4-6 shows that the model's predictions for nitric acid were more accurate than those for aerosol nitrate. The observed diurnal pattern of HNO_3 is quite pronounced, with low nighttime concentrations and high afternoon concentrations at most sites. This pattern reflects the high rates of photochemical production from NO_x in the daytime. The model tracks the diurnal pattern well at Altamont Pass, Crows Landing, Buttonwillow, and Edison. The model underestimates HNO_3 concentrations at Academy on all days and at Yosemite on August 6. The observed nitric acid levels at Yosemite were less than 2 ppb until August 6, when they increased to 11 ppb; the model predictions at Yosemite did not show the increase on August 6. Similarly, the model fails to predict the increases in nitric acid at Pacheco Pass on August 5 and 6. The model underpredicted the nitric acid at Sequoia, however, the observed levels were low (<1.5 ppb) on all days. The mean predicted HNO_3 concentrations were 1.4, 1.5, 1.4, and 1.4 ppb when 1.5, 1.6, 1.8, and 3.2 ppb were observed on August 3, 4, 5, and 6, respectively. The mean normalized bias ranges from - 33 percent to +17 percent and the mean normalized error ranges from ± 40 to ± 62 percent.

A comparison of predicted and observed total nitrate (TNO_3) concentrations, shown in **Figure 4-7**, shows underprediction everywhere except at the Edison station. The total nitrate predictions were better than those for nitrate but worse than those for nitric acid. The data shows that most of the inorganic nitrate existed as nitric acid, rather than nitrate, in the daytime. The model predicts a diurnal pattern that is similar to the observed pattern at most sites, except the modeled concentrations are generally lower than observed. The model predicted mean total nitrate concentrations of 4.8, 4.6, 4.2, and 3.7 $\mu g/m^3$ when 5.9, 6.4, 7.1, and 10.0 $\mu g/m^3$ were observed on August 3, 4, 5, and 6, respectively. The mean normalized bias ranges from - 60 percent to -5 percent and the mean normalized error ranges from ± 44 to ± 67 percent.

The bias in total nitrate was somewhat surprising given that the model's performance for ozone was acceptable. In theory, accurate simulation of NO_x oxidation and NO_2 concentrations are needed to achieve good ozone performance. However, past experience has indicated that comparable ozone performance can be achieved with varying levels of NO_x and VOC emissions, and that regional air quality models rarely predict accurate NO_2 concentrations. Since nitric acid is formed from NO_2, errors in NO_2 will directly affect nitric acid predictions. The underestimation of total nitrate in this simulation could be caused by a

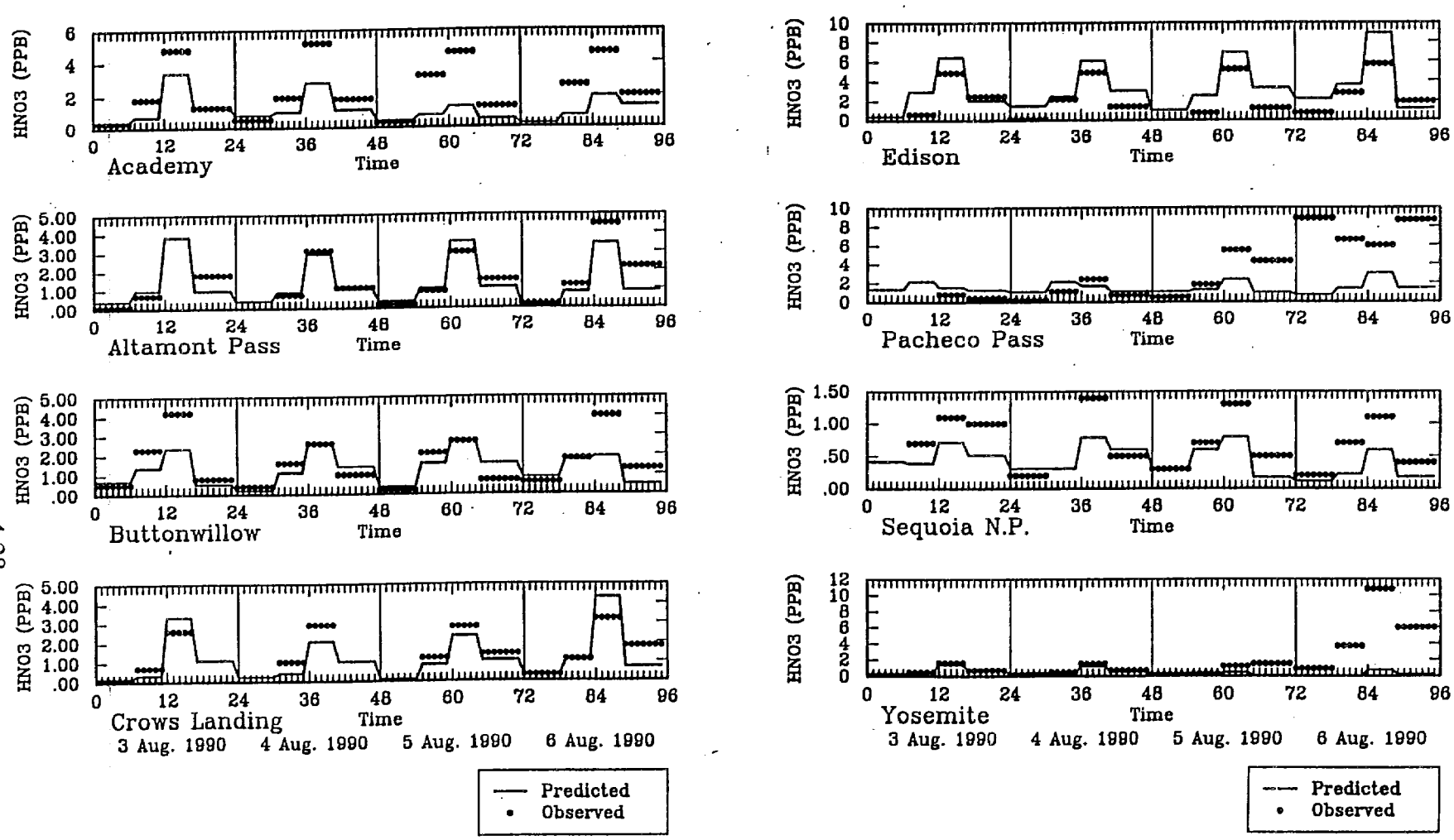

Figure 4-6. Time-series plot of observed (•••) and predicted (—) HNO_3 concentrations.

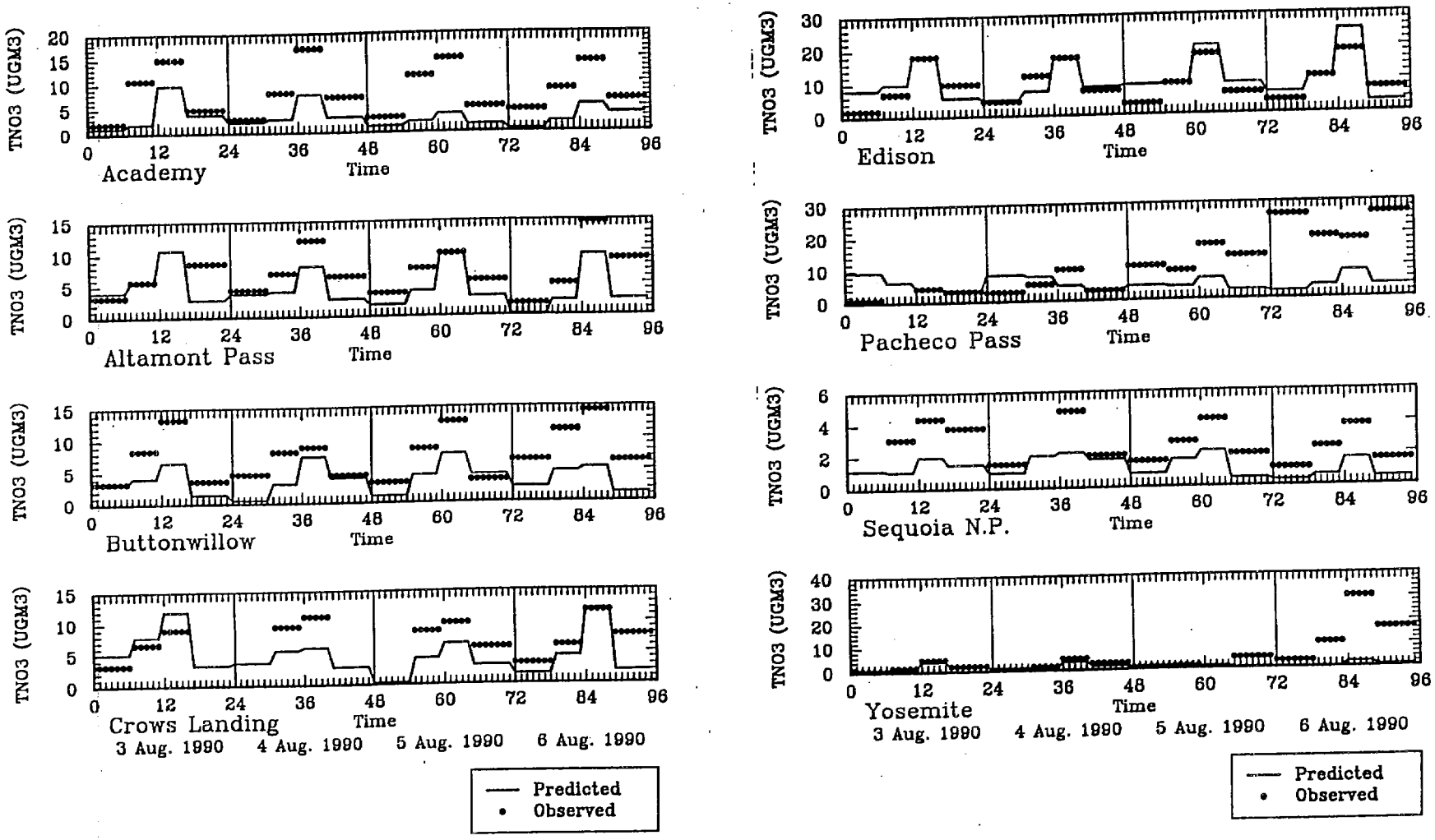

Figure 4-7. Time-series plot of observed (•••) and predicted (—) TNO3 concentrations.

number of factors, including underestimation of NO_x emissions, underestimation of VOC emissions or VOC reactivity, underestimation of nitric acid formation in the gas-phase chemical mechanism, and/or overestimation of total nitrate dry deposition. With regard to the last factor, recall that the dry deposition velocity of nitric acid is much higher than aerosol nitrate, so the model's errors in gas-aerosol partitioning, which favored nitric acid, probably caused underestimation of total nitrate.

4.3.2.3 Ammonium, Ammonia, and Total Ammonium

The model predictions of PM_{10} ammonium were in the same range as the observed levels (1 to 3 $\mu g/m^3$) which were quite low (see **Figure 4-8**). At most stations, the observed ammonium was underpredicted by 0.5 to 1.5 $\mu g/m^3$. On average, the model predicted 1.3, 0.9, 1.0 and 0.8 $\mu g/m^3$ of ammonium when 1.5, 1.6, 1.7 and 1.5 $\mu g/m^3$ were observed on August 3, 4, 5 and 6, respectively. The mean bias ranged from -0.2 to -0.8 $\mu g/m^3$ and the mean error ranged from ± 0.5 to ± 0.8 $\mu g/m^3$. The mean normalized bias ranged from -20 to -48 percent and the mean normalized error ranged from ± 41 to ± 48 percent. The observed data do not show a consistent diurnal pattern and the model's predictions do not track the diurnal patterns well. The model underestimated the highest observed concentrations which occurred at Academy, Altamont, and Buttonwillow. Overall, the most notable feature of the comparison is that the model and the data are roughly in the same low range in the summer episode.

The model results for ammonia are mixed. While the model predicted mean ammonia concentrations that are comparable to the observed concentrations, the model only tracked the observed diurnal variations well at one station, Buttonwillow. **Figure 4-9** shows that the temporal correlation of the predicted and observed concentrations was poor at most stations. On average, the model predicted concentrations of 7.9, 8.3, 11.7, and 13.9 ppb of ammonia when 9.4, 8.1, 10.6, and 11.5 ppb were observed on August 3, 4, 5, and 6, respectively (excluding the Crows Landing predictions). The mean biases ranged from -1.5 to 2.4 ppb and the mean error ranged from ± 3.7 to ± 6.9 ppb. On a percentage basis, the mean normalized biases and error were large (up to +58 percent bias and ± 91 percent error). The large errors confirm the lack of dynamic tracking of the observation, which is particularly evident at Academy and Sequoia. At certain stations, the predicted ammonia concentrations were much higher than the observations on any one of the four days or on all four days. The discrepancy is largest at Crows Landing where the model predicted up to 150 ppb at night when only 5 ppb was observed. The Crow Landing observations were overpredicted in the mornings and evenings, but not in the afternoon when the strong sea breeze occurred. At Altamont Pass, the model predicted 75 ppb early on the morning of August 6 when 15 ppb was observed. It should be recognized that there is very little transfer of ammonia to the aerosol phase in these simulations, so the errors cannot be ascribed to the gas-aerosol partitioning. Instead, the results suggest that the timing of ammonia emissions may be inaccurate and the magnitude of the ammonia emissions in certain portions of the domain may be overestimated. Inaccuracies in the wind fields, particularly at night may also contribute to the large discrepancies. For example, the highest ammonia emissions area is located 20 to 40 km east of the Crows Landing

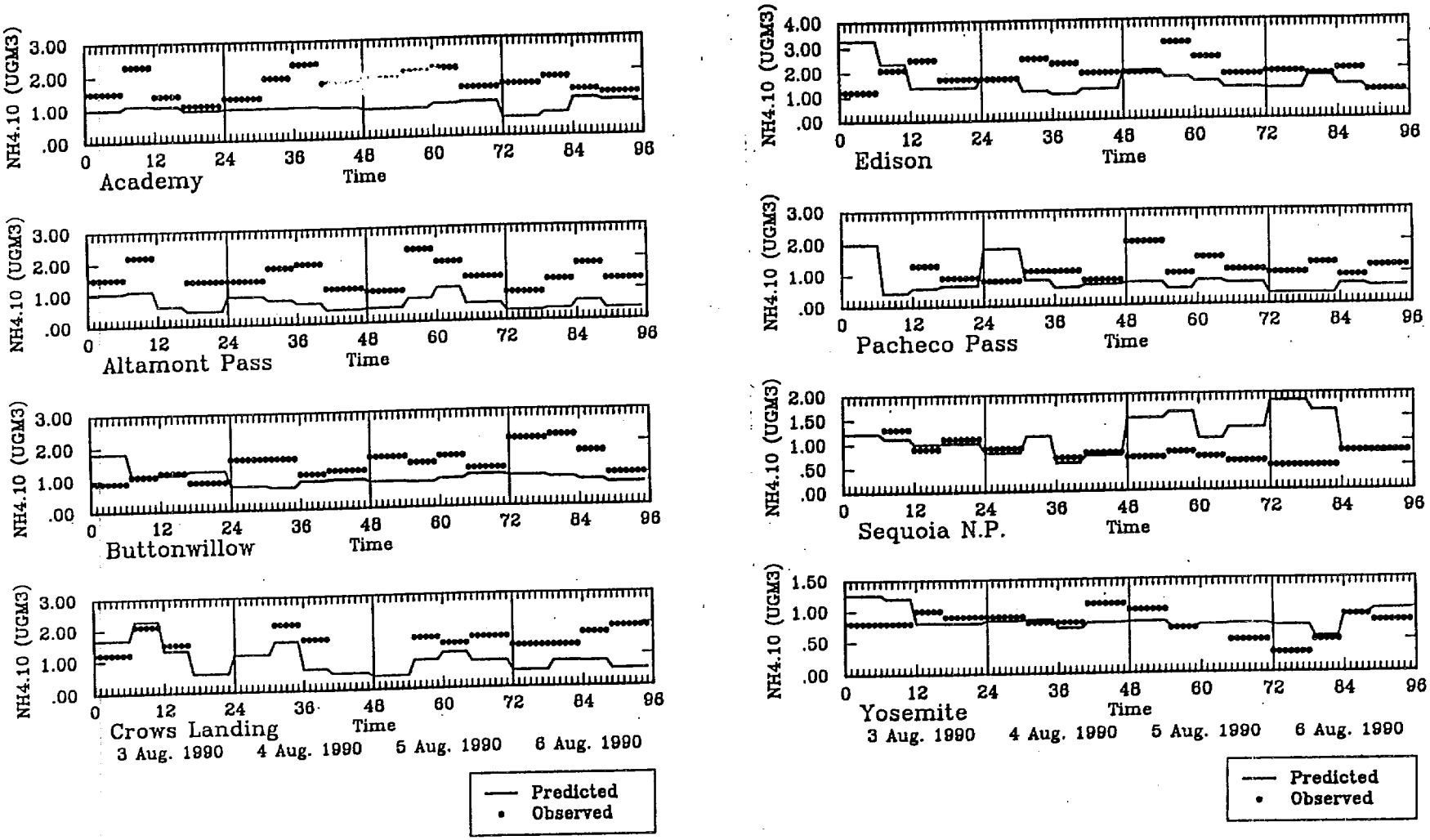

Figure 4-8. Time-series plot of observed (•••) and predicted (—) PM_{10} NH_4 concentrations.

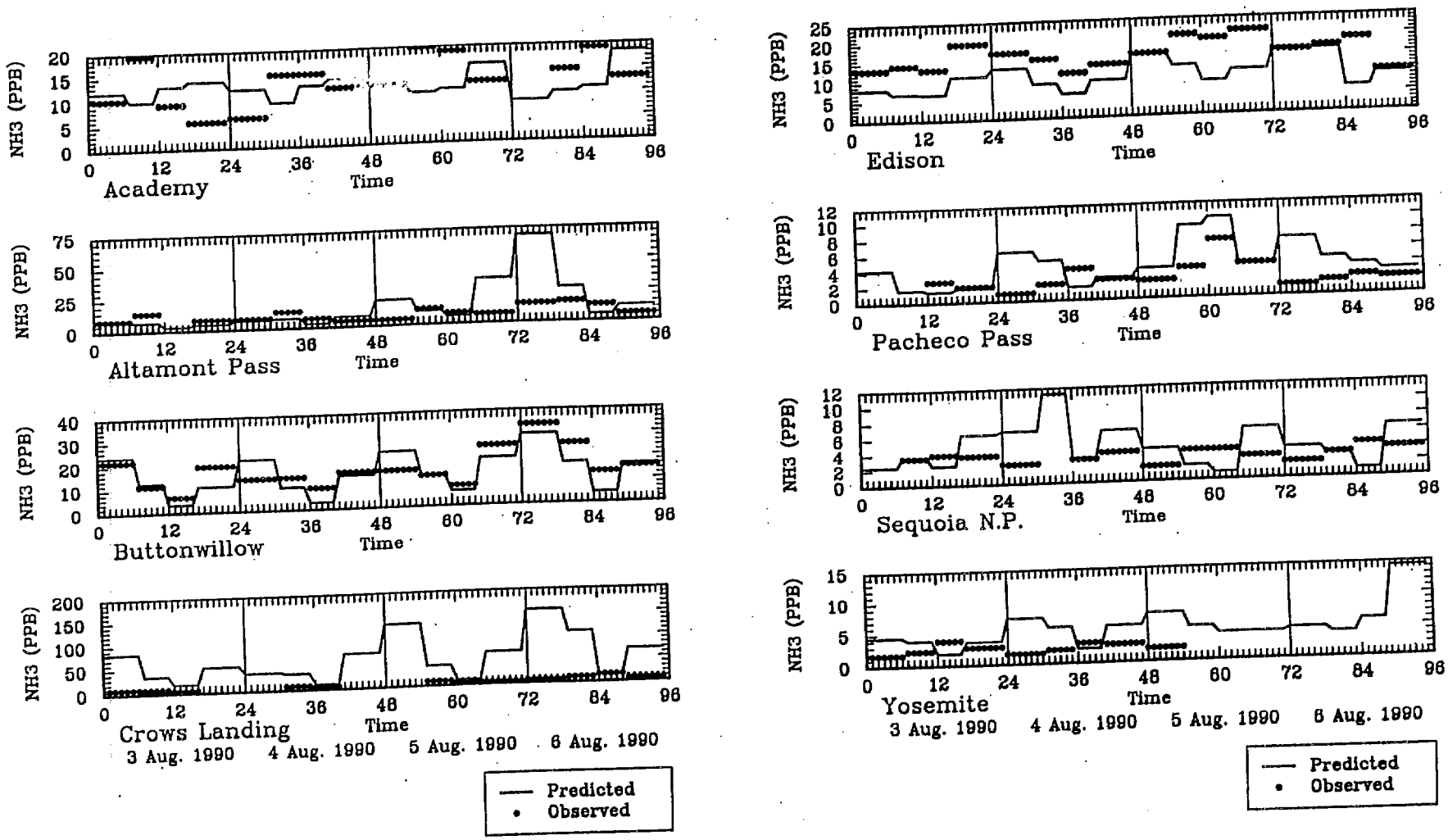

Figure 4-9. Time-series plot of observed (•••) and predicted (—) NH_3 concentrations.

station where only small amounts of ammonia were observed. Inaccuracies in the winds near large sources can cause large discrepancies, especially at night when the surface-based emissions are trapped in the shallow surface layer. These results point out the need for further refinement of ammonia emissions for the SJV.

The observed and predicted total ammonium concentrations, shown in **Figure 4-10**, compare somewhat better than those for ammonia alone. The observed data show that the total ammonium is composed of about 15 percent aerosol ammonium and 85 percent gaseous ammonia, on average, in this summer episode. The model predictions of total ammoniumconcentrations were often in the same range as the observed concentrations, however, the model predictions did not track the observed dynamic patterns closely. The mean predicted concentrations were 7.6, 7.5, 10.4, and 12.0 $\mu g/m^3$ when 11.2, 9.9, 12.7, and 13.4 $\mu g/m^3$ of total ammonium were observed on August 3, 4, 5, and 6, respectively (excluding Crows Landing). The mean biases ranged from -3.7 $\mu g/m^3$ to -1.4 $\mu g/m^3$ and the mean errors ranged from ± 4.4 $\mu g/m^3$ to ± 7 $\mu g/m^3$. The mean normalized biases ranged from -20 percent to +10 percent and the mean normalized error ranged from ± 41 to ± 60 percent. On average, the total ammonium was underpredicted, yet Figure 4-10 shows significant overpredictions occurred at Altamont Pass on August 6 and at Crows Landing. At Academy the model underpredicted the peak concentrations. At Altamont the model predictions were close to observations on August 3, 4, and 5. At Buttonwillow the model followed the observed levels fairly well. At Edison the modeled total ammonium was about 50 percent lower than the observed levels most the of time. At Sequoia Pass, Pacheco Pass, and Yosemite the model predictions were slightly higher than the observed levels. Overall, the total ammonium results are consistent with those for ammonia and aerosol ammonium.

4.3.2.4 Organic Material and Elemental Carbon

Organic material is the next largest component of the PM_{10} aerosol after crustal material in this summer episode, comprising about 25 percent of the PM_{10} mass. The model predictions of PM_{10} organic material concentrations were lower than the observed values at most sites except at Edison where the model overpredicted OM (see **Figure 4-11**). The model severely underpredicted the peak OM concentrations at Sequoia Pass, Pacheco Pass, and Yosemite. The model predicted mean OM concentrations of 7.2, 8.0, 9.7, and 10.9 $\mu g/m^3$ when 11.9, 11.3, 12.8, and 13.6 $\mu g/m^3$ were observed on August 3, 4, 5, and 6, respectively. The mean normalized bias ranged from -40 percent to -21 percent and the mean normalized error ranged from ± 45 to ± 53 percent. The model did not trace the dynamic patterns of OM well. The principle source of OM in the simulations is primary emissions, rather than secondary formation from VOCs (based on sensitivity tests), and the uncertainties in the OM emissions are believed to contribute substantially to the bias and errors in the predictions. Uncertainties in VOC emissions and secondary aerosol yields also contribute to the discrepancies. There is also concern that the coarse horizontal resolution used for this simulation contributes to the errors in predictions of all primary species in the model. For example, Blumenthal et al. (1997) compared 4 and 12 km resolution MM5 wind fields to observations for this episode and

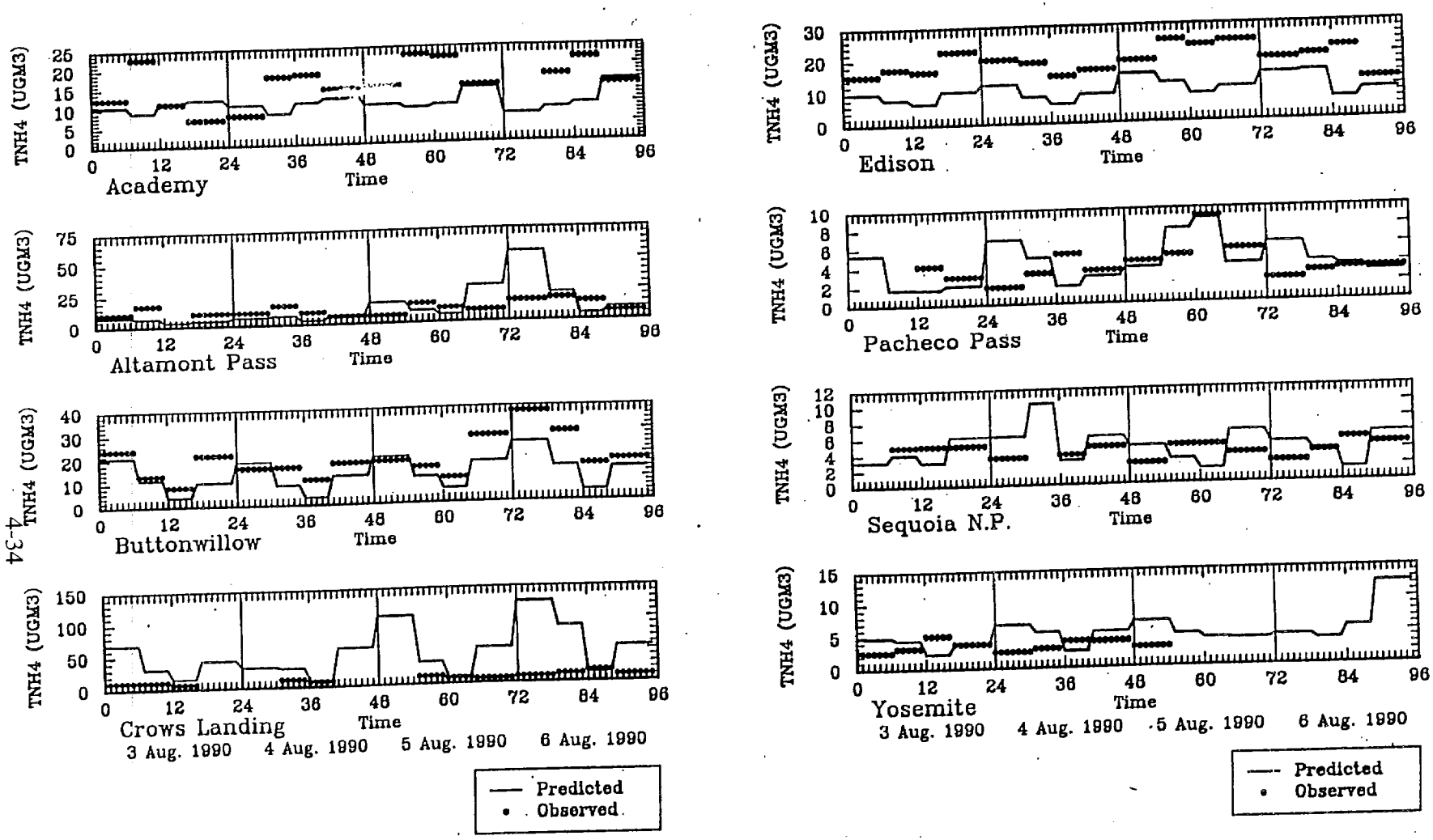

Figure 4-10. Time-series plot of observed (•••) and predicted (—) TNH4 concentrations.

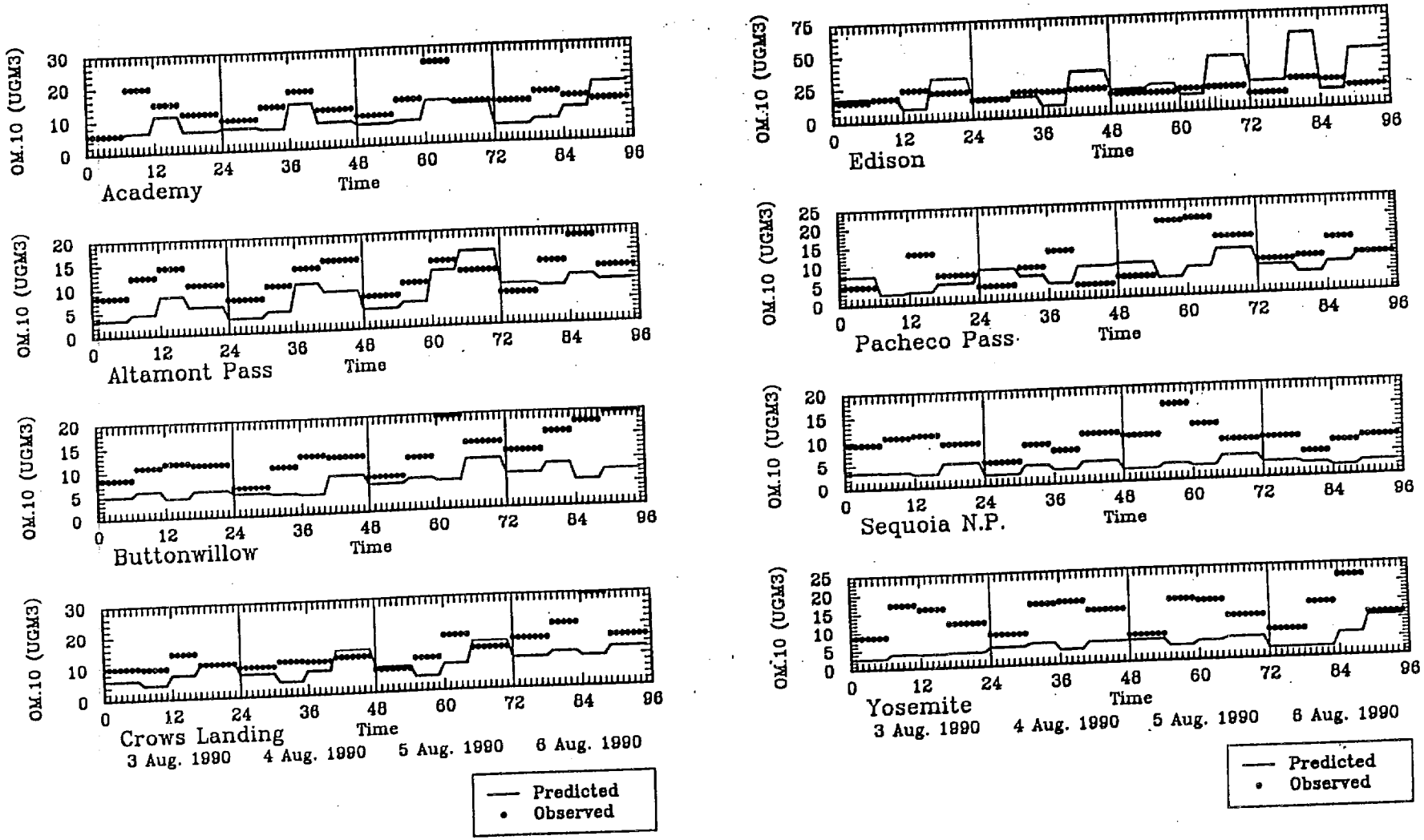

Figure 4-11. Time-series plot of observed (•••) and predicted (—) PM_{10} OM concentrations.

found that the 12 km wind fields did not capture numerous aspects of the local scale and mesoscale flows that were observed and that were captured in the 4 km wind fields.

The model predictions of PM_{10} elemental carbon, displayed in **Figure 4-12**, show varying degrees of agreement with the observations. Both the predicted and observed concentrations were fairly low (0.5 to 10 $\mu g/m^3$). The model predicted mean concentrations of 1.5, 1.7, 2.1, and 2.4 $\mu g/m^3$ when 2.6, 2.3, 2.3, and 2.7 $\mu g/m^3$ were observed on August 3, 4, 5, and 6, respectively. The mean normalized bias ranges from - 40 percent to -2 percent and the mean normalized error ranges from ± 46 to ± 57 percent. On an absolute basis, the model bias ranged from 0.3 to 1.1$\mu g/m^3$ and the model error ranged from ± 1.1 to ± 1.8 $\mu g/m^3$. At Academy the model predictions of PM_{10} Elemental Carbon (EC) were similar to the observed values except that the model underestimates the peak on the morning of August 3. At Altamont, the model underpredicted the peak PM_{10} EC on all days. At Buttonwillow, the model underpredicted the peak on August 3, 4, and 6. At Crows Landing the model did fairly well on August 3 and 4, but then underpredicted on August 5 and 6. At Edison the model followed the observed values well on August 3 and 4, but severely overestimated the peak on August 5 and 6. The model underestimated the elemental carbon at Sequoia Pass and Yosemite. The model predictions are quite close to observations at Pacheco Pass, though the peak is underestimated on August 5 and 6. Overall, the accuracy of the EC predictions was comparable or slightly better than those for OM. The uncertainty in EC emissions and the coarse spatial resolution probably contributed to the model error for this species.

4.3.2.5 PM_{10} Mass

The PM_{10} mass was mostly comprised of crustal and organic material in the summer episode. As shown in **Figure 4-13**, the model underpredicted the PM_{10} mass concentrations at most sites. The temporal patterns of PM_{10} were not tracked closely by the model, as was the case for many of the PM_{10} constituents. The highest observed PM_{10} mass concentration was 170 $\mu g/m^3$ at Crows Landing on the morning of August 6, when the model predicted a concentration of 30 $\mu g/m^3$. The model predictions were equal to or lower than the observations at Academy, Buttonwillow, and Crows Landing. The predictions were equal to or higher than the observations only at Altamont Pass. Predictions at Edison, Pacheco Pass, Sequoia, and Yosemite showed some overpredictions, but mostly underpredictions of PM_{10} mass. The model predicted mean PM_{10} mass concentrations of 25.0, 26.0, 30.5, and 30.4 $\mu g/m^3$ when 36.6, 36.1, 39.9, and 52.1 $\mu g/m^3$ were observed on August 3, 4, 5, and 6, respectively. The mean normalized bias ranges from -18 percent to -3 percent and the mean normalized error ranges from ± 46 to ± 57 percent.

The 24-hr average PM_{10} concentrations were available for numerous routine monitoring stations on August 3. **Table 4-10** shows the observed and predicted PM_{10} mass at these stations. The model mostly underpredicted the observed values at sites in the southern San Joaquin Valley, and overpredicted at sites in the San Francisco Bay Area (SFBA) and in the

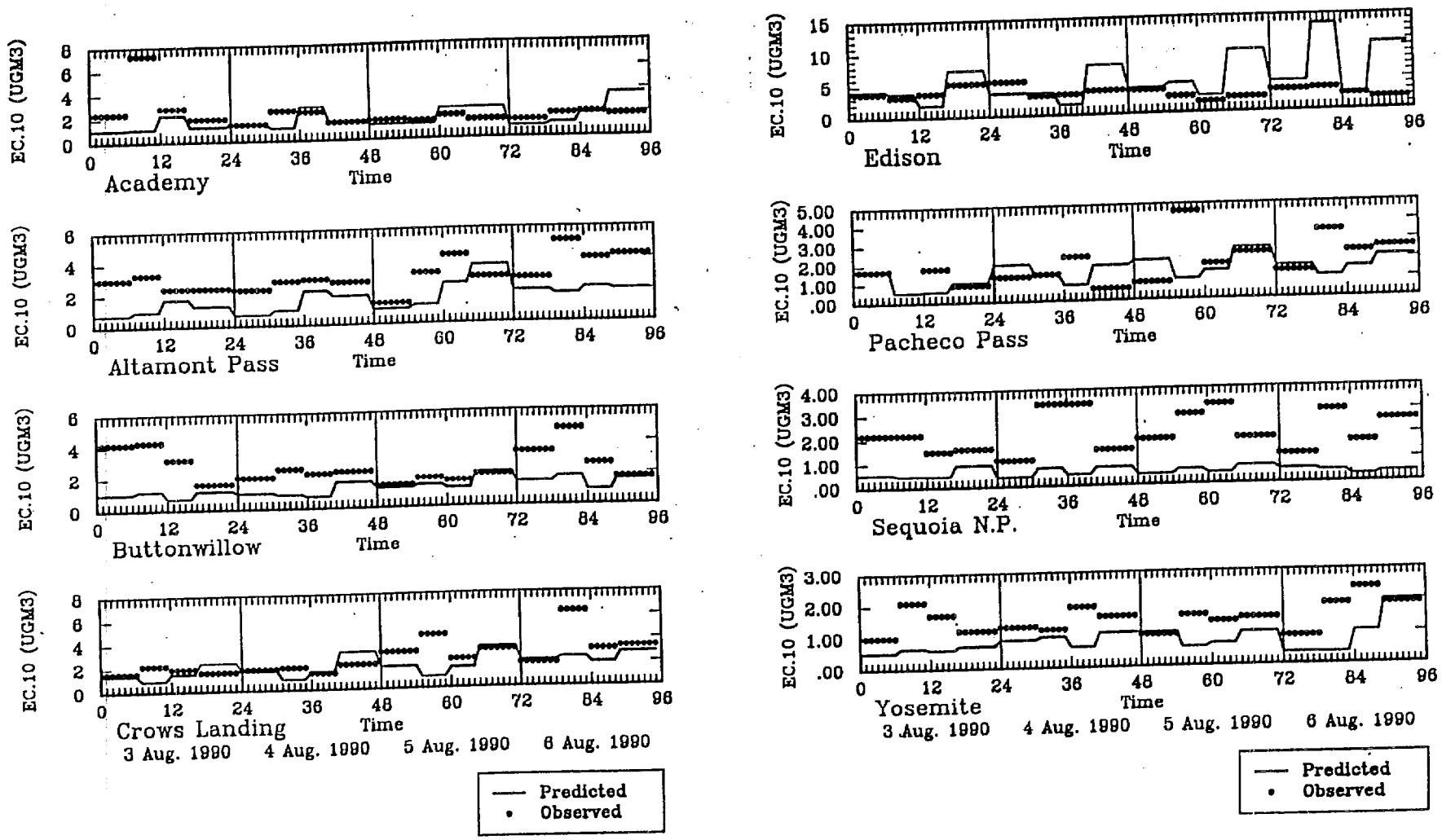

Figure 4-12. Time-series plot of observed (•••) and predicted (—) PM_{10} EC concentrations.

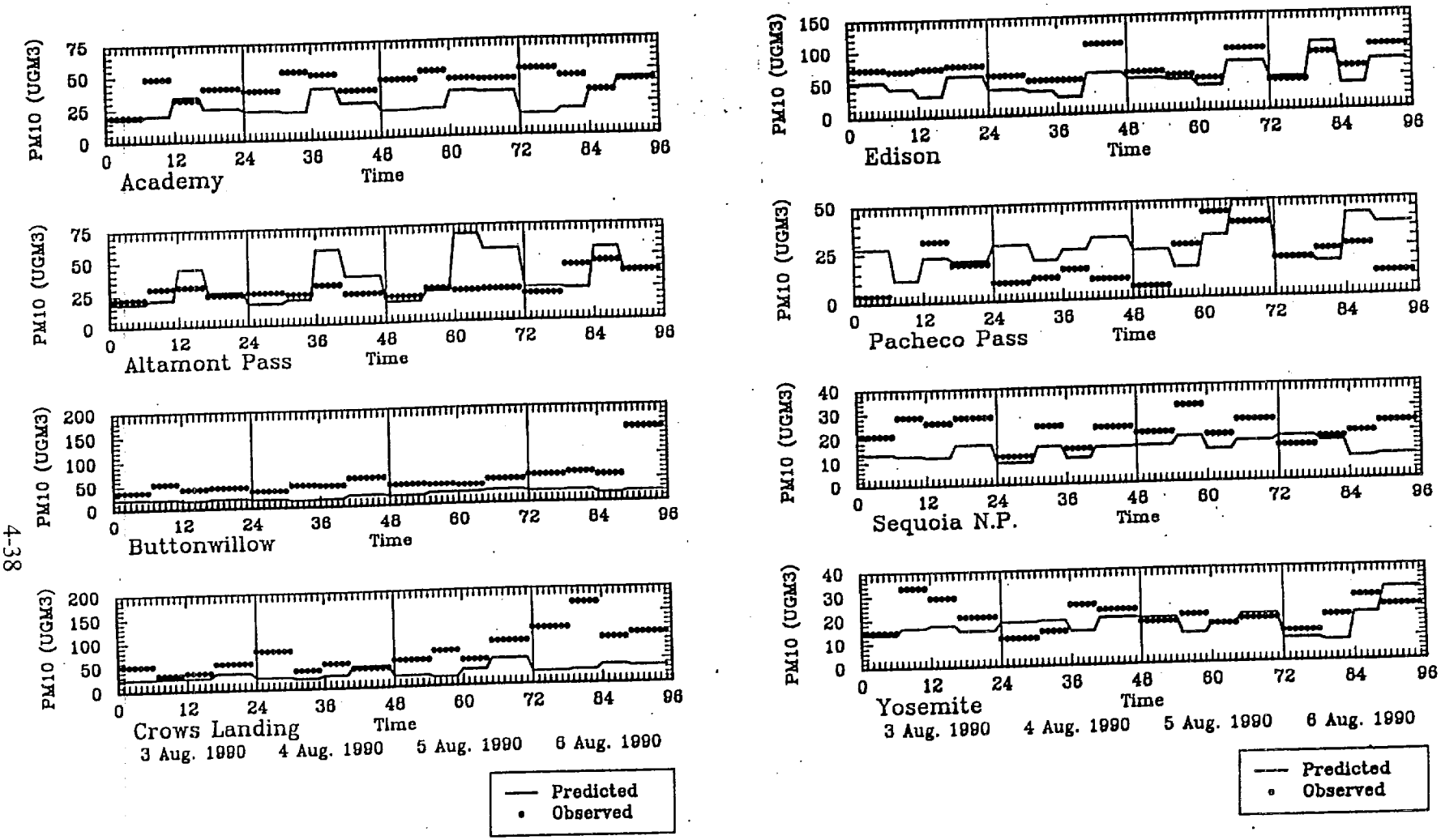

Figure 4-13. Time-series plot of observed (•••) and predicted (—) PM_{10} mass concentrations.

Table 4-10. Observed and predicted PM_{10} mass concentrations ($\mu g/m^3$) at routine monitoring stations on August 3, 1990.

Location	Observed	Predicted
Santa Rosa	17	21
San Rafael	21	78
San Francisco	20	34
Richmond	16	46
Concord	17	32
Redwood City	42	78
Livermore	28	34
San Jose	23	88
Fremont	30	39
Vallejo	21	22
Pittsburg	47	24
Vacaville	46	19
Woodland	37	19
Sacramento	22	34
Citrus Heights	30	41
Rocklin	26	41
Salinas	18	40
Atascadero	26	16
San Luis Obispo	21	21
Crows Landing	71	27
Madera	35	46
Stockton	55	34
Fresno	51	62
Visalia	57	45
Handford	50	30
Corcoran	49	35
Kern Refuge	37	34
Oildale	60	30
Taft College	57	30
Bakersfield	57	44
Westley	37	28
Yosemite	40	14
Average	36	37

northern portions of the valley. At Richmond and Concord the model predictions of PM_{10} mass were twice the observed value. At Fresno the model slightly overpredicted the observed value. At Bakersfield it underpredicted the observed value by 10 $\mu g/m^3$. The model prediction was close to the observed value at Kern Refuge. The model underestimated the observed values by more than 50 percent at Oildale, Taft College, Hanford, Yosemite Village, Stockton, Atascadero, Vacaville, Crows Landing, Woodland, and Pittsburg. Whereas, at San Rafael the model predicted 80 $\mu g/m^3$ compared to the observed value of 20 $\mu g/m^3$. The model also overestimated the 24-hr PM_{10} concentrations at Salinas, Rocklin, Citrus Heights, Sacramento, San Jose, Redwood City, Fremont, and San Francisco. The model predictions are close to observations at San Luis Obispo, Westley, Livermore, Vallejo, and Santa Rosa. Overall, the mean bias and mean error in PM_{10} concentrations were $+1$ $\mu g/m^3$ and ± 19 $\mu g/m^3$. The average predicted and observed PM_{10} concentrations were 37 and 36 $\mu g/m^3$ at the routine monitoring stations on August 3.

The pattern of PM_{10} overprediction in the SFBA and underprediction in the SJV is probably due to the approximate method used to estimate the PM emissions. The preliminary PM emission estimates were uniformly increased throughout the modeling domain, even though the missing PM emissions, such as from wind blown dust and agricultural tillage, are probably greater in the SJV than in the SFBA. The spatial pattern of model bias is consistent with the PM emissions being overestimated in the SFBA and underestimated in the SJV.

4.3.2.6 Spatial Distributions of Predicted Concentrations

Figures 4-14 through 4-21 show the spatial distribution of predicted PM_{10} SO_4, PM_{10} NO_3, HNO_3, PM_{10} NH_4, NH_3, PM_{10} OM, PM_{10} EC, and PM_{10} mass 24-hr average concentrations, respectively, on August 6, 1990. The highest SO_4 concentrations were predicted in Sacramento, Fresno, Bakersfield, and Sequoia National Park (east of the monitoring site). Much of the SJV and San Francisco Bay Area (SFBA) have more than 3 $\mu g/m^3$ of sulfate on August 6. August 6 was the warmest of the four episode days and had the lowest predicted nitrate concentrations.

Figure 4-15 shows that the 24-hr NO_3 concentrations were below 0.4 $\mu g/m^3$ at most locations and the highest nitrate concentrations, which were only 3 to 4 $\mu g/m^3$, were predicted east of Crows Landing in the area with high ammonia levels. Predicted nitric acid levels (see Figure 4-16) were highest near Fresno and Bakersfield (up to 4 ppb), and generally between 1 and 3 ppb throughout the SJV. Fairly low nitric acid levels were predicted for the SFBA, except for downwind of San Jose.

The predicted PM_{10} NH_4 concentrations were low (<1.5 $\mu g/m^3$) in most of the modeling domain (see Figure 4-17). The highest ammonium concentration (2.5 $\mu g/m^3$) was predicted east southeast of Crows Landing, near Modesto. The predicted ammonia concentrations (see Figure 4-18) were fairly high (>8 ppb) throughout the SJV on August 6. The highest ammonia concentrations (between 140 and 200 ppb) were predicted northwest of

Crows Landing. Ammonia levels in the SFBA and in most of the coastal areas were predicted to be lower than in the SJV.

The predicted spatial patterns for organic material and elemental carbon were quite similar (see Figures 4-19 and 4-20). The model predicted high OM and EC concentrations in San Jose, Sacramento, and Fresno. The predicted OM was also quite high near Modesto (42 to 60 $\mu g/m^3$) and fairly high from Stockton to Visalia, and in Bakersfield. The OM and EC spatial pattern corresponds closely with the spatial pattern of emissions for these species.

The predicted pattern of 24-hr PM_{10} mass concentrations showed modest to high concentrations in the SFBA and in a narrow band extended from Sacramento to Bakersfield (see Figure 4-21). A very high concentration (between 280 and 400 $\mu g/m^3$) was predicted south of Oakland, which probably reflects uncertainties in the crustal PM emission inventory.

4.4 SUMMARY AND RECOMMENDATIONS

Significant progress was made in this study towards the goal of having a scientifically credible aerosol and acid deposition model based on SAQM. The software engineering to incorporate aerosol species and the dominant aerosol processes in the SAQM model was completed. Initial testing of the model against the AUSPEX PM and acid data for the August 3-6, 1990 was completed using preliminary PM and NH_3 emission estimates.

The model testing showed varying degrees of agreement with observations in the SFBA and SJV. Overall, the performance was not nearly as good as was achieved in the ozone modeling of this episode. The two principle problems were that (1) the model often did not track the diurnal patterns of the observed data (causing significant error) and (2) the model tended to underestimate the concentrations of most PM_{10} aerosol species (causing significant bias). The concentrations of PM_{10} nitrate, ammonium, and organic material were consistently underestimated. The concentrations of nitric acid, PM_{10} sulfate, and EC showed a mixture of underestimation and overestimation. PM_{10} mass was mostly underestimated. The only new species for which the simulations predominantly overestimated observations was ammonia.

Further testing of the model is needed to evaluate its performance and perhaps refine its algorithms before it is used for assessing emissions control options. Testing of the model for other types of PM episodes, especially ones with high concentrations of secondary PM constituents and with fogs, which are common in California episodes, is needed. The model's ability to simulate the evolution of the ambient aerosol size distribution, or at least its ability to estimate fine (0-2.5 μm) and coarse (2.5-10 μm) PM species concentrations, should be evaluated. In addition, testing should be conducted using finer spatial resolution than 12 km grids in order to improve the resolution of transport and local source influences.

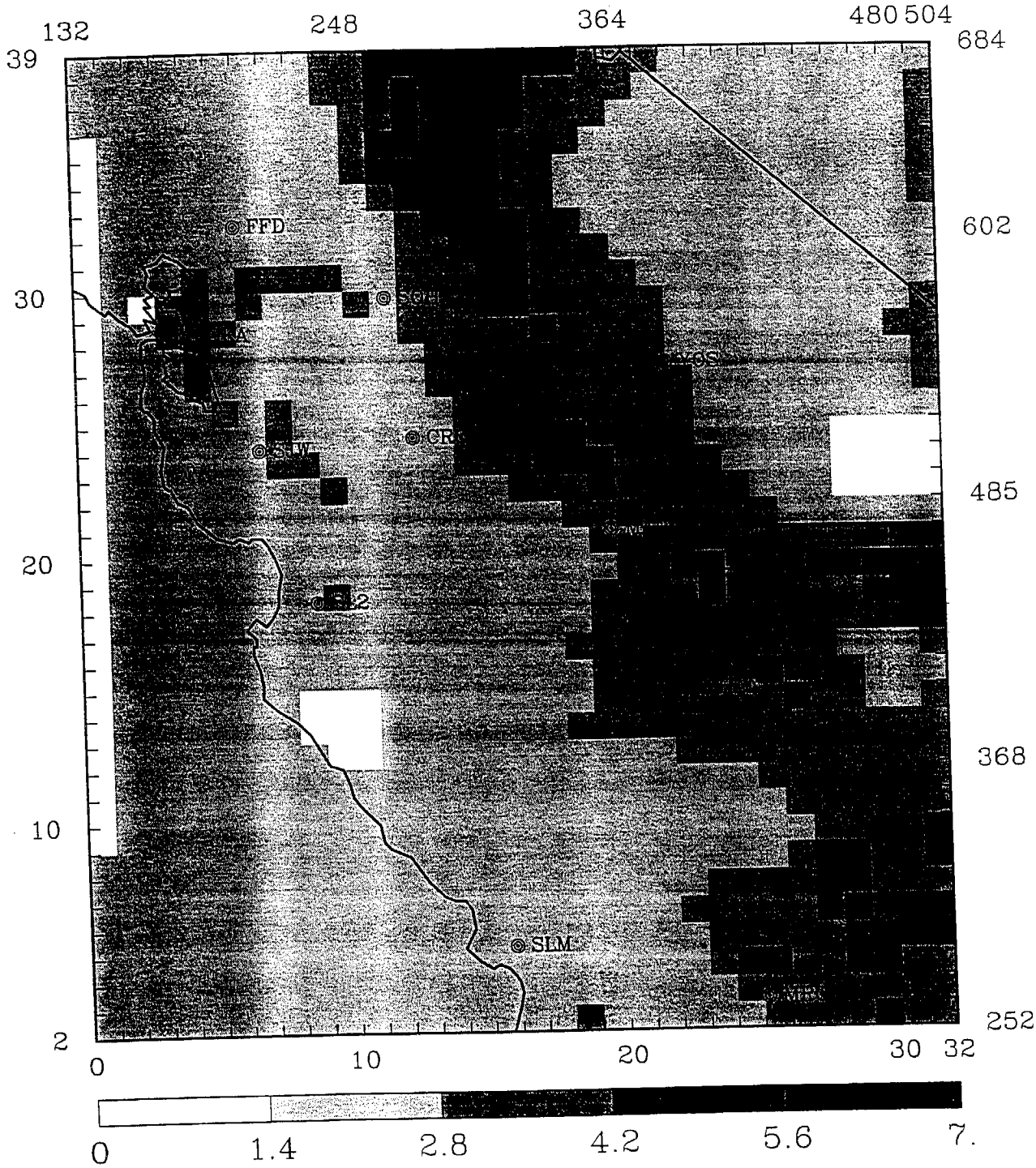

Figure 4-14. Spatial distribution of predicted PM_{10} SO_4 concentrations on August 6, 1990.

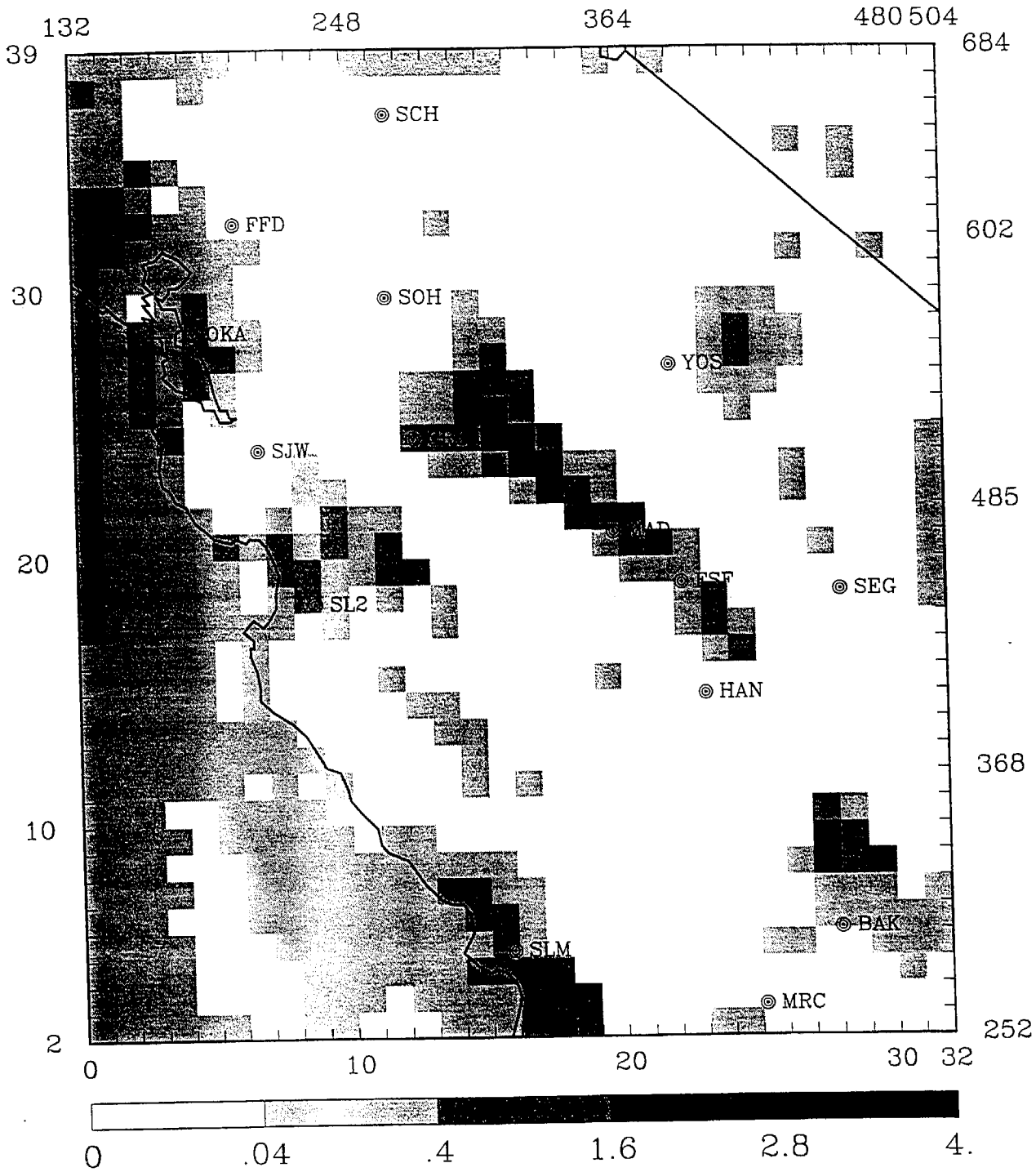

Figure 4-15. Spatial distribution of predicted PM_{10} NO_3 concentrations on August 6, 1990.

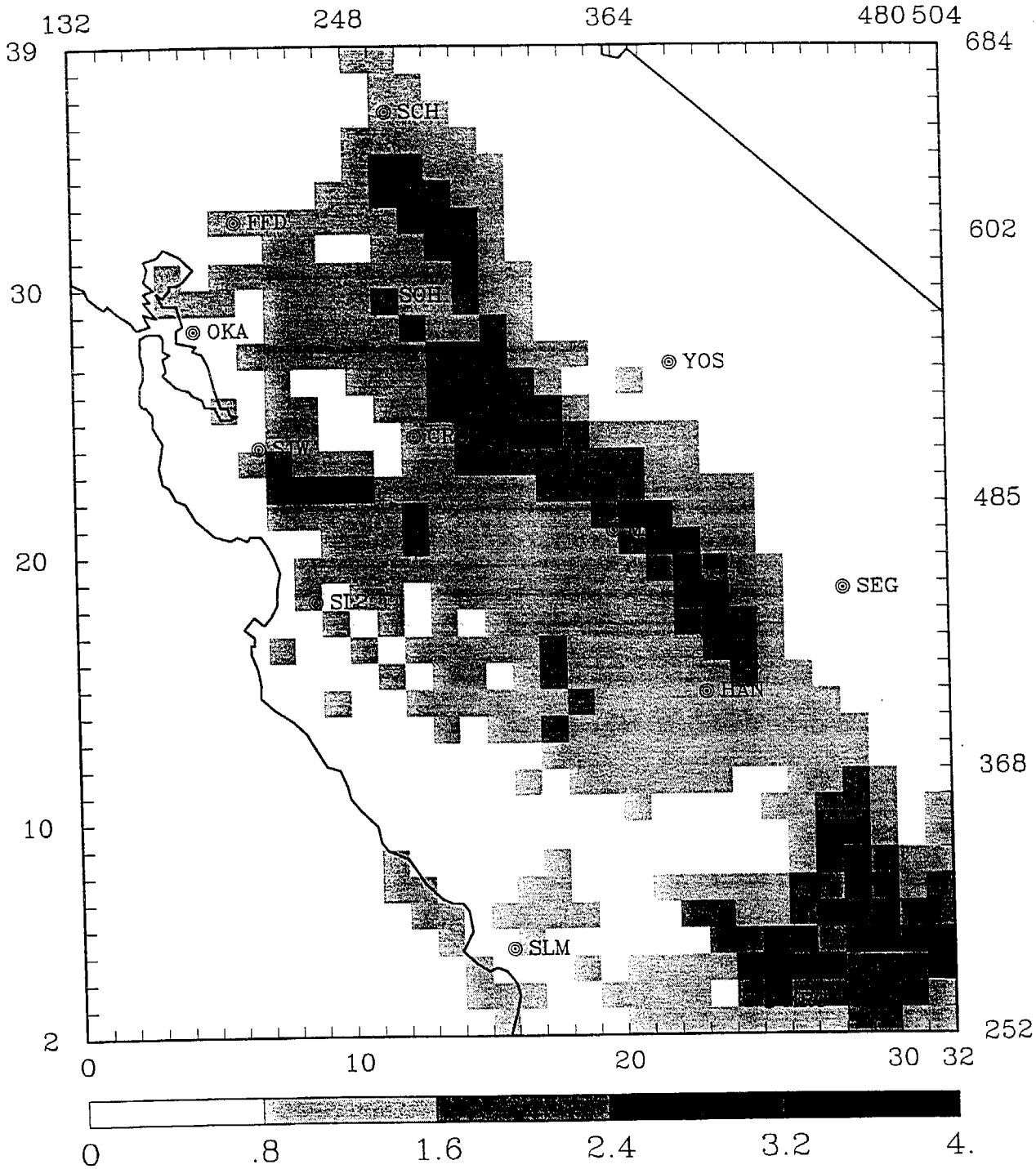

Figure 4-16. Spatial distribution of predicted HNO_3 concentrations on August 6, 1990.

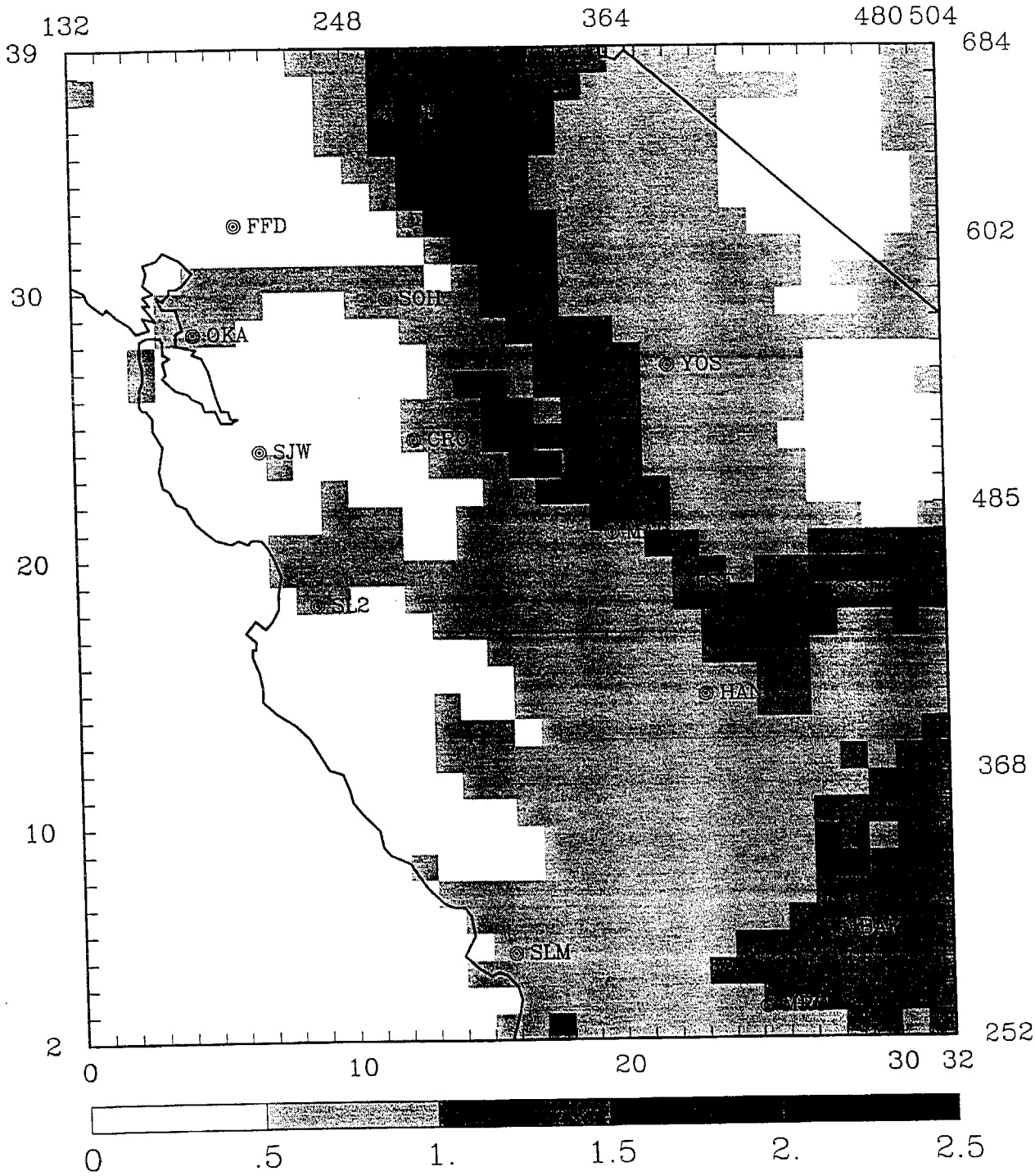

Figure 4-17. Spatial distribution of predicted PM_{10} NH_4 concentrations on August 6, 1990.

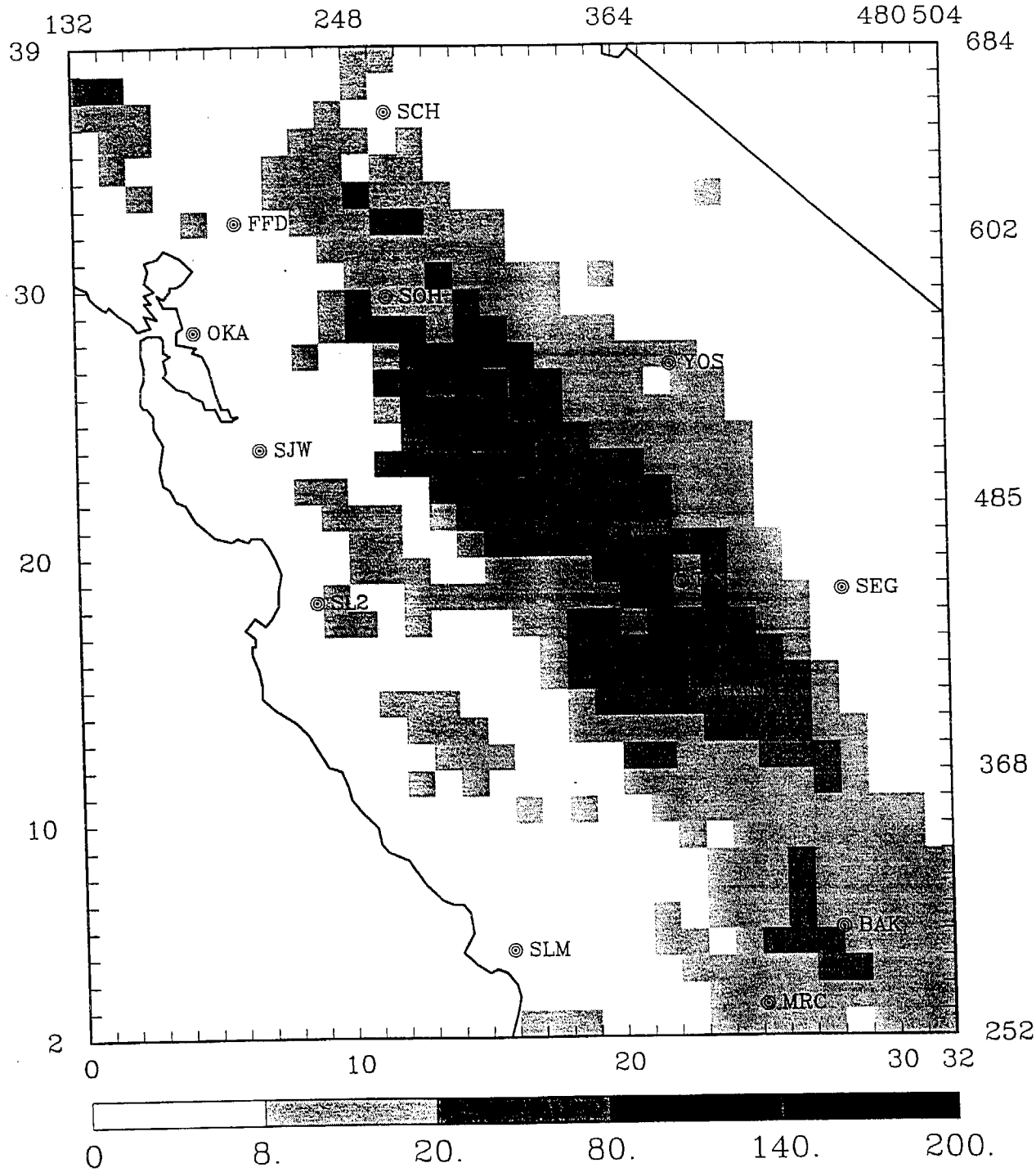

Figure 4-18. Spatial distribution of predicted NH_3 concentrations on August 6, 1990.

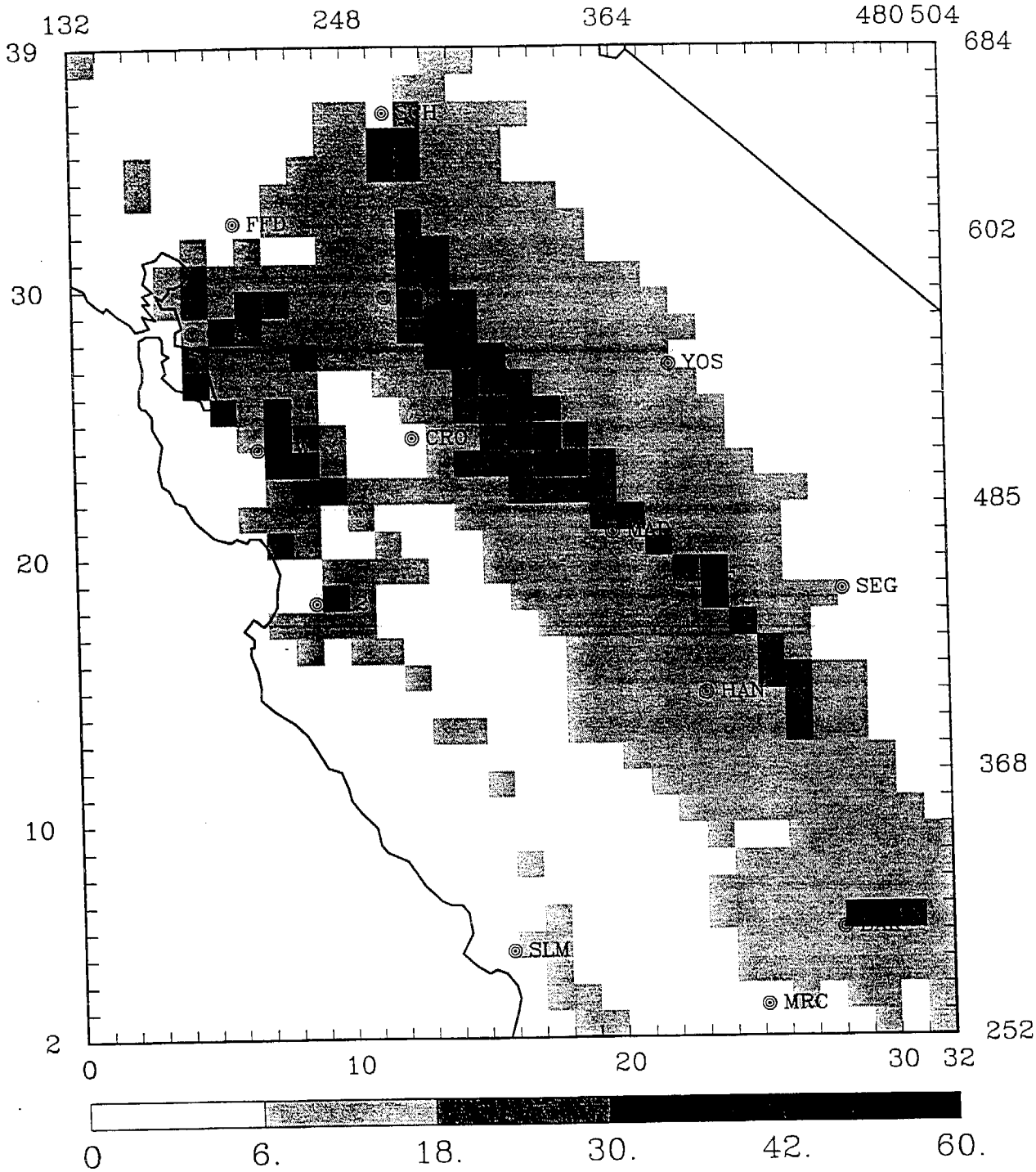

Figure 4-19. Spatial distribution of predicted PM_{10} OM concentrations on August 6, 1990.

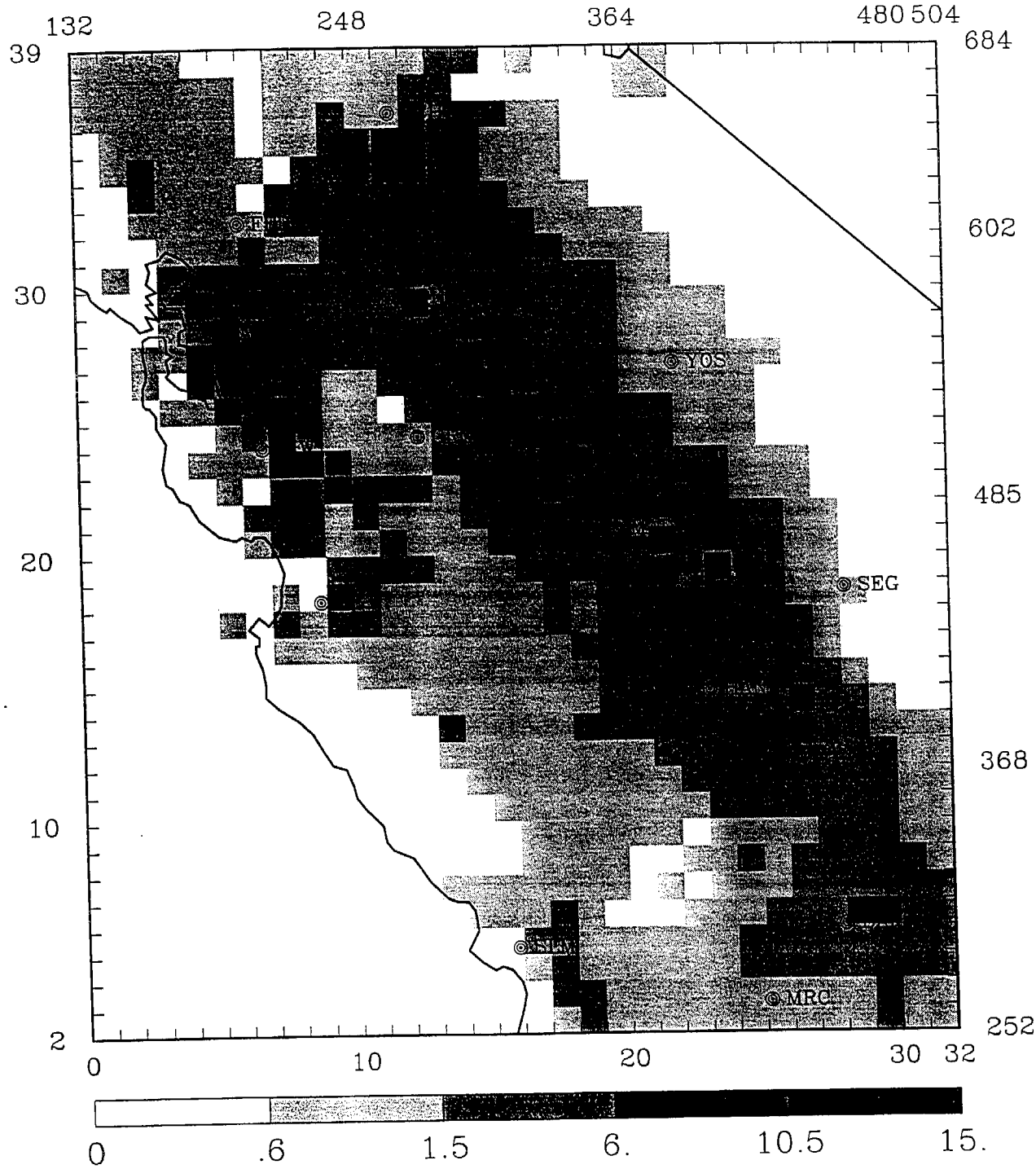

Figure 4-20. Spatial distribution of predicted PM_{10} EC concentrations on August 6, 1990.

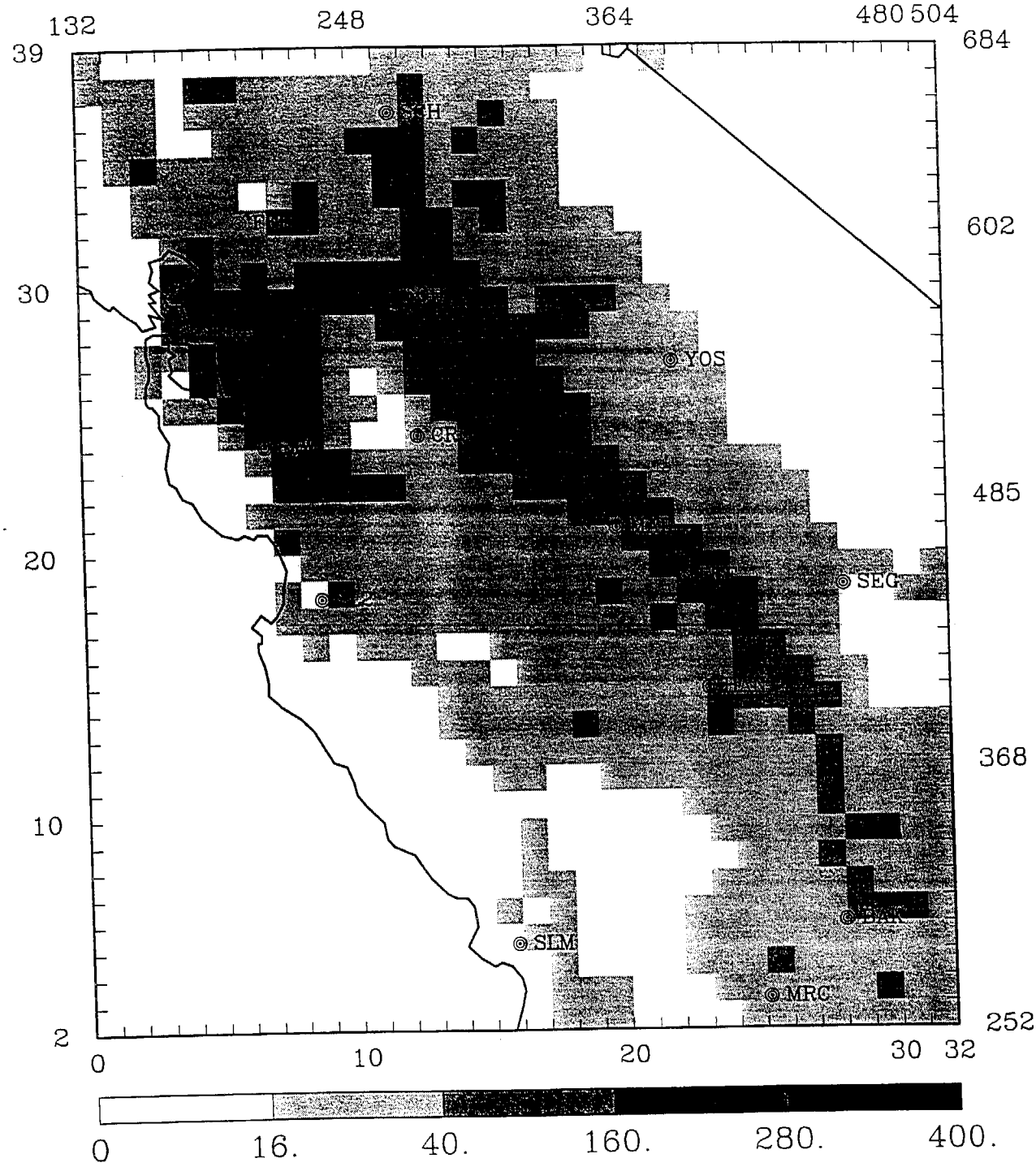

Figure 4-21. Spatial distribution of predicted PM_{10} mass concentrations on August 6, 1990.

5. A NEW TIME STEP ALGORITHM

In reviewing the logic incorporated into the SAQM model for ways to improve its computational efficiency, we discovered that the model did not check that the time step used for horizontal advection would ensure numerical stability. In the SAQM the chemistry integration time step is a user-defined input and the transport time step is calculated as half of the chemistry time step. This design assumes the user will check the stability criteria ($\Delta t < \Delta x / u_{max}$) for each hour and level of the wind field before specifying the chemistry time step. The default time steps are 150 and 300 s for the transport and chemistry operators. The model uses the Bott scheme (Bott, 1989) to solve for the advection in the horizontal and vertical directions. The Bott scheme requires that the Courant stability criteria be fulfilled for numerical stability of the solution. For small grid spacing, the 150 s default time step would often result in unstable solutions at the higher levels of the model where the highest wind speeds typically occur. The SAQM model checks for Courant stability when performing vertical advection and if the stability criteria is not satisfied, it takes multiple vertical advection steps to ensure numerical stability. Hence, the main problem with the SAQM design is that it is not robust because the horizontal advection solutions may be numerically unstable if a user changes the wind field and forgets to adjust the maximum chemistry time step for the maximum wind speeds in the new wind field.

A more robust design is to assign an upper limit on the integration time step and then choose the actual time step based on the Courant stability criteria (both for the horizontal and vertical advection) at the beginning of each hour of simulation. This may lead to a variable number of time steps for each hour, but ensures numerical stability under all conditions. A new subroutine TMSTPS was written to calculate the transport time step based on the Courant limit in the horizontal and vertical directions. A new variable DTMAX was added to the user input file to specify the maximum time step to be used by the model for transport operator. The default value for DTMAX is 450 s. The model interpolates the meteorological variables between the even hours and subroutine TMSTPS is called to calculate the time steps corresponding to the beginning and end of the hour. The minimum of the two time steps is selected as the actual time step for integration. This scheme of selecting integration time step strictly ensures numerical stability at all times during integration. The model was tested on the August 3-6, 1990 episode using the new time step algorithm. Note there was a 9 percent increase in the CPU time used in the simulation (compared to the base case) because of high winds in the upper layers of the models. That is, all of the previous 12 x 12 km resolution runs for the August 3-6 episode may have had some numerical instability in the higher layers of the model.

Tables 5-1 and 5-2 list the 24-hr average concentrations of aerosol and gas-phase species predicted in the base case and the new time step algorithm case on August 6, 1990. Only the last day of the simulation is shown because the differences between the two runs are small and similar on all days. The biggest differences between the two simulations were for PM_{10} NO_3 and PM_{10} NH_4 concentrations for which the percent differences are large, but absolute differences are still small. The differences in predicted PM_{10} SO_4 , OM, EC, and

mass are less than 1.2 percent at all stations. The 24-hr ozone and NO_2 concentrations compare well for the two cases; the largest differences are about 3 percent. For nitric acid and ammonia, the differences are up to 3 and 4 percent. Overall, the results show slightly higher concentrations are predicted for the surface layer with the new time step algorithm. It was reassuring to find that the differences were small. The accurate portion of the base case solutions were probably in the highest layers of the model and had little effect on the surface layer predictions. Use of the new time step algorithm is recommended because it is numerically correct and more robust than the original procedure.

Table 5-1. 24-hr average predicted concentrations of PM species (in $\mu g/m^3$) for the base case and alternate time step case on August 6, 1990.

Species	Station	Base Case Prediction	Alternate Case Prediction	Percent Change
PM_{10} SO_4	Academy	2.94	2.92	-0.7
PM_{10} SO_4	Altamont Pass	1.96	1.96	0.0
PM_{10} SO_4	Buttonwillow	3.06	3.05	0.4
PM_{10} SO_4	Crows Landing	2.22	2.22	-0.1
PM_{10} SO_4	Edison	5.19	5.17	-0.4
PM_{10} SO_4	Pacheco Pass	1.94	1.93	-0.1
PM_{10} SO_4	Sequoia N. P.	4.45	4.43	-0.4
PM_{10} SO_4	Yosemite	2.62	2.61	-0.3
PM_{10} NO_3	Academy	0	0	0.0
PM_{10} NO_3	Altamont Pass	0	0	0.0
PM_{10} NO_3	Buttonwillow	0	0	0.0
PM_{10} NO_3	Crows Landing	0.52	0.53	2.7
PM_{10} NO_3	Edison	0.24	0.48	101.
PM_{10} NO_3	Pacheco Pass	0.03	0.03	14.
PM_{10} NO_3	Sequoia N. P.	0	0	17.
PM_{10} NO_3	Yosemite	0	0	-14.
PM_{10} NH_4	Academy	0.8	0.69	-13.
PM_{10} NH_4	Altamont Pass	0.39	0.27	-30.
PM_{10} NH_4	Buttonwillow	0.86	0.78	-9.8
PM_{10} NH_4	Crows Landing	0.62	0.49	-21.
PM_{10} NH_4	Edison	1.31	0.78	-41.
PM_{10} NH_4	Pacheco Pass	0.44	0.34	-22.
PM_{10} NH_4	Sequoia N. P.	1.37	1.36	-0.9
PM_{10} NH_4	Yosemite	0.78	0.74	-5.3
PM_{10} EC	Academy	1.67	1.67	0.1
PM_{10} EC	Altamont Pass	1.99	1.99	0.3
PM_{10} EC	Buttonwillow	1.45	1.45	0.0
PM_{10} EC	Crows Landing	2.33	2.34	0.2
PM_{10} EC	Edison	7.18	7.22	0.6
PM_{10} EC	Pacheco Pass	1.61	1.61	-0.4
PM_{10} EC	Sequoia N. P.	0.46	0.45	-0.7
PM_{10} EC	Yosemite	0.82	0.82	-0.2
PM_{10} OM	Academy	8.9	8.9	0.1
PM_{10} OM	Altamont Pass	8.84	8.86	0.2
PM_{10} OM	Buttonwillow	7.42	7.42	0.0
PM_{10} OM	Crows Landing	10.52	10.54	0.2
PM_{10} OM	Edison	31.23	31.4	0.5
PM_{10} OM	Pacheco Pass	7.39	7.36	-0.4
PM_{10} OM	Sequoia N. P.	2.9	2.89	-0.4
PM_{10} OM	Yosemite	5	5	-0.1
PM_{10} mass	Academy	25.84	25.84	0.0
PM_{10} mass	Altamont Pass	34.05	34.19	0.4
PM_{10} mass	Buttonwillow	22.36	22.38	0.1
PM_{10} mass	Crows Landing	30.46	30.54	0.3
PM_{10} mass	Edison	62.47	63.25	1.2
PM_{10} mass	Pacheco Pass	27.41	27.45	0.1
PM_{10} mass	Sequoia N. P.	14.54	14.49	-0.3
PM_{10} mass	Yosemite	15.76	15.76	-0.0

Table 5-2. 24-hr average predicted concentrations of gas-phase species (in ppb) for the base case and alternate time step case on August 6, 1990.

Species	Station	Base Case Prediction	Alternate Case Prediction	Percent Change
Ozone	Academy	50.0	50.1	0.2
Ozone	Arvin	61.6	62.5	1.5
Ozone	Crows Landing	49.3	49.5	0.4
Ozone	Corcoran	49.5	49.8	0.6
Ozone	Edison	54.3	55.8	2.6
Ozone	Fresno	49.3	49.5	0.5
Ozone	Gilroy	38.4	38.5	0.4
Ozone	Kern Refuge	53.1	53.9	1.5
Ozone	Livermore	38.8	38.8	0.0
Ozone	Oildale	45.0	45.8	1.8
Ozone	Citrus Heights	44.6	44.7	0.1
Ozone	Stockton	37.9	37.7	-0.4
NO_2	Academy	2.22	2.29	3.0
NO_2	Arvin	7.29	7.33	0.5
NO_2	Crows Landing	10.88	10.96	0.7
NO_2	Corcoran	3.1	3.15	1.6
NO_2	Edison	6.53	6.58	0.7
NO_2	Fresno	16.34	16.52	1.1
NO_2	Gilroy	6.39	6.43	0.7
NO_2	Kern Refuge	7.11	7.08	-0.4
NO_2	Livermore	11.7	11.78	0.7
NO_2	Oildale	18.3	18.55	1.4
NO_2	Citrus Heights	13.82	13.96	1.0
NO_2	Stockton	7.22	7.30	1.1
HNO_3	Academy	0.87	0.86	-0.5
HNO_3	Altamont Pass	1.04	1.02	-2.7
HNO_3	Buttonwillow	1.16	1.17	0.8
HNO_3	Crows Landing	1.35	1.32	-2.0
HNO_3	Edison	3.6	3.54	-1.8
HNO_3	Pacheco Pass	1.47	1.46	-0.7
HNO_3	Sequoia N. P.	0.24	0.24	-1.6
HNO_3	Yosemite	0.22	0.22	-1.1
NH_3	Academy	11.17	11.3	1.2
NH_3	Altamont Pass	36.48	36.83	1.0
NH_3	Buttonwillow	19.47	19.57	0.5
NH_3	Edison	13.06	13.61	4.2
NH_3	Pacheco Pass	5.26	5.34	1.6
NH_3	Sequoia N. P.	3.68	3.67	-0.1
NH_3	Yosemite	6.8	6.87	1.0

6. REFERENCES

Blumenthal D.L., Lurmann F.W., Roberts P.T., Main H.H., MacDonald C.P., Knuth W.R., and Niccum E.M. (1997) Three-dimensional distribution and transport analyses for SJVAQS/AUSPEX. Draft final report prepared for San Joaquin Valley Air Pollution Study Agency, Sacramento, CA by Sonoma Technology, Inc., Santa Rosa, CA, Technical & Business Systems, Santa Rosa, CA, and California Air Resources Board, Sacramento, CA, STI-91060-1705-DFR, February.

Bott A. (1989) A positive definite advection scheme obtained by nonlinear renormalization of the advective fluxes. *Mon. Wea. Rev.* **117**, 1006-1015.

Bromley L.A. (1973) *AIChE J.* **19**, 313-320.

Chang J.S., Brost R.A., Isaksen I.S.A., Madronich S., Middleton P., Stockwell W.R., and Walcek C.J. (1987) A three-dimensional Eulerian acid deposition model: physical concepts and formulation. *J. Geophys. Res.* **92**, 14681-14700.

Chinkin L.R., Main H.H., and Coe D.L. (1996) Evaluation and improvement of methods for determining ammonia emissions in the San Joaquin Valley. Technical support study 15. Technical memorandum prepared for California Air Resources Board, Sacramento, CA by Sonoma Technology, Inc., Santa Rosa, CA, March.

Chow J.C., Watson J.G., Lowenthal D.H., Solomon P.A., Magliano K., Ziman S., and Richards L.W. (1992) PM_{10} source apportionment in California's San Joaquin Valley. *Atmos. Environ.* **26A**, 3335-3354.

Chow J.C., Watson J.G., Zhiqiang L., Lowenthal D.H., Frazier C.A., Solomon P.A., Thuillier R.H., and Magliano K. (1996) Descriptive analysis of $PM_{2.5}$ and PM_{10} at regionally representative locations during SJVAQS/AUSPEX. *Atmos. Environ.* **30**, 2079-2112.

Gear C.W. (1971) *Numerical Initial Value Problem in Ordinary Differential Equations*. Prentice-Hall, Englewood Cliffs, NJ.

Gelbard F. (1990) Modeling multicomponent aerosol particle growth by vapor condensation. *Aerosol Sci. Technol.* **12**, 399-412.

Gelbard F., Tambour Y., and Seinfeld J.H. (1980) Sectional representation for simulating aerosol dynamics. *J. Colloid Interface Sci.* **76**, 541-556.

Gery M.W., Whitten G.Z., and Killus J.P. (1988) Development and testing of the CBM-IV for urban and regional modeling. Report prepared by Systems Applications Inc., San Rafael, CA, EPA Contract No. 68-02-4136.

Grosjean D. and Seinfeld J.H. (1989) Parameterization of the formation potential of secondary organic aerosols. *Atmos. Environ.* **23**, 1733-1747.

Hesstwedt E., Hov O., and Isaksen I.S.A. (1978) Quasi-stead-state approximation in air pollution modeling. *Int. J. Chem. Kinet.* **10**, 971-994.

Hildemann L.M., Russell A.M., and Cass G.R. (1984) Ammonia and nitric acid concentrations in equilibrium with atmospheric aerosols: experiment vs. theory. *Atmos. Environ.* **18**, 1737-1750.

Kim Y.P. and Seinfeld J.H. (1990) Simulation of multicomponent aerosol condensation by the moving sectional method. *J. Colloid Interface Sci.* **135**, 185-199.

Kim Y.P., Seinfeld J.H., and Saxena P. (1993a) Atmospheric gas - aerosol equilibrium I. Thermodynamic model. *Aerosol Sci. Technol.* **19**, 157-181.

Kim Y.P., Seinfeld J.H., and Saxena P. (1993b) Atmospheric gas - aerosol equilibrium II. Analysis of common approximations and activity coefficient calculation methods. *Aerosol Sci. Technol.* **19**, 182-198.

Kumar N., Lurmann F.W., and Carter W.P.L. (1995) Development of the flexible chemical mechanism version of the urban airshed model. Final report prepared for the California Air Resources Board, Sacramento, CA by Sonoma Technology, Inc., Santa Rosa, CA, STI-94470-1508-FR, August.

Kumar N., Lurmann F.W., Wexler A.S., Pandis S., and Seinfeld J.H. (1996) Development and application of a three-dimensional aerosol model. Paper presented at *A&WMA's Speciality Conference on Computing in Environmental Resource Management, Raleigh-Durham, NC, December 2-4*, STI-1609.

Kusik C.L. and Meissner H.P. (1978) *AIChE Symp. Ser.* **173**, 14-20.

Lamb R.G. (1982) A regional scale (1000 km) model of photochemical air pollution. 1, Theoretical formulation. Report prepared by Office of Research and Development, U.S. Environmental Protection Agency, Research Triangle Park, NC.

Lurmann F.W. and N. Kumar (1997) Application of the UAM-AERO model to two 1995 PM10 episodes in the South Coast Air Basin. Report prepared for South Coast Air Quality Management District, Diamond Bar, CA by Sonoma Technology, Inc., Santa Rosa, CA, (in preparation).

Lurmann F.W., Kumar N., Loomis C., Cass G.R., Seinfeld J.H., Lowenthal D., and Reynolds S.D. (1996) PM_{10} air quality models for application in the San Joaquin Valley PM_{10} SIP. Final report prepared for San Joaquin Valleywide Air Pollution Study Agency, Sacramento, CA by Sonoma Technology, Inc., Santa Rosa, CA, STI-94250-1595-FR, ARB Contract No. 94-1PM, September.

Lurmann F.W., Wexler A.S., Pandis S., Musarra S., Kumar N., Seinfeld J.H., and Hering S.V. (1997) Development of an acid deposition model (UAM-AERO) for the South Coast Air Basin. Final report prepared for California Air Resources Board, Sacramento, CA by California Institute of Technology, Pasadena, CA, Sonoma Technology, Inc., Santa Rosa, CA, and Aerosol Dynamics, Inc., Berkeley, CA, ARB Contract No. 92-311, August.

Pandis S.N. (1996) Equil 2.1 user's guide. Report prepared for California Air Resources Board, Sacramento, CA.

Pilinis C. and Seinfeld J.H. (1987) Continued development of a general equilibrium model for inorganic multicomponent atmospheric aerosols. *Atmos. Environ.* **21**, 2453-2466.

Pilinis C. and Seinfeld J.H. (1988) Development and evaluation of an Eulerian photochemical gas-aerosol model. *Atmos. Environ.* **22**, 1985-2001.

Pandis S.N., Harley R.A., Cass G.R., and Seinfeld J.H. (1992) Secondary organic aerosol formation and transport. *Atmos. Environ.* **26A**, 2269-2282.

Pandis S.N., Wexler A.S., and Seinfeld J.H. (1993) Secondary organic aerosol formation and transport - II. Predicting the ambient secondary organic aerosol size distribution. *Atmos. Environ.* **27A**, 2403-2416.

Pitzer K.S. (1979) In *Activity Coefficients in Electrolyte Solutions*, Vol. 1, Ptykowicz R.M., ed., CRC Press, Boca Raton, FL, p. 157.

Ranzieri A. (1996) Personal communication with F.W. Lurmann regarding the draft updated SJV ammonia emissions inventory.

Saxena P., Hildemann L.M., McMurry P.H., and Seinfeld J.H. (1995) Organics alter hygroscopic behaviour of atmospheric particles. *J. Geophys. Res.* **100**, 18755-18770.

Seigneur C., Hudischewskyi A.B., Seinfeld J.H., Whitby K.T., Whitby E.R., Brock J.R., and Barnes H.M. (1986) Simulation of aerosol dynamics: a comparative review of mathematical models. *Aerosol Sci. Technol.* **5**, 205-222.

Slinn S.A. and Slinn W.G.N. (1980) Predictions for particle deposition on natural waters. *Atmos. Environ.* **24**, 1013-1016.

Slinn W.G.N., Hasse L., Hicks B.B., Hogan A.W., Lai D., Liss P.S., Munnich K.O., Sehmel G.A., and Vittori O. (1978) Some aspects of the transfer of atmospheric trace constituents past the air-sea interface. *Atmos. Environ.* **12**, 2055-2087.

Stelson A.W., Friedlander S.K., and Seinfeld J.H. (1979) A note on the equilibrium relationship between ammonia and nitric acid and particulate ammonium nitrate. *Atmos. Environ.* **13**, 369-371.

Stokes R.H. and Robinson R.A. (1966) *J. Phys. Chem.* **70**, 2126-2130.

Sun P., Chock D.P., and Winkler S.L. (1994) An implicit-explicit hybrid solver for a system of stiff kinetic equations. Paper presented at the *Air & Waste Management Association 87th Annual Meeting, Cincinnati, OH, June 19-24.*

Voldner E.C., Barrie L.A., and Sirois A. (1986) A literature review of dry deposition of oxides of sulphur and nitrogen with emphasis on long-range transport modeling in North America. *Atmos. Environ.* **20**, 2101-2123.

Watson J.G., Chow J.C., Lurmann F.W., and Musarra S.P. (1994) Ammonium nitrate, nitric acid, and ammonia equilibrium in wintertime Phoenix, Arizona. *J. Air & Waste Manag. Assoc.* **44**, 405-412.

Wexler A.S. and Seinfeld J.H. (1990) The distribution of ammonium salts among a size and composition dispersed aerosol. *Atmos. Environ.* **24A**, 1231-1246.

Wexler A.S. and Seinfeld J.H. (1992) Analysis of aerosol ammonium nitrate: departures from equilibrium during SCAQS. *Atmos. Environ.* **26A**, 579-591.

Wexler A.S., Lurmann F.W., and Seinfeld J.H. (1994) Modeling urban and regional aerosols: I. model development. *Atmos. Environ.* **28**, 531-546.

6. References (cont.)

Blumenthal D.L. (1993) Field Study Plan for the San Joaquin Valley Air Quality Study (SJVAQS) and the Atmospheric Utility Signatures, Predictions, and Experiments (AUSPEX) Program. Final report to California Air Resources Board, STI-98020-1241-FR, Sacramento, CA.

Bott A. (1989a) A positive definite advection scheme obtained by nonlinear renormalization of the advective fluxes. *Mon. Weather Rev.* **117**, 1006-1015.

Bott A. (1989b) *Reply Mon. Wea. Rev.* **117**, 2633-2636.

Chang J.S., R.A. Brost, I. Isaksen, S. Madronich, P. Middleton, W.R. Stockwell, and C.J. (1987) A three-dimensional Eulerian acid deposition model: physical concepts and formation. *J. Geophys. Res.* **92**, 14681-14700.

Chang, J.S., S. Jin, Y. Li, M. Beauharnois, K-H. Chang, H-C. Huang, C-H. Lu, G. Wojcik, S. Tanrikulu, and J. DaMassa (1996) The SARMAP Air Quality Model. Part 1 of SAQM Final Report. California Air Resources Board, Sacramento, CA.

Crowley, W. P. (1968) Numerical advection experiments. *Mon. Weather Rev.* **96**, 1-11.

Dabdub D. and J. H. Seinfeld (1996) Parallel computation in atmospheric chemical modeling. *Parallel Computing* **22**, 111-130.

DaMassa J., S. Tanrikulu, K. Magliano, A. J. Ranzieri, and L. Niccum (1996) Performance Evaluation of SAQM in Central California and Attainment Demonstration for the August 3-6, 1990 Ozone Episode. California Air Resources Board, Sacramento, CA.

Gery M. W., G. Z. Whittenm J. P. Killus, and M. C. Dodge (1989) A photochemical kinetics mechanism for urban and regional scale computer modeling. *J. Geophys. Res.* **94**, 12925-12956.

Grell G. A., J. Dudhia and D. R. Stauffer (1993) A Description of the Fifth-generation Penn State/NCAR Mesoscale Model (MM5). NCAR Tech. Note, NCAR/TN-398+1A.

Hubbe J. M., and J. R. Pederson (1994) Dry deposition Study Planning. *Planning and Managing Regional Air Quality*, edited by P. A. Solomon, Lewis Publishers, Florida, in conjunction with Pacific Gas and Electric Company.

Lagarias J. S., and W. W. Sylte (1991) Designing and Managing the San Joaquin Valley Air Quality Study. J. Air Waste Manage. Assoc. **41**, 1176-1179.

Lurmann F. W., M. Gery, and W. P. L. Carter (1991) Implementation of the 1990 SAPRC Chemical Mechanism in the Urban Airshed Model. Final Report to the California South Coast Air Quality Management District, Sonoma Technology, Inc. Report STI-y99290-1164-FR, Santa Rosa, CA.

Magliano, K. L. (1994) Summary of SARMAP emissions modeling. Technical Support Division, California Air Resources Board, Sacramento, CA.

McRae G. J., W. R. Goodin and J. H. Seinfeld (1982) Numerical solution of the atmospheric diffusion equation for chemically reacting flows. *J. Comp. Phys.* **45**, 1-42.

Ranzieri A. J., and R. H. Thuillier (1994) SJVAQS and AUSPEX: a Collaborative Air Quality Field Measurement and Modeling Program. *Planning and Managing Regional Air Quality*,

edited by P. A. Solomon, Lewis Publishers, Florida, in conjunction with Pacific Gas and Electric Company.

Roberts P. T., C. G. Lindsey, and T. B. Smith (1995) Analyses of San Joaquin Valley Air Quality and Meteorology. Planning and Managing Regional Air Quality}, edited by P. A. Solomon, Lewis Publishers, Florida, in conjunction with Pacific Gas and Electric Company.

San Joaquin Valley Air Quality Study Policy Committee (1996) *San Joaquin Valley Air Quality Study, Policy-Relevant Findings.*

Seaman N. L., D. R. Stauffer and A. M. Lario-Gibbs (1995) A multiscale four dimensional data assimilation applied in the San Joaquin Valley during SARMAP. Part I: Modeling design and basic performance characteristics. *J. Applied Met.* **34**, 1739-1761

Tesche, T. W., P. Georgopoulos, J. H. Seinfeld, G. Cass, F. L. Lurmann, and P. M. Roth (1990) Improvement of Procedures for Evaluating Photochemical Models, California Air Resources Board.

Yanenko N. N. (1971) *The Method of Fractional Steps.* Springer, New York.

APPENDIX A

MODIFICATIONS IN THE SAQM CODE

A1. MODIFICATIONS IN THE SAQM CODE

This appendix describes the changes that were made in the SAQM code to develop the aerosol version of the computationally efficient acid deposition model (SAQM-AERO) for California. The code changes were principally made to install a new gas-phase chemistry solver and the aerosol module. The types of modifications included 1) major changes in existing subroutines, 2) minor changes in existing subroutines, 3) addition of new subroutines, and 4) elimination of old subroutines. **Tables A-1 and A-2** list the SAQM subroutines that were modified in major and minor ways to create to new model. **Tables A-3 and A-4** list the subroutines that were added to and eliminated from the model. **Table A-5** lists subroutines that remain the same as in the SAQM code.

Table A-1. List of FORTRAN subroutines changed in major ways.

bcflow.f	buffioc_sls.f	fileini1.f	vdiffex_sls.f	a_cmmns.com
bcflow_sls.f	chem.f	initer.f	vdiffim.f	
blk_data.f	chem_sls.f	mydummy.f	vdiffim_sls.f	
blk_data_sls.f	drivern.f	saqm2c.f	vdiffj.f	
buff_sls.f	driver_sls.f	vdiffex.f	vmix.f	

Table A-2. List of FORTRAN subroutines changed in minor ways.

addaqc.f	eddym4.f*	foutc1_ha.f	klsour_sls.f	vadvcoef.f*
aqchem.f	eddym4_sls.f*	foutc1_sls.f	mapref_sls.f*	vadvcoef_sls.f*
buffinm.f*	edycofn.f*	foutc1_slsha.f	mratio.f	vadvec.f*
cblcalc.f	edycofn_sls.f*	foutn1.f	mratio_sls.f	vadvec_sls.f*
cksumer.f*	fileinbc.f	foutn1_ha.f	nstpc.f	a_b1desc.com
cksumer_sls.f*	fileinc1_ha.f	foutn1_sls.f	omegas.f*	a_c1desc.com
cldprc.f	fileinee.f*	foutn1_slsha.f	omegas_sls.f*	a_cmmnw.com
concdmp.f	fileinjv.f	hadvec.f*	phot.f*	a_datas.com
couple.f	fileinm1.f	hadvec_sls.f*	prcout.f*	a_eedesc.com
couple_sls.f	fileinm2.f	hdiff.f*	rdsour.f	a_filfmt.com
decouple_sls.f	finc1_sls.f	hdiff_sls.f*	sfcconc.f	a_i1desc.com
delconc.f*	finc1_slsha.f	interi.f*	sfcconc_sls.f	a_iopts.com
delconci.f*	floor.f*	interp.f*	sumchem.f	a_n1desc.com
eddycof.f*	floor_sls.f*	interp_sls.f*	sumchem_sls.f	a_params.com
eddycof_sls.f*	foutc1.f	klsour.f	timeswap.f*	a_units.com

Table A-3. List of new FORTRAN subroutines added.

addaerem.f	chemi.f	hdiffaer_sls.f	pblmod.f	a_aero.com
addaerem_sls.f	chkneg.f	jacbnd.f	second.f	chparm.com
adddep.f	chread.f	lsfun.f	spline.f	dep.inc
adddep_sls.f	equil1_5.f	lsodef1.f	sprate.f	nsect.inc
aeroaq.f	equil2_0.f	newrk.f	stodef1.f	param.inc
blk_dat2.f	equil2_1.f	nitbal.f	tmstps.f	
blk_dat3.f	hdiffaer.f	opena.f	vdep.f	

Table A-4. List of FORTRAN subroutines eliminated from the original SAQM.

fileinc2_ha.f	foutc2.f	foutn2_sls.f	predrate_sls.f	a_data1.com
fileini2.f	foutc2_sls.f	foutn2_slsha.f	produc.f	a_i2desc.com
finc2_sls.f	foutc2_slsha.f	integ1.f	setdtc.f	a_n2desc.com
finc2_slsha.f	foutn2.f	integ1_sls.f	setdtc_sls.f	
finsls2.f	foutn2_ha.f	predrate.f	a_c2desc.com	

Table A-5. List of FORTRAN subroutines unchanged from the original SAQM.

alldone.f	fileopen.f	rdufh.f	a_cmmnw1.com	a_oddmet.com
blnk.f	j2g.f	tridiag.f	a_cmmnw2.com	a_parmj.com
blnkal.f	oiwait.f	wrfd.f	a_datfmt.com	a_paramw.com
bott_h.f	rabort.f	wrspr.f	a_expname.com	a_r2fd.com
charout.f	rdfd.f	wrtext.f	a_jvdesc.com	a_r2sp.com
const.f	rdspr.f	wrtsh.f	a_logdb.com	a_ufhead.com
crayrtns.f	rdtext.f	wrufh.f	a_m1desc.com	
expment.f	rdtsh.f	a_cmmnj.com	a_m2desc.com	

The FORTRAN subroutines from the original SAQM code that are no longer used (Table A-4) were either specific to the chemical mechanism/integrator (*integ1.f, integ1_sls.f, predrate.f, predrate_sls.f, produc.f, setdtc.f, setdtc_sls.f*, and *a_data1.com*) or correspond to second concentration input/output subroutines. As described below, instead of separating each of the initial conditions and concentration output files into two different files (as is done in the SAQM), a single input and output file is used to store concentrations of all species. Thus, the FORTRAN code specific to reading/writing the second concentration input/output files is no longer needed.

A1.1 NEW FORTRAN SUBROUTINES ADDED

Table A-3 lists the new FORTRAN subroutines which have been added to the SAQM code. Most of these subroutines are part of the new chemical mechanism/solver or the aerosol module. In addition, there are three new subroutines (*opena.f, second.f,* and *tmstps.f*) that are called by the main program. The subroutine OPENSAQM reads the input and output files from the input file "saqm.input" and opens those files for I/O purposes. **Table A-6** describes the order in which the file names should appear in the file "saqm.input". The subroutine SECOND emulates the CRAY timer routine SECONDS and is used to calculate the wall clock time taken per time step. The subroutine TMSTPS is used to calculate the integration time step based on the Courant stability limit.

Table A-6. Order of files appearing in the SAQM.INPUT file.

Order	File
1	Diagnostic output file
2	Hourly instantaneous concentration output file
3	Meteorological data input file 1
4	Meteorological data input file 2
5	Initial conditions file
6	Emissions input file
7	Chemical parameter (CHEMPARAM) input file
8	Photolytic rate data file
9	DB output file
10	Boundary conditions input file
11	Simulation control input file
12	Diagnostic output file to check concentrations at specific locations
13	Instantaneous concentration output file for RESTART
14	Diagnostic output file for aerosol module
15	Output file for aerosol box model (it is written if the model crashes in the aerosol module)
16	Hourly average concentration output file
17	Hourly instantaneous concentration output file for surface sub-layer module
18	Hourly average concentration output file for surface sub-layer module
19	Instantaneous concentration output file for RESTART for surface sub-layer module
20	Surface roughness file (only if USEDEFRF = .FALSE.)
21	Initial conditions file for surface sub-layer (only if RESTART = .TRUE.)

A1.1.1 Chemical Mechanism Specific Subroutines

The FORTRAN subroutines, which are specific to the chemical mechanism or the chemical solver, are *blk_dat2.f, chemi.f, chkneg.f, chread.f, jacbnd.f, lsfun.f, lsodef1.f, newrk.f, nitbal.f, sprate.f, stodef1.f*, and *chparm.com.*

Blk_dat2.f is a FORTRAN block data file that defines the names of the gas-phase species and their molecular weights, and maps the species to the corresponding species in the emission input file (see Figure 3-6 of the report). The *chemi.f* file contains three mechanism-dependent subroutines that are produced by the FCM interface, which was used to implement the IEH solver in the SAQM. These three subroutines are called RATES, CHMFST, and CHMSLO. The RATES subroutine calculates the reaction throughput rates of all the reactions at each time step. CHMSLO and CHMFST subroutines calculate the net rate of change (time derivatives) of concentrations of slow- and fast-reacting species, respectively. Subroutine RATES is called every time (and before) CHMSLO or CHMFST is called. All three subroutines have eight real arguments, listed below in the order in which they appear on the argument list:

1. Array A0 which contains the constant and slow species concentrations (input)
2. Array A1 which contains the reaction rate constants (input)
3. Array A2 which contains the reaction throughput rates (output from RATES; input for CHMSLO and CHMFST)
4. Array A3 which contains the constant coefficients (input)
5. Array A4 which contains the time derivatives of each species (output from CHMSLO and CHMFST; not used in RATES)
6. Array A5 which contains the fast species concentrations (input)
7. Array A6 which contains the concentration of steady-state species (output from RATES; not used in CHMFST and CHMSLO)
8. Real scalar variable TIME which contains the current time (currently not used)

Subroutine CHKNEG checks if the concentration of fast-reacting species (other than the radical species) becomes negative. This subroutine is called by the chemical integrator during integration to check for negative concentration; if the concentration of any species (other than the radical species) becomes negative, the integrator time step is reduced and the integration step is performed again until those species have positive concentrations. Subroutine CHREAD reads the CHEMPARAM input file.

Subroutines LSODEF1 and STODEF1 contain the main code for the IEH solver, whereas LSFUN contains various utility routines that are called by both LSODEF1 and STODEF1. Subroutine JACBND contains the code to calculate the Jacobian (the derivatives of the rate of change of species concentrations with respect to other species concentrations) for fast-reacting species. The IEH solver options are currently set to estimate the Jacobian rather than explicitly evaluating the Jacobian in subroutine JACBND.

Subroutine NEWRK calculates the reaction rates for nonphotolytic reactions based on the data read from the CHEMPARAM input file and the temperature. This routine is called

before the beginning of integration for each grid cell. Subroutine SPRATE is called every time (and after) NEWRK is called to calculate the rates of "special" reactions (to match the reaction rates in the SAQM) and to update the photolytic reaction rates. Subroutine SPRATE has hardwired code in it and must be updated whenever the chemical mechanism is changed in the model. Subroutine NITBAL can be used to force the nitrogen balance while integrating the chemistry. This subroutine is called after every integration step if the logical variable LNITBAL is .TRUE. This subroutine assigns the lost or gained nitrogen mass to HNO_3 and NO_2 equally immediately after the integration step.

CHPARM.COM is a FORTRAN include file that contains parameter statements and common blocks specific to the chemistry. Figure 3-5 (in the report) shows the CHPARM.COM file used in the model. LSPEC is the number of advected gas-phase species used in the model; NREAC is the number of chemical reactions; NCMAX is the maximum number of constant coefficients; MAXKON is the maximum number of constant species; MAXFST is the maximum number of fast species; and MAXSLO is the maximum number of slow species. The parameter MSPEC defines the maximum number of species including both the gas-phase and the aerosol-phase species. NSECT and NDROP are defined in a FORTRAN include file, NSECT.INC, and refer to the number of aerosol size-sections and the number of droplet size-sections used in the aerosol module, respectively. The NSECT.INC include file must always be included before the CHPARM.COM include file in any subroutine. The integer array LDUM refers to pointers to different species, and common block KCHNM defines those pointers.

A1.1.2 Aerosol Module Specific Files

The FORTRAN files that are specific to the aerosol module are: *addaerem.f, addaerem_sls.f, adddep.f, adddep_sls.f, aeroaq.f, blk_dat3.f, equil1_5.f, equil2_0.f, equil2_1.f, hdiffaer.f, hdiffaer_sls.f, pblmod.f, spline.f, vdep.f, a_aero.com, dep.inc, nsect.inc*, and *param.inc*.

Subroutines ADDAEREM and ADDAEREM_SLS add aerosol emissions to the concentration arrays in the old layer module (OLM) and the surface sublayer module of the SAQM, respectively. The model includes numerous routines that are similar for the OLM and sublayer module; however, only changes in the OLM versions are described below. In ADDAEREM, the aerosol emissions are added as a step function to the concentration array after each call to the chemistry module. Subroutine ADDDEP subtracts the effect of particle deposition from the concentration array for aerosol species. Deposition for aerosol species is treated like a step function (like emissions) and the subroutine ADDDEP is called immediately after the call to ADDAEREM.

Subroutine AEROAQ is the main subroutine for the aerosol module, which calls other routines. Subroutine AEROAQ has nine arguments listed in the order in which they appear on the argument list:

1. Array "gas" which contains the concentrations of gas-phase species in ppm (input array which is updated with new concentrations before the subroutine returns to the calling program)
2. Array "aero" which contains the concentrations of aerosol-phase species in $\mu g/m^3$ (input array which is updated with new concentrations before the subroutine returns to the calling program)
3. Scalar "temp" which specifies the temperature in Kelvin (input)
4. Scalar "rh" which specifies relative humidity as a fraction (input)
5. Logical scalar variable "fogcell" which defines if the grid cell has heavy fog, (fogcell = .TRUE.) light fog, or no fog (fogcell = .FALSE.) (input)
6. Scalar "nsect" which specifies the number of aerosol sections (input)
7. Scalar "ndrop" which specifies the number of fog droplet sections (input)
8. Scalar "naspec" which specifies the number of aerosol and fog species (input)
9. Scalar "ngtotal" which specifies the number of gas-phase species (input)

The file *blk_dat3.f* contains FORTRAN block data, which define the names of the aerosol species and the names of the condensable gas-phase species, and a subroutine BLOCK, which is called at the beginning of the simulation. Subroutine BLOCK adds subscripts to the names of the aerosol species based on the number of aerosol and droplet sections. For example, the species sodium is defined as NA+ in the block data and becomes NA+1, NA+2, etc. in subroutine BLOCK depending on the number of sections used in the simulation.

The subroutines *equil1_5.f, equil2_0.f,* and *equil2_1.f* contain three different versions of the equilibrium routines (EQUILIB15, EQUILIB20, and EQUILIB21), respectively. These subroutines contain the original and updated code for the SEQUILIB model of Pilinis and Seinfeld (1987). EQUILIB15 is the fastest and the least accurate (it also gives warning messages due to some logical flaws in the code). EQUILIB21 is the most accurate, but the least efficient. EQUILIB20 lies between the other two versions in terms of accuracy and efficiency. EQUILIB15 is about 5 times faster than EQUILIB21 and about 2 times faster than EQUILIB20. In a box model where these three versions were run for 2857 cases under different initial conditions, results from EQUILIB15 differed from those from EQUILIB21 for 1 percent of the cases, and results from EQUILB20 differed from those from EQUILB21 for about 0.1 percent of the cases. Thus, for most applications, the three versions give the same results. EQUILB20 is recommended for most applications.

Subroutine HDIFFAER performs horizontal diffusion calculations for the aerosol species. The only difference between HDIFFAER and the routine for gas-phase species, HDIFF, is that for the gas-phase the concentrations are converted from the density units to mixing ratios before the diffusion calculation, whereas for the aerosol species the concentrations are always in units of $\mu g/m^3$. Subroutine PBLMOD calculates the friction

velocity, Monin-Obhukov length, and 10 m wind speed. This subroutine is called before the deposition velocities for the aerosol species are calculated.

Subroutine SPLINE performs LOG_{10} spline interpolation to fit the aerosol mass to fixed size bins. This subroutine is called after every equilibrium calculation for aerosol species. Subroutine VDEP calculates deposition velocities for the aerosol species and is called before the call to subroutine ADDDEP.

The include file *a_aero.com* contains the common block statements specific to the aerosol module. The include file *dep.inc* contains the common block statements required for particle deposition routines. The include file *nsect.inc* contains the parameter statements specifying the number of sections, number of droplet sections, number of aerosol species, number of emitted aerosol species, and common block statements for the aerosol species names. The include file *param.inc* contains more parameter statements specific to the aerosol module.

A1.2 FORTRAN SUBROUTINES CHANGED IN MAJOR WAYS

Table A-1 lists the subroutines that were changed significantly from the original SAQM code. When the changes in the routines for the OLM and the sublayer module are similar, only the changes for the OLM are described below (e.g., the changes to *bcflow.f* described below also apply to *bcflow_sls.f*). Almost every FORTRAN subroutine that has changed contains two additional include files, *chparm.com* and *nsect.inc*. These files were included in all of the routines in this section unless mentioned otherwise.

The main change in subroutine BCFLOW is that it now processes the boundary conditions for the aerosol species as well as for the gas-phase species. The boundary condition arrays (for example, BNORTH, BSOUTH, etc.) contain the values for both the aerosol and gas-phase species and are transferred to the corresponding concentration arrays (at the boundary cells). In the original SAQM the species order in boundary condition arrays matched the order in concentration arrays, but in the SAQM-AERO the order may be different. Hence, the species in the boundary condition arrays are matched to the species in the concentration arrays using the array ISMAP before the values are transferred from one array to another.

The FORTRAN block data file *blk_data.f* was modified to delete the mechanism-specific data, which are now either read from the CHEMPARAM file or specified in the *blk_dat2.f* block data file. The subroutine CHEM was rewritten as the chemistry integrator in the SAQM-AERO and is completely different from the one in the SAQM.

Subroutine DRIVERN was modified extensively. It includes seven additional FORTRAN include files: *param.inc, a_paramw.com, nsect.inc, dep.inc, chparm.inc, a_units.com,* and *a_aero.com*. Several local arrays were added for the deposition and aerosol modules. The subroutine DRIVERN processes the gas-phase and aerosol-phase species (if the logical flag DOAERO = .TRUE.). New code was added to write concentrations of species after the call to each operator if debugging information is requested for a particular grid cell.

Subroutine DRIVERN now calls additional routines: HDIFFAER, ADDAEREM, PBLMOD, VDEP, ADDDEP, and AEROAQ. Subroutine HDIFFAER is called immediately after the call to HDIFF. ADDAEREM, PBLMOD, VDEP, and ADDDEP routines are called after the chemistry calculations followed by the call to subroutine AEROAQ (if logical variable CALLAERO = .TRUE.). The aerosol routine AEROAQ is not necessarily called after every time step. The value of CALLAERO is dictated by the number of aerosol calls per hour (NTAERO) and the number of time steps per hour. The default value of NTAERO is 3, but it is also a user-specified input. Changes in subroutine DRIVER_SLS are similar to those in the subroutine DRIVERN.

Subroutine FILEINI1 was modified because the SAQM-AERO uses only one initial concentration file instead of two files as the SAQM does. After the species names are read from the initial concentration file, they are matched against the names stored in the block data file *blk_dat2.f* and the species map array ISMAP is used to store the information. This subroutine now also includes an additional common block include file *a_cmmns.com*.

Subroutine INITER has also been significantly changed. It contains the additional common block include file *a_aero.com*. Additional variable names were added in NAMELIST to control the simulation. **Table A-7** describes the additional simulation control variables added to NAMELIST. The code which initialized chemistry arrays corresponding to the chemical solver in the SAQM was deleted. Default values of certain new variables were added (shown in Table A-7). Code was added to open the input file "saqm.input" and to call the subroutine OPENSAQM to open the input/output files. Code was also added to call the subroutine CHREAD to read the CHEMPARAM input file, and to either read the surface roughness file or use a default surface roughness at each grid point.

The *mydummy.f* file contains utility subroutines for I/O operations. Two new subroutines were added to this file. Subroutine BUFFERIN2 is used to read the input data in double precision. This is used to read the initial conditions file when the model is restarted from an aborted run. Subroutine BUFFEROUT2 is used to write the data in single precision. This subroutine is used to write the hourly average concentration file and the hourly instantaneous concentration file in the SAQM-AERO.

SAQM2C is the main program of the SAQM-AERO and SAQM models. In the SAQM-AERO it contains the additional common block include files *a_aero.com*, *a_c1desc.com*, and *a_units.com*. It also contains code to determine the wall clock time used for each time step and contains logic to determine when to call the aerosol module. Calls to subroutine TMSTPS were added to determine the integration time step for each hour of a simulation. All the hourly output files are closed and then opened again as "append" files after the call to BUFFIOC and BUFFIOC_SLS. This is done to force the output buffers to be written to the output files after every hour so that output files contain the latest results in case the program aborts prematurely. The instantaneous concentration file (N1 file which is used to restart the program) is overwritten every two hours of model simulation.

Subroutines VDIFFEX, VDIFFIM, VDIFFJ, and VMIX were modified to account for the aerosol species. Unlike gas-phase species, which undergo unit conversion in these

Table A-7. Description of new variables added to NAMELIST in subroutine INITER.

Variable Name	Variable Type	Description
RELERR	Real	Relative tolerance for chemical integrator in the IEH solver; default = 0.01
ABSERR	Real	Absolute tolerance for chemical integrator in the IEH solver; default = 1.0E+06 molecules/cm^3
DTMAX	Real	Maximum operator time step (seconds) for advection
DOAERO	Logical	Flag to specify whether to call aerosol module during the simulation (.TRUE. means aerosol module is called); no default
NTAERO	Integer	Number of times aerosol module is called per hour; default = 3
RHMAX	Real	Maximum relative humidity (as a fraction) to be used in the aerosol module; default = 0.95
DEFRUF	Real	Default surface roughness (m); no default
USEDEFRF	Logical	Flag to specify whether default surface roughness is used in all grid cells (.TRUE. means use default surface roughness). If .FALSE., then a gridded surface roughness file must be read; no default
IVEREQ	Integer	Flag to specify which EQUILIB version to use for equilibrium calculation in the aerosol module; IVEREQ = 1 means to use EQUIL1_5; IVEREQ = 2 means to use EQUIL2_0; IVEREQ = 3 means to use EQUIL2_1; default = 2
AEROBUG	Logical	Option to print detailed aerosol resizing data; should be set to .TRUE. for printing detailed information; default = .FALSE.
ALLLAYERS	Logical	Option to write output concentrations for all vertical layers (.TRUE. => print all layers; .FALSE. => print only first three layers); default = .FALSE.
ICBUG, JCBUG, KCBUG	Integer	The x, y, and z indices of a grid cell which is to be debugged and for which large volumes of extra outputs will be produced. Input zeroes for a normal (no debug) run; default = zeroes

routines, the aerosol species are always in mass units (μg/m^3), hence the code for treating aerosol species in these subroutines is different than that for treating gas-phase species. The common block include file *a_cmmns.com* contains the main common block statements of the program and is included in almost all subroutines. This file was modified to delete the common blocks specific to old chemistry solver, and to add the common blocks for the IEH solver. The dimension statements for boundary condition arrays, emission arrays, and concentration arrays were changed to account for both the gas-phase and aerosol-phase species. Surface roughness array was added to the common block VMVARS. A variable DTMAX (which defines the maximum integration time step for advection) was added to the common block RCNTRL.

A1.3 SUBROUTINES CHANGED IN MINOR WAYS

Table A-2 lists the subroutines that were modified in minor ways. The subroutines shown with an asterisk were modified only to include two new common block and parameter statement include files, *chparm.com* and *nsect.inc*. Most subroutines which were modified include these two common block files (they were added to all of the subroutines in this group unless noted in the following discussion).

In subroutine ADDAQC the variable LPRED is replaced by LSPEC. In subroutine AQCHEM pointers to species indices start with the prefix K instead of L (for example, KSO2 instead of LSO2 to refer to species SO2). Similarly, in subroutine CBLCALC the position index for saving dry deposition starts with the prefix K instead of L. Subroutine CLDPRC was modified in a similar manner as the subroutine AQCHEM. Subroutine CONCDMP, which writes concentrations for predetermined grid cells, was modified to use the ISMAP array to determine the species indices. Subroutines COUPLE and DECOUPLE were modified to change the variable LPRED to LSPEC and to transfer the deposition arrays to the appropriate position in the concentration array. Subroutine FILEINBC was modified to change the variable LSPEC to MSPEC to include the aerosol species.

Subroutine FILEINC1_HA does not include the *chparm.com* and *nsect.inc* include files. The only change is the replacement of variable LC3D1E with LC3D2E. Subroutine FILEINJV also does not include the *chparm.com* and *nsect.inc* include files; the only change in this routine is that the photolytic data file opens in subroutine OPENSAQM rather than in FILEINJV. Subroutine FILEINEE only includes the additional common block file *nsect.inc*. Subroutines FILEINM1 and FILEINM2 were modified to not open the meteorological data files as those files are opened in the subroutine OPENSAQM. Subroutine FINC1_SLS was changed not to open the surface-layer module instantaneous concentrations file. The unit variable "c1_unit_sls" was replaced by "i1_unit_sls" and variable LC3D1E was replaced by LC3D2E.

In subroutine FOUTC1, the variable LC3D1E was replaced by LC3D2E; variable I2HSTR was replaced by I1HSTR; NSPEC was changed from 15 to 47; the call to subroutine FILEOPEN was deleted; and the *a_i2desc.com* include file was deleted. The same changes were made in subroutines FOUTC1_HA, FOUTC1_SLS, and FOUTC1_SLSHA. In subroutine FOUTN1, the variable FOUTTP was added in the argument list (FOUTTP = 1 means that header information gets written). Also, the variable LC3D1E was replaced by LC3D2E and NSPEC was changed from 15 to 47. Similar changes were made in subroutines FOUTN1_HA, FOUTN1_SLS, and FOUTN1_SLSHA.

In subroutine KLSOUR, the variable LPRED was replaced by LSPEC. Also, the indices of the two-dimensional array PRODS were interchanged. In subroutine MRATIO, the variable LPRED was replaced by LSPEC. In subroutine NSTPC, the write statements specific to chemistry time step were deleted. In subroutine RDSOUR, the variable LEMIS was replaced by (LEMIS + LAEROEM) to account for the aerosol emission species. A call to subroutine BLOCK was also added which is invoked only the first time subroutine RDSOUR is

called. In subroutine SFCCONC, variable LCHJ1 was replaced by KCHJ1. In subroutine SUMCHEM, the variable LPRED was replaced by LSPEC.

Apart from the FORTRAN subroutines, some of the common block files were also changed. In file *a_bcdesc.com,* the variable LSPEC was replaced by LC3D2E-2. In file *a_c1desc.com,* the variable LC3D1E was replaced by LC3D2E and an additional common statement C1FILE was added which contains the names of all the hourly concentration output files. In file *a_cmmnw.com,* the array LDUM was deleted. In file *a_datas.com,* the data statements for WTM, SIGMAF, and INTGRT were deleted. In file *a_eedesc.com,* variable LEMIS was replaced by (LEMIS + LAEROEM). In file *a_i1desc.com,* the variable LC3D1E was replaced by LC3D2E. In file *a_iopts.com,* a logical variable ALLLAYERS was added. In file *a_n1desc.com,* the variable LC3D1E was replaced by LC3D2E. In file *a_units.com,* unnecessary unit names were deleted.

In file *a_params.com,* the parameters IDTCSET, NREAC, NREACK, LPRED, LSS, LDIAG, LSPEC, LSSS, and LSSE were deleted. Parameter LEMIS was changed from 14 to 16.

A1.4 CHANGES IN I/0

In the SAQM there are two files for each category of concentration input and output file. The first 15 species in the SAQM are stored in the first file and second 16 species are stored in the second file. For example, the hourly average concentration output files are stored as C1_HA and C2_HA, which are first and second hourly average concentration files, respectively. The reason for storing input and output in two separate files may have been the large size of a single input/output file which earlier computers could not handle. To keep the I/O operations simple, it was decided to use a single file for input and output concentration storage in the SAQM-AERO. Hence, there is only one initial condition file (I1_2), one hourly average concentration output file (C1_HA), one hourly instantaneous concentration output file (C1), and similarly, one output file in each category (i.e., hourly average and hourly instantaneous) for the surface-layer module.

Another modification was to use a logical variable ALLLAYERS to specify whether output for all layers or only the lowest layers should be stored. If ALLLAYERS is set to .FALSE., then output arrays for only the first three vertical layers are stored, otherwise the output arrays for all layers are stored. This is useful when one is only interested in concentrations at the surface and there is no need to store large output files. All the output files are stored in "single precision" to reduce storage space, except the hourly restart file (N1), which is written in "double precision" because it may be needed to restart a run. The N1 file is written every two hours of simulation because the meteorological data used in the model is still stored in such a way that the model can only be started at an even number hour. The N1 file is overwritten at the end of every two hours and can be used to restart a simulation if a simulation aborts prematurely. The hourly instantaneous file for surface sub-layer module (N1SLS) is also written in "double precision" and is overwritten every two hours.

The N1 and the N1SLS files can be used to restart a simulation if a run is aborted prematurely. To restart a simulation the user should set the RESTART option in the simulation control file to .TRUE. and use the N1 and N1SLS files as initial conditions files. The average concentration output files obtained from two runs (one prior to and one after RESTART) can be combined into one file for post-processing using a FORTRAN program JOINC1, which is provided with the model.

Both the *buffioc.f* and the *buff_sls.f* files were modified extensively to implement the features described above. The changes in the two files were similar and only the changes in the file *buffioc.f* are described here. In the argument list of the subroutine BUFFIOC, the unit number for the second file was deleted. The *a_i2desc.com, a_c2desc.com,* and *a_n2desc.com* FORTRAN include files were deleted. All the calls to process second input/output files were deleted. Code was added to transfer the data read from the initial condition file (I1_2) to the appropriate location in the concentration array based on the species mapping array ISMAP. Code was added to either print the number 3 or KMAX vertical layer data, based on the value of variable ALLLAYERS.

The concentration input files can have species in any order, but they should follow the file conventions used in the SAQM, i.e., the header should contain the names of the species in the order in which they appear. The aerosol species must be listed after the gaseous species. The species are written in the output files in the same order as they appear in the input files. The model maps the species read from the initial conditions files to the internal order of species using the array ISMAP. The internal order of gas-phase species in the model is shown in Figure 3-6 and the internal order of aerosol-phase species is shown in Table 4-6. The order of gas-phase species in the emissions input file is dictated by the array MAPSP defined in the block data file blk_dat2. The aerosol phase species can be in any order in the emissions input file, but must occur after the gas-phase species. The names of the species in the input files must match those shown in Figure 3-6 and Table 4-6. The current order of gas-phase species in the emissions input file is the same as in the emissions file used in the SAQM except that the species OLE2 and ammonia were added (in that order).

A1.4.1 Changes in Simulation Control Input File

The Simulation Control input file (referred to as the UI file in the SAQM) was modified to introduce new variables as shown in Table A-7 and to delete certain variables as discussed in Section A1.2 The variables that are used in the SAQM, but are no longer used in the SAQM-AERO are: SPFLAG_ON, INUMHO, and INUMHOX. Two of these variables are not needed because the chemistry solver in SAQM-AERO is different than the one in the SAQM. SPFLAG_ON is not needed because the I/O structure has been changed so that the average concentration files are always written in single precision and the instantaneous concentration files are always written in double precision. The new variable DOAERO acts as a "switch" to turn the aerosol module on or off (as described in Table A-7).